Long-Term Behavior of Support Elements in NATM Tunnels

Dissertation

Submitted to the Institute of Subsurface Engineering, Department of Mineral Resources and Petroleum Engineering and the Committee on Graduate Studies of Montanuniversität Leoben, Austria in Partial Fulfilment of the Requirements for the Degree of Doktor der Montanistischen Wissenschaften

Author:

Muhammad Usman

Supervisor:

Univ. Prof. Dipl. Ing. Dr.mont
Robert Galler

August, 2012

Dedication

To my mother who supported me throughout my life, to my wife who has always stood by me and whose motivation infused in me a passion to improve my qualification, to my children Aiyna, Malaika, Omaima and Mahad who dealt with all sufferings due to my absence from family.

Affidavit

I declare in lieu of oath, that I wrote this thesis and performed the associated research myself, using only literature cited in this volume.

Muhammad Usman **M.Sc. Engg.** Leoben, 2012

Abstract

The long-time behavior of support elements in New Austrian Tunneling Method (NATM) tunnels was studied by applying finite element method using new findings from laboratory tests based on 30 years old tunnel support elements. The gradual degradation of reinforced shotcrete support over a period of time, its perpetual deterioration under the influence of different physical, chemical, mechanical and biological agents and ground pressure was simulated by the reduction of Young's Modulus, cohesion and friction angle to study the impact of this reduction on the stress distribution and overall stability of the tunnel support system consisting of rock mass, shotcrete and the inner lining. The degradation of sprayed concrete linings may contribute to destabilization of the rock mass, resulting in increased maintenance costs, reduced service life, as well as a potential safety risk. A three-dimensional finite element model involving dual-lining system consisting of primary shotcrete support, and the inner cast in place concrete liner was modeled using the general purpose code ABAQUS. The tunnel excavation was simulated using top-heading, bench and invert techniques with simultaneous installation of the shotcrete support. The emphasis was on the prediction of deformation and stresses acting on the primary shotcrete lining during the excavation in soil modeled with Mohr-Coulomb elasto-plastic material behavior. The material parameters used in the analysis were derived from the 30 years old shotcrete, concrete, steel anchors, and waterproofing geomembranes samples from different Austrian tunnel sites tested in the laboratories of the Montan University. The samples of the inner lining were tested at the Graz University of Technology. Using a parametric study, different deterioration processes were simulated by defining suitable interaction between the shotcrete shell and the ground, and the interaction between the shotcrete shell and the inner liner. Substantiating shotcrete shell deterioration, the progressive increase of stresses in the inner lining and stress dissipation into the surrounding ground was observed. This provided the possibility to illustrate the main attribute of a particular deterioration process on the basis of the obtained stress distributions and displacements of the support elements. The evaluated results furnished important information to devise a virtual relationship governing the quantum of load shared by inner liner and construing practical solutions for dimensioning of inner lining thickness and reinforcement requirements.

Kurzfassung

Das Langzeitverhalten der Stützelemente in NÖT Tunnels wurde mittels Finite-Elemente-Methode auf Basis von neuen Erkenntnissen aus Laborversuchen, die an 30 Jahre alten Proben aus verschiedenen Tunnels in Österreich entnommen wurden, untersucht. Die Verwitterung des Spritzbetons unter dem Einfluss von verschiedenen physikalischen, chemischen, mechanischen und biologischen Prozessen sowie die Gebirgsspannungen wurden simuliert; dies geschah durch die Reduktion des E-Moduls, der Kohäsion und des Reibungswinkels. Die Verwitterung von Spritzbeton kann zu einer Destabilisierung des Tunnelbauwerkes beitragen, was zu erhöhten Wartungskosten und einer geringeren Lebensdauer führt. Gleichzeitig kann daraus ein potentielles Sicherheitsrisiko resultieren. Das dreidimensionale Finite-Elemente-Modell mit zweischaligem Ausbau, bestehend aus dem primärem Spritzbeton und der Ortbeton-Innenschale wurde mit ABAQUS untersucht. Der Tunnelvortrieb wurde in Kalotte, Strosse und Sohle unterteilt. Der Schwerpunkt lag auf der Vorhersage der Verformungen und Spannungen insbesonders in der Innenschale. Gerechnet wurde mit dem Mohr-Coulomb'schen Materialgesetz. Die Materialparameter, die in der Analyse verwendet wurden, stammen aus 30 Jahre altem Spritzbeton, Beton, Ankern und Dichtungsbahnen aus verschiedenen österreichischen Tunneln. Die Versuche wurden in den Labors der Montan-Universität, betreffend die Innenschale auch in den Labors der Technischen Universität Graz, durchgeführt. Mit Hilfe einer Parameterstudie wurden verschiedene Prozesse der Verwitterung simuliert. Mit der Verwitterung der Aussenschale konnte eine progressive Zunahme von Spannungen in der Innenschale und Spannungsänderungen im umgebenden Erdreich beobachtet werden. Die Ergebnisse der Untersuchungen brachten wichtige Informationen für die Beurteilung der Wechselwirkungen zwischen Innenschale, Spritzbetonschale und umgebendem Gebirge sowie die Dimensionierung der Innenschale.

Acknowledgements

First and foremost I acknowledge and offer my sincerest gratitude to **Professor Robert Galler** who always supported and guided me patiently during my entire study period at the Institute of Subsurface Engineering Montan University Austria. His diligent and consistent supervision made it possible for me to achieve this feat. His huge breadth and depth of knowledge always helped me steer in the right direction. He has always supported me regarding any problem that I have shared with him. I cannot find enough words to thank him. I would like to thank **Dr. Gerhard Pittino** for his support and guidance in the laboratory testing of materials. I am also thankful to Lab. Technician **Gerhard Cevela** for his cooperation in laboratory work. I thank my colleagues **Erik Schuller, Gunter G. Gschwandtner, Christian Volderauer** for providing their ever ready help through their expertise and cooperation. I also acknowledge the efforts of **Miss Schmid Michaela** for her help and support regarding administrative matters. I like to thank my friend **Hojjat Gholizadeh** for his continuous invaluable support especially in installing Linux operating system and compilers on my computer. I am grateful to Higher Education Commission of Pakistan (HEC), for financially supporting my studies abroad. I would also avail the opportunity to thank OEAD Austria specially **Miss Nadja Juritsch** and **Madam Dagmar Holzapfel** for their efforts regarding the administrative aspects. I also pay thanks to my parent organization Pakistan Atomic Energy Commission (PAEC), for granting study leave. Last but never the least, I thank to my mom and my wife **Hayat** for being supportive and cooperative on all occasions and my daughters **Aiyna**, **Malaika**, **Omaima** and my son **Mahad**.

List of Abbreviations

ACN	acrylonitrile
ATR	attenuated total reflection
2D	two dimensional
3D	three dimensional
C	concrete
c	cohesion
C-DLS	dual lining systems with composite linings
C3D8	three-dimensional 8-node linear brick elements
C3D8R	three-dimensional 8-node linear brick elements with reduced integration
DHC	dehydrochlorination
DMA	dynamic mechanical analysis
DOP	di-(2 ethylhexyl) phthalate
DSC	differential scanning calorimetry
E	Young's modulus
EPB	earth-pressure balance machines
ESI	electro spray ionization
g	plastic potential function
HDPE	high density polyethylene
GROUND	numerical model of ground
H	overburden
HB	Brinnel hardness
HV	Vicker hardness
IR	infrared
K	lateral earth-pressure coefficient
LINER	numerical model of inner liner
LLDPE	linear low-density polyethylene
MDPE	medium-density polyethylene
MeOH	methyl hydroxide
NATM	New Austrian Tunneling Method
ÖVBB	Österreichische Vereinigung für Beton- und Bautechnologie
P	contact pressure
PP	polypropylene
PVC	polyvinyl chloride
Rm	ultimate stress
Rp	yield stress
RV	reduced viscosity
RVS	Richtlinien und Vorschriften für das Straßenwesen
SEM	scanning electron microscopy
S22	tangential stress in shotcrete shell or inner liner
S-DLS	dual lining systems with separate linings
SS	slurry shield machines
TBM	tunnel boring machine
T_g	glass transition temperature
UV	ultra violet

List of Symbols (Greek symbols)

ε	strain
ε^e	elastic strain
ε^p	plastic strain
λ	scalar function in strain vector
σ	stress
σ_H	horizontal stress field
σ_V	vertical stress field
σ_b	failure stress
ε_b	failure strain
γ	specific weight; unit weight
γ_{elast}	elastic slip
ν	Poisson's ratio
ψ	dilation angle
ϕ	friction angle
ϕ_i	internal friction angle
ρ	density
μ	friction coefficient
τ	shear stress
τ_{crit}	maximum transferable shear stress
δ	deformation vibration
δu	shear displacement
Δv	dilation
v	wave number

Contents

Chapter 1

Introduction

1.1 Historical preview

In some western countries, sufficient number of tunnels have stepped into aged phase. The increased age of road and railway tunnels has intensified the realization for proper maintenance and sustainability of the structure. Tunnel is always subject to the influence and control of surrounding environment during its service life. The long-time behavior and assessment of the stability and serviceability of the tunnel lining is an important issue of modern tunneling industry. In dual-lining systems, fiber reinforced shotcrete is widely used as a primary support in tunnel lining. It is generally believed that under the influence of different deterioration processes the shotcrete support looses its characteristics and is unable to fully support the structure in the long-term. No support contribution may be derived from shotcrete support for long-term assuming shotcrete deterioration [1, 2]. According to [3], until 1999 there were approximately 346 km of highway and rail transit tunnels in U.S.A. more than 50 years old where support elements were deteriorated and needed repair. The current international guidelines [4], recognize shotcrete as a temporary support which looses its effectiveness after some time of the construction of the inner lining. Shotcrete lining deterioration is the outcome of aging, deformations and fracturing due to ground pressure. Environmental factors (e.g. moisture, temperature) and operating conditions (traffic, de-icing salts) also contribute to lining degradation. Anomalies associated with shear deformation caused by the instability due to excavation work in the neighboring area or seismic activity are direct evidence of ambient stress variations and indicate potential damage in terms of cracking and failure of lining [5]. The progressive growth of plastic zone around the tunnel due to weathering could be the reason of increased ground pressure loading the tunnel support [6]. On the other hand, presence of aggressive ground water in the surrounding of tunnel environment could cause deterioration of the shotcrete support. Due to the fact that mostly in tunnels with dual-lining systems a waterproofing geomembrane is installed between shotcrete shell and the inner lining, only the shotcrete shell is exposed to hostile environment. Different processes that are generally held responsible for the deterioration of tunnel support are enumerated below;

- Physical processes
- Chemical processes

- Biological processes
- Other processes

Almost thirty years old samples of support elements representing degraded shotcrete, concrete, steel rock bolts and geomembranes were obtained from different locations (crosscuts) of the five highway tunnel sites named Tanzenberg, Ganzstein, Katschberg, Ropenner and Bosruck tunnels in Austria. The samples were tested in different institutes of Montan University for observing the possible causes and extent of deterioration. The inner lining samples were tested at the Technical University of Graz. The change in properties and strength characteristics of the support elements with ageing under the given service conditions was analyzed. The results of the degraded samples were also compared with the results obtained from fresh samples to measure the extensity of deterioration and serviceability of the old samples. The derived parameters from the testing of different samples were used in developing a three-dimensional finite element model for carrying out a numerical study of a tunnel constructed with a dual-lining system to investigate the long-time deterioration processes of the shotcrete shell and their impacts on the combined support system including shotcrete shell, inner liner and the surrounding ground. The initial support included steel fiber reinforced shotcrete and the final lining constructed of cast-in-place concrete after the initial support and waterproofing had been placed. The effect of installing a geomembrane was included in the model by defining a suitable interaction between the shotcrete shell and the inner liner whereas the effect of rock bolts was taken into account by an increased cohesion of the ground. The long time behavior of steel fiber reinforced shotcrete support and its degradation under the influence of different physical, chemical, mechanical and biological agents was simulated by the reduction of the Young's Modulus, cohesion and friction angle to study the impact of this reduction on the stress distribution and overall stability of the tunnel support system. The obtained results were discussed in terms of stresses and displacements of the support elements, which evolved during deterioration.

1.2 Thesis outline

This thesis is organized with a view that the reader gets the essential scoops of all the relevant work areas before numerical model development is discussed.
Chapter 1. gives a short introduction and historical overview of the problem.
Chapter 2. delineates a brief introduction to modern tunnel support systems, which includes single-lining and dual-lining systems. A short discussion of the main deterioration processes (physical, chemical, biological and others) of the tunnel support system is presented. Results of the uniaxial and triaxial tests on the samples of shotcrete and concrete are also presented.
Chapter 3. contains details about deterioration of steel rock bolts. Different tests (mechanical, chemical, microstructure analysis) conducted on the degraded steel bolts samples are described.
Chapter 4. has a discussion about different tests conducted on the samples of deteriorated waterproofing geomembranes collected from different tunnel sites. It furnishes information regarding composition, strength characteristics and causes of degradation of the examined samples.

Chapter 5. entails the description of the numerical model construction of a tunnel with a dual-lining system, excavation sequence and investigation of the time dependent deterioration of the primary shotcrete shell and its impacts on the inner liner. The results and discussion of the stresses and displacements of the parametric study showing different deterioration processes of the primary shotcrete shell are also presented.
Chapter 6. lists the conclusions and recommendations for future development.

Chapter 2

Deterioration of Tunnel Lining

2.1 Lining configuration

Nowadays most tunnels are constructed with a double lining system usually called primary and secondary lining [7, 8].The role of the primary lining or support is to withstand the loads that arise during tunnel excavation. Usually the secondary lining is installed much later than the primary support. The Austrian guideline for inner lining recommends to bring in the inner (secondary) lining by observing a deformation velocity of the primary (outer) lining less than 4mm/month [9]. The tunnel lining, as final support for the ground has to ensure stability, durability and serviceability for the entire period of use of the facility. It protects the interior against any pressure from the surrounding ground or water ingress into the tunnel environment. In this particular study a tunnel construction utilized a dual lining system consisting of both primary support and final lining separated by a waterproofing and drainage system. The initial support included shotcrete with reinforcement using wire mesh and the final lining constructed of cast-in-place unreinforced concrete after the waterproofing system had been placed. It was assumed that the initial support deteriorates over time and all the loads were transferred to and supported by the final lining. The initial support was based on the principles of the New Austrian Tunneling Method (NATM). A brief overview of the tunnel support describing single-lining and dual-lining systems is presented below.

2.1.1 Single-lining system

A tunnel lining system where only one lining is installed which serves as both the initial support and the final lining, is called single-lining or single-pass lining system. Common examples are bolted, gasketed precast concrete segmental systems, liner plate systems and most widely used reinforced sprayed concrete (shotcrete). Single-lining systems of tunnel support could be applied to different excavation methods. Shotcrete with its superb properties like bonding to the rock and remarkable ductility is widely used as a support material in conventional tunneling methods done by drill and blast, using excavators and roadheaders; sometimes shotcrete is also used by doing excavation by open tunnel boring machines (TBMs). The segmental ring consisting of reinforced concrete, sometimes of cast iron or steel are commonly used today, including TBM tunneling. Liner plates are curved sheeting screwed together through their raised edges and are typically used for

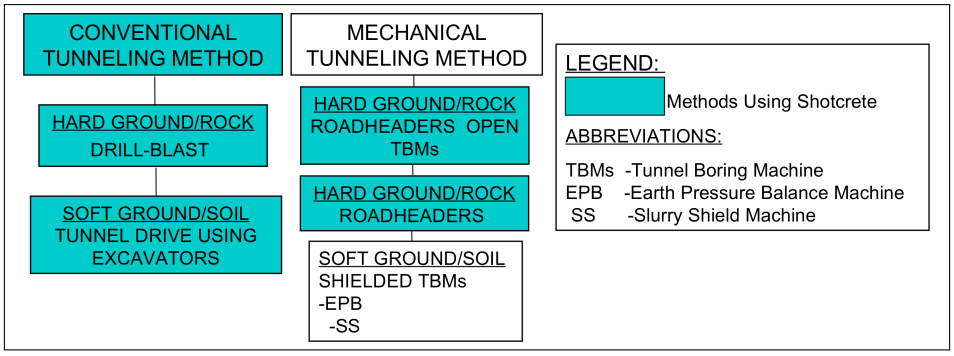

Figure 2.1: Overview of tunneling methods; turquoise colored methods provide the possibility to use shotcrete as support; [8].

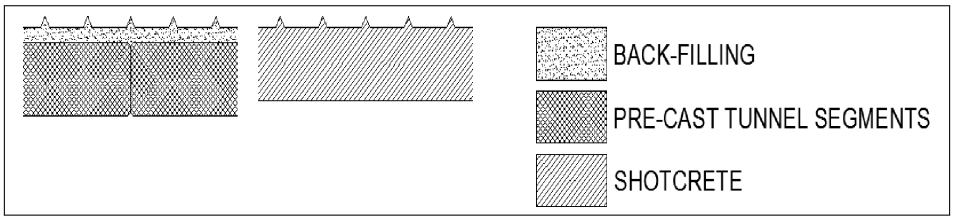

Figure 2.2: Different types of single-lining systems; adapted from [10].

small cross section soft-ground conditions where immediate support is required. Fig. 2.1 illustrates different excavation methods used today, whereas those employing shotcrete as a support are highlighted.

Shotcrete lining is usually fissured and thus water permeable. Due to water leakage problems infrastructure tunnels (e.g road-tunnels, railway-tunnels) make seldom use of single-lining systems. From the construction operation point of view shotcrete should be applied in several layers to the tunnel walls and reinforcement should be used either with wire mesh or steel fibre shotcrete. Reinforcement of shotcrete with steel fibres, steel nets or wire mesh will also contribute towards increased tensile strength and reduced cracking of lining. Grouting could help to some extent in achieving subsequent waterproofing. Fig. 2.2 illustrates two different types of single-lining systems.

2.1.2 Dual-lining systems composite lining (C-DLS)

In the dual-lining systems with composite lining (C-DLS), primary and secondary liners are applied one after the other. The two liner are in fixed contact with each other and depending on the method of spraying, the lining either act as a composite shell or shows a reduced shear interaction when subjected to load. Initial support to rock is usually provided with shotcrete. Pre-cast tunnel segments could also be used instead.The cast-in-place concrete is usually used for the secondary inner liner. Fig. 2.3 shows different types of C-DLS. This system of lining suffers from one serious disadvantage that due to the absence of a geomembrane between the two liners there is no efficient drainage effect as occur in S-DLS (Sec. 2.1.3), and the secondary liner may be subjected to ground water seepage through the shotcrete shell. Therefore, C-DLS are recommended to be used in relatively dried environment.

The sprayed waterproof lining is a special type of C-DLS systems with a waterproofing

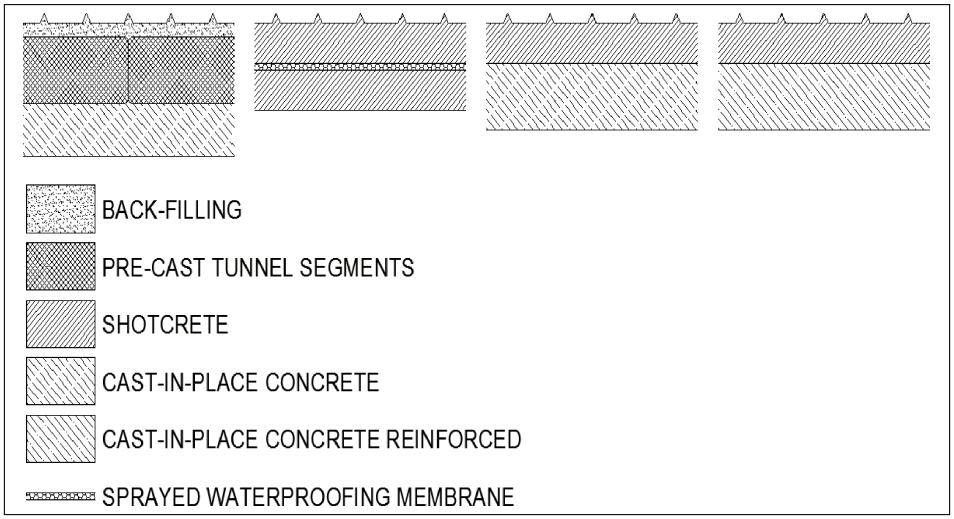

Figure 2.3: Different types of dual-lining systems with composite linings (C-DLS); adapted from [10].

membrane between primary and secondary liner. The sprayed water proofing membranes application system is more flexible and can be readily adopted in tunnels with complex geometries (e.g. junctions, bays), while maintaining the tied contact between primary and secondary liner.

2.1.3 Dual-lining systems–separate linings (S-DLS)

Dual-lining systems with separate linings (S-DLS) incorporate the placement of geomembranes between primary and secondary liner independently installed one after the other. In such a system there is a constructive and functional separation of the individual shells with a waterproofing membrane, which is applied after the primary liner is installed. S-DLS can be used with all tunneling methods. Shotcrete or pre-cast tunnel segments are the common support types employed as primary lining in both cases of conventional and mechanical excavation methods. The secondary liner can be either cast-in-place or sprayed concrete. The cast-in-place concrete is usually the standard method adopted for secondary lining. Fig. 2.4 illustrates different types of S-DLS. Secondary liner is constructed after installation of geomembrane which prevent leakage of ground water into the tunnel and protect inner liner against any agressive attack.

The presumption as to which extent the primary shotcrete lining attribute to permanent support depends on as far it is affected by degradation. The secondary cast-in-place concrete inner liner has to withstand all loads resulting from the deterioration of the primary support. The design of concrete inner liner takes into acccount all requirements regarding long-term stability and serviceability of the tunnel structure.

2.1.4 Structural requirements-single lining system vs. dual lining system

The German guideline [11] states that in C-DLS the inner liner could be shotcrete alone when there is no presence of ground water. The Austrian guideline for shotcrete [12]

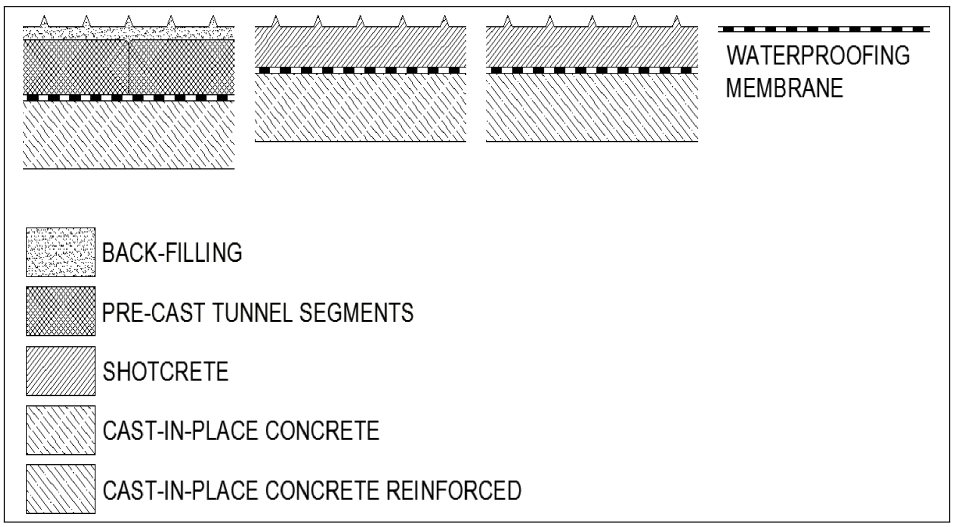

Figure 2.4: Different types of dual-lining systems with separate linings (S-DLS); adapted from [10].

recommends single-lining systems with shotcrete only in dry environment or alternatively subsequent grouting should ensure water tightness in the presence of an effective tunnel-drainage system. In the presence of aggressive groundwater the only solution will be adopting dual lining systems with a geomembrane (S-DLS) and use of special shotcrete-quality to protect shotcrete shell against detrimental effects. The Austrian guideline for inner linings [9] advocate that the concrete-quality of the inner-liner should be better in case of C-DLS as compared to that of S-DLS. The Austrian guideline [10] mentions that under no circumstances shotcrete should be applied for single-lining if water pressure can act on the tunnel. In case of S-DLS, the shotcrete is required to provide initial support during construction of the tunnel. Geotextile is placed over the rough surface of shotcrete liner to provide smooth and even surface for the geomembrane to be placed between shotcrete shell and the cast-in-place concrete inner liner. Geomembrane control water ingress into the tunnel and protects inner liner against any deleterious effects of ground water. The concrete inner liner is responsible for providing over all long-term stability of the tunnel. The inner liner has also to cater for preservation of tunnel integrity during fire hazards, accidental collisions and seismic loading etc. It is the consolidated opinion of above mentioned guidelines that single-lining systems assume no deterioration of the shotcrete. The basis of this assumption is the fact that no or very little groungdwater is present and unable to cause any considerable disturbance. Dual-lining systems are state-of-the-art construction methods for infrastructure tunnels in Europe.

2.2 Conclusion-single lining system vs. dual lining system

As discussed earlier that single-lining systems and dual-lining systems with composite linings (C-DLS) lack in providing efficient waterproofing characteristics, consequently they are not ideally used when aggressive groundwater is present, which is believed to play a crucial role in lining degradation. On the other hand dual-lining systems with separate linings (S-DLS) are more versatile and could be successfully used under adverse

Table 2.1: Evolution in material mechanical properties

Parameter	Trend over time	Bibliographical reference
Young's modulus	−	Wiid and Colback (1965)
Poisson's ratio	+	Hencher et al. (1990) & Stead et al. (2000)
Compressive strength	−	Wiid and Colback (1965)
Tensile strength	−	Wiid and Colback (1965)
Cohesion	−	Wiid and Colback (1965)
Density	+/−	Sorgi et al. (2004)
Permeability	+	Sorgi et al. (2004)
Degree of saturation	+	Sorgi et al. (2004)
Porosity	+/−	Sorgi et al. (2004)
Shear strength	+	Hencher et al. (1990) & Stead et al. (2000)
Friction angle	−	Wiid and Colback (1965)

+: Tendency to increase; −: Tendency to decrease.

environmental conditions to effectively safeguard the inner liner against belligerent environment. In the numerical calculations dual-lining systems with separate linings (S-DLS), whereby the waterproofing membrane is placed between the primary shotcrete shell and the secondary cast-in-place concrete inner liner using contact formulations that allow finite sliding, is investigated.

2.3 Degradation of tunnel support

Structural and mechanical characteristics of tunnel support undergo significant changes during the life-time of a tunnel. Long-term structural assessment of support elements is one of the key activities in maintaining the performance of a tunnel during its service life. The lining structure of a tunnel is subjected to both external loads and environmental effects. Under the given circumstances the support elements are subjected to mechanical, physical, chemical and biological actions of numerous hostile agents [13]. The physical and chemical properties of construction materials are thus sensitive to these processes, and their evolution over time produces material ageing (see Tab 2.1). Short-term time-dependent instabilities are mostly attributed to the rock behaviour (i.e viscosity) and may exhibit large deformations like for squeezing and swelling rocks [14]. Long-term changes in strains are associated with deterioration in the mechanical characteristics and ageing of the rock. It may also involve changes in hydraulic conditions (pore pressure), chemical transformation and even, in some cases, thermal effects [15]. This evolution depends on the category of material, environmental conditions, type of degradation process and time. Typically the primary and secondary linings are not mechanically connected and can deform independently. The secondary support has to withstand those loads that arise from tunnel operation, change in groundwater conditions, deterioration of ground strength and/or primary support with time, or from other changes of stresses in the ground around the tunnel studied by KGS [1996] and cited by [16]. The causes of deterioration were broadly classified into two types by [17] as under:

1. Those caused by external pressure, including earth pressure and freezing pressure; and

2. those caused by the deterioration of materials.

Due to the increasing age of tunnels worldwide there is growing concern about the safety and serviceability of tunnels built long time ago. The investigation of time-effect on the stability of a tunnel structure has become an important feature and different points which have to be considered, are:

- As a basic requirement of NATM, monitoring of the tunnel is done during construction (and on some very specific points, where problems during construction occured) and also during its life-time to collect information about the geotechnical behaviour (system behaviour). Material properties of the support elements are normally measured continuously during the construction process only.

- Investigation of the long-time deterioration phenomena in tunnel structures including different degradation processes.

Different processes that are generally held responsible for the deterioration of tunnel support are given below;

1. Physical processes

2. Chemical processes

3. Biological processes

4. Other processes

2.3.1 Physical processes

The time-dependent changes that affect the internal characteristics of concrete support and other support elements can be sorted out as the physical processes responsible for support deterioration. According to [18], stiffness reduction or strain increase could be used to model such processes in the numerical simulations. In physical processes the support material is subjected to mechanical disintegration and breakdown under the action of different agents including heating and cooling, frost action, organisms, and tectonic effects. This includes concrete deterioration by surface wear, cavitation, crystallization of salts in the pores of concrete. The time dependent conditions of water flow pattern, water pressure around the tunnel as well as over- consolidation may significantly contribute to the physical degradation of tunnel support systems. Changing conditions may lead to swelling or creeping of the ground. It was concluded by [19], that an increase of water pressure may be the result of sintering of the tunnel drainage system which in turn induces higher loads on the support. The presence of visoplastic rocks such as phyllites and schist/slates in the tunnel vicinity lead to creep deformation which ultimately load the final lining. Interestingly, [20], postulated that the effect of consolidation has to be considered if highly cohesive soils are encountered in the surrounding of tunnel. With the

release of stresses upon tunnel excavation in such areas, negative pore water pressures may initially build up and at first loads the support to a small extent. Eventually with the reduction of negative pore water pressure over time, the tunnel support elements are more heavily loaded. The impacts from mass movements and tectonics have to be considered as well. Similarly [6], suggested the load on the tunnel crown by considering the weight of the plastic zone for deep tunnels. Acording to German guidelines [11] water submersion in surroundings of tunnel can result in degradation of ground in a way that a tunnel built in an aquifer can act like a drainage system. Consequently the plastic zone around the tunnel grows further with the erosion of surrounding ground.

2.3.2 Chemical processes

Chemical processes usually play very active role in the degradation of tunnel support elements. Chemical processes introduce a series of surface reactions between the material, the atmosphere and water. The stability of the entire support system may change over a period of time as a result of change in the chemical composition of support elements and the surrounding ground. Chemical deterioration mechanisms generally involve the penetration of external ions into material pores structure and /or the dissolution of chemical species from its hydrated and unhydrated phases [21]. According to [22], the adhesion of shotcrete linings may be substantially affected by small amounts of interactions on the interface by the action of water due to its thin structure and inhomogeneities regarding the distribution of porosity. Long-time deterioration by chemical processes causing reduction of rock mass strength properties was analyzed by [23]. It was stated by [18], that chemical processes reduce the mechanical strength properties and cause thickness reduction due to weathering of the exposed liner material. In the absence of adequate waterproofing systems the inner liner is exposed to external attacks of aggressive groundwater (e.g. sulphates corrosion, calcium leaching). When a water proofing membrane is placed between shotcrete and inner liner, shotcrete support will deteriorate and degradation may occur at the inner liner intrados with eventual reduction of final lining thickness caused by de-icing salts corrosion. In many investigated tunnels concrete structures in contact with ground water, the processes of leaching and the formation of sulfate minerals, predominantly thaumasite, have been detected. As a consequence thaumasite may be a very common cause controlling the course of concrete deterioration [22]. Chemical attacks are mainly referred to erosion on concrete and corrosion on steel. Erosion can occur in different forms. Continuous intrusion of CO2 usually makes a carbonized incrustation on concrete cover, which makes concrete brittle to scale or to spall [24]. Under continuous erosion of acid action or sulfites media, voids or cavitations will develop within the concrete structure.

2.3.3 Biological processes

Bio degradation of concrete is thought to occur when microorganisms are present in the environment to produce mineral or organic acids that dissolve or disintegrate the concrete matrix. According to [25] live organisms under favorable conditions, in the presence of water and appropriate temperature can readily settle on low pH concrete. They form a film called biofilm, which is followed by the chemical biodeterioration of concrete.

2.3.4 Other processes

The damage in concrete structures can also arise from a variety of additional reasons. These might include overloading and accidental actions such as fire, impacts and accidents, events like earthquake ice-and frost-actions etc. Such damages in exceptional cases may change tunnel equilibrium with time and need to be considered in service life or durability issues.

2.4 Testing of old shotcrete samples

Almost thirty years old samples of shotcrete (primary lining) obtained from different cross-cuts of five highways tunnel sites in Austria, named Tanzenberg, Ganzstein, Katschberg, Roppener, and Bosruck were tested in the material testing laboratory of the Subsurface and Geotechnical Institute of Montan University Leoben, Austria. After preparation these samples were subjected to different tests such as uniaxial compression and tri-axial compression tests to determine uniaxial compressive strength UCS, Poisson's ratio ν, Young's modulus E, deformation modulus V and shear strength parameters like cohesion c, and angle of friction ϕ using multiple failure tests. The tests were conducted to investigate material degradation and strength reduction with the passage of time and any influence from the above mentioned deteriorating processes. Fig. 2.5 shows uniaxial compression testing of the shotcrete sample and the resultant stress-strain diagram is illustrated in Fig. 2.6. The relevant details about samples diameter, length, mass, density and calculated values from the uniaxial compression tests of shotcrete are presented in Tab. (2.2). The Mohr-Coulomb and Hoek-Brown failure envelopes of the triaxial testing of the shotcrete sample are depicted in Fig. 2.7. The samples description and obtained results are presented in Tab. (2.3).

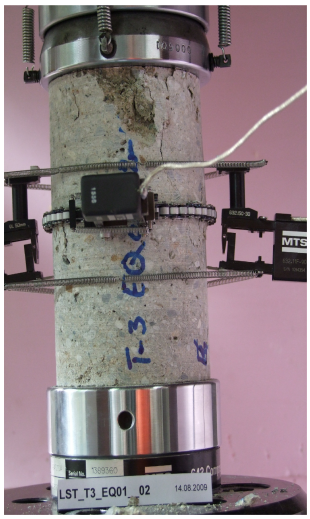

Figure 2.5: Uniaxial compression testing of the shotcrete sample using MTS test equipment

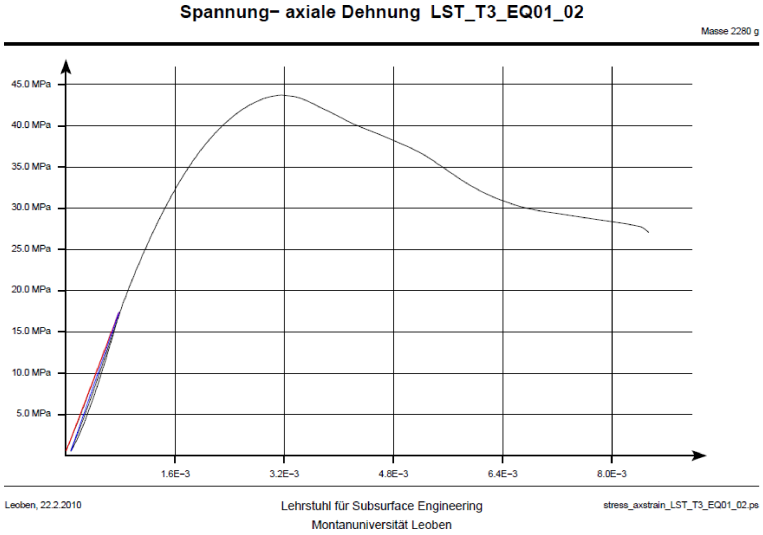

Figure 2.6: Stress-strain diagram of the UCS testing of shotcrete sample

Table 2.2: Values of different parameters obtained as a result of the uniaxial testing of shotcrete samples

						Elastic Parameter			Uniaxial Comp. Strength
Reference	Cross section	Diameter	Length	Weight	Density	E-Modul	V-Modul	Poisson's ratio ν	UCS
		[mm]	[mm]	[kg]	[kg/m^3]	[GPa]	[GPa]	[-]	[MPa]
Tanzenberg	EQ-02/3	104.20	167.00	3.360	2359	38.35	37.44	0.09	70.13
Tanzenberg	EQ-03/2	104.30	100.20	2.030	2371	28.10	24.94	0.08	68.88
Ganzstein	EQ-01/2	93.20	185.50	3.000	2370	46.18	45.27	0.13	69.68
Ganzstein	EQ-02/3	93.20	116.30	1.810	2280	24.59	22.26	0.11	31.11
Ganzstein	EQ-02/6	93.30	82.70	1.312	2321	18.30	13.59	0.05	33.45
Katschberg	EQ-01/2	93.80	147.30	2.280	2240	23.85	21.70	0.09	43.73

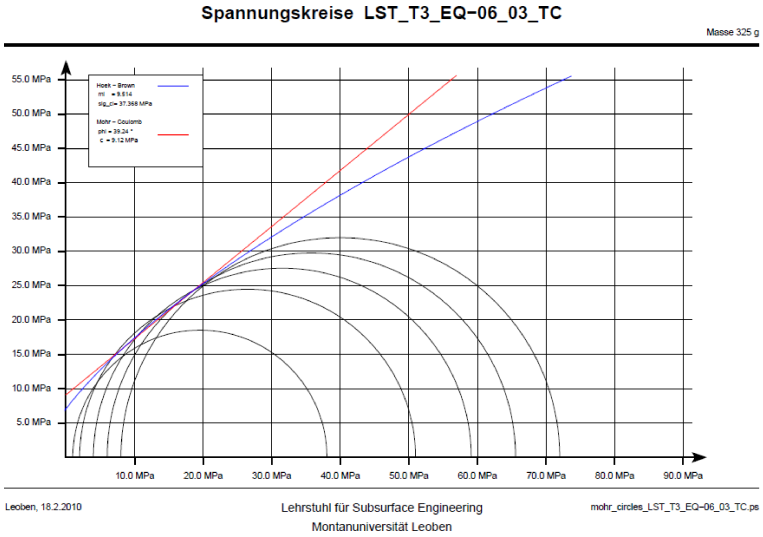

Figure 2.7: Mohr circles from the multiple failure testing of the shotcrete sample

Table 2.3: Values of different parameters obtained as a result of the triaxial testing of shotcrete samples

						Elastic Parameter			Mohr-Coulomb		Hoek-Brown	
Reference	Cross section	Diameter	Length	Weight	Density	E-Modul	V-Modul	Poisson's ratio ν	c	ϕ	σ_{ci}	m_i
		[mm]	[mm]	[kg]	[kg/m^3]	[GPa]	[GPa]	[-]	[MPa]	[°]	[MPa]	[-]
Tanzenberg	EQ-01/2	98.90	166.30	3.030	2371	33.79	27.93	0.09	17.04	35.83	65.11	7.191
Tanzenberg	EQ-02/2	98.80	200.20	3.630	2364	64.28	22.66	0.19	18.86	34.74	70.87	6.513
Tanzenberg	EQ-03/1	98.90	141.80	2.580	2369	36.31	11.19	0.13	12.99	40.97	54.81	10.65
Ganzstein	EQ-01/1	93.20	199.00	3.237	2383	-	20.28	-	19.24	32.49	67.47	6.478
Ganzstein	EQ-02/7	93.10	200.20	3.097	2274	28.02	12.33	0.21	8.79	36.43	33.24	8.392
Katschberg	EQ-06/3	49.20	77.50	0.325	2205	29.62	18.04	0.11	9.12	39.24	37.37	9.514
Roppener	ASN-07/2	98.40	201.80	3.300	2150	16.86	12.68	0.13	5.26	38.43	16.96	15.13
Bosruck	GQ-06/2	94.60	167.60	2.770	2351	20.36	17.12	0.11	12.65	31.00	43.09	6.209

In a study conducted on the shotcrete samples from different cross-cuts of Bosruck tunnel [26], the increase in uniaxial compressive strength of shotcrete with time was investigated. UCS results of the samples after 7 and 28 days of installation in the cross-cuts GQ-1, EQ-5 and LQ-N were compared with the values of UCS for the mentioned cross-cuts after it served for 30 years. It was observed that shotcrete gained strength with the passage of time. The relationship showing increase in UCS over a period of many years from green to old shotcrete are illustrated in Fig. 2.8, Fig. 2.9 and Fig. 2.10

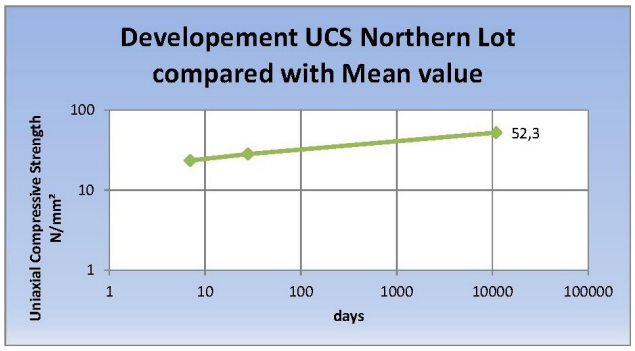

Figure 2.8: Diagram of the developement of the UCS during excavation of the first tube (northern lot) and comparison with the mean value from all of the 30 year old specimens (in double logarithmic scale); [26]

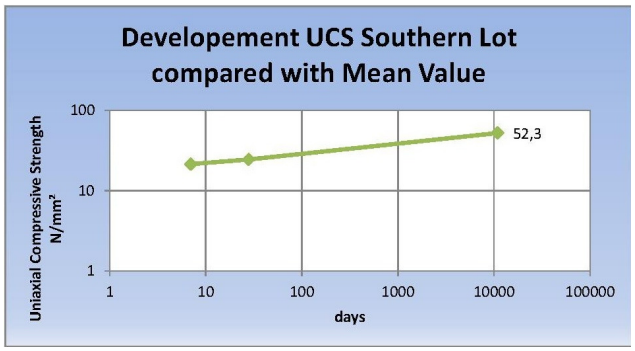

Figure 2.9: Diagram of the developement of the UCS during excavation of the first tube (southern lot) and comparison with the mean value from all of the 30 year old specimens (in double logarithmic scale); [26]

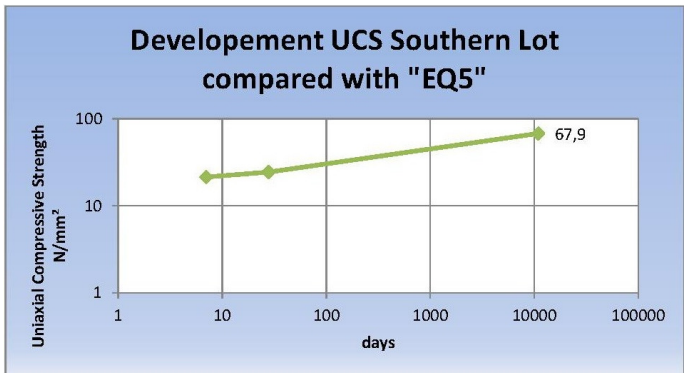

Figure 2.10: Diagram of the developement of the UCS during excavation of the first tube (southern lot) and comparison with the mean values from EQ-5 of the 30 year old specimens (in double logarithmic scale); [26]

2.5 Testing of old concrete samples

The samples of concrete (secondary lining) from the previously mentioned tunnel sites, Tanzenberg, Ganzstein, Katschberg, Roppener, and Bosruck were tested at the Institute for Rock Mechanics and Tunnelling Technical University Graz, Austria. After preparation these samples were subjected to different tests such as uniaxial compression and tri-axial compression tests to determine uniaxial compressive strength UCS, Poisson's ratio ν, Young's modulus E, deformation modulus V and shear strength parameters like cohesion c, and angle of friction ϕ using multiple failure tests. The tests were conducted to investigate the durability and behavior of inner linings in a dual-lining system after many years of service. The samples description and the derived parameters of the uniaxial and triaxial compression testing of the concrete samples are presented in Tab. (2.4) and Tab. (2.5) respectively.

Table 2.4: Values of different parameters obtained as a result of the uniaxial testing of concrete samples

						Elastic Parameter			Uniaxial Comp. Strength
Reference	Cross section	Diameter	Length	Weight	Density	E-Modul	V-Modul	Poisson's ratio ν	UCS
		[mm]	[mm]	[kg]	[kg/m^3]	[GPa]	[GPa]	[-]	[MPa]
Tanzenberg	EQ-02/IS	104.1	193.4	3.877	2355	41.81	31.80	0.13	25.15
Tanzenberg	EQ-01/IS	104.1	205.5	4.185	2393	40.62	34.37	0.09	41.22
Ganzstein	EQ-01	94.0	188.2	2.966	2271	30.38	21.17	0.10	26.69
Ganzstein	EQ-02	94.0	189.0	3.070	2341	34.15	25.81	0.07	41.50
Katschberg	EQ-1/3	94.0	184.1	2.997	2346	38.18	30.75	0.11	46.29
Katschberg	EQ-3/3	94.0	189.9	3.160	2398	31.34	23.25	0.08	40.35
Roppener	ASN-7	98.5	196.4	3.610	2412	44.60	35.79	0.12	45.88
Roppener	FQ-12	93.80	172.8	2.839	2378	37.79	29.49	0.11	30.85
Bosruck	GQ-06	98.5	167.0	3.066	2410	39.39	30.28	0.11	31.65
Bosruck	GQ-01	94.8	184.7	3.222	2472	52.55	43.98	0.11	34.51

Table 2.5: Values of different parameters obtained as a result of the triaxial testing of concrete samples

						Elastic Parameter			Mohr-Coulomb		Hoek-Brown	
Reference	Cross section	Diameter	Length	Weight	Density	E-Modul	V-Modul	Poisson's ratio ν	c	ϕ	σ_{ci}	m_i
		[mm]	[mm]	[kg]	[kg/m^3]	[GPa]	[GPa]	[-]	[MPa]	[°]	[MPa]	[-]
Tanzenberg	EQ-04/IS	83.8	169.9	2.111	2253	41.74	39.41	0.10	10.44	34.3	34.07	9.83
Tanzenberg	EQ-03/IS	83.8	159.0	1.948	2222	35.70	35.95	0.10	11.28	33.6	40.57	6.68
Ganzstein	EQ-01	83.8	169.9	2.110	2252	28.14	22.07	0.07	8.91	35.9	33.96	7.28
Ganzstein	EQ-02	83.8	169.8	2.095	2238	28.88	26.13	0.06	10.19	35.2	33.94	10.33
Katschberg	EQ-5/3	83.8	168.3	2.153	2319	31.89	29.03	0.12	11.11	36.2	37.92	10.81
Katschberg	EQ-3/1	83.8	169.9	2.185	2332	37.14	36.68	0.09	11.69	35.8	40.85	9.85
Roppener	ASN-7	98.4	197.9	3.644	2422	52.29	48.36	0.07	11.87	37.0	42.02	10.92
Roppener	FQ-12	83.8	170.1	2.290	2441	34.69	31.89	0.10	8.85	35.7	27.92	12.10

2.6 Conclusion

Almost thirty years old samples of shotcrete (primary lining) and concrete (secondary lining) obtained from different cross-cuts of five highway tunnel sites were conducted to investigate material degradation and strength reduction with the passage of time and any influence from the above mentioned deteriorating processes on the durability and behavior of dual-lining systems. Putting together with shotcrete, the results of inner linings could deliver useful information in adopting optimum design of the combined support system. The authenticity of the assumption of total decadence of shotcrete support with time could not be verified. Some samples of shotcrete had incredibly higher values of UCS, E-modulus; in some cases even higher than concrete. This may partially be attributed to the optimum dry-mix design of shotcrete and partially to the specific geoenvironmental conditions encountered at the sites. Considering the long-time stability and durability of the shotcrete as witnessed, inner lining thickness or reinforcement could be debated. Also implementation of cost effective single shell steel or synthetic fiber reinforced shotcrete shell in areas above watertable could be envisaged as an alternate solution. It is pertinent to mention that the obtained results relate to a particular set of environment over a specific period of time, any generalization of the results would need collection of first hand information of the prevailing conditions on case to case basis.

Chapter 3

Deterioration of Rock bolts

3.1 Steel rock bolts/dowels

Ground control and stability is one of the most important aspects of under ground construction works affecting safety, production and efficiency. Steel rock bolts are the commonly used elements for reinforcement of underground structures in rock and soil, installed separately or in combination with other support elements. The rock bolts reinforce the rock by binding the stratified or broken blocks together through the friction forces generated by physical interlocking at the bolt rock interface. They tend to increase the shear strength or bearing capacity of the rock mass or rock joints by providing confining stresses. Reinforcement of the rock mass by means of rock bolting involve one or more of the following methods: suspension of loosened rock to more competent layers, beam building, formation of internal pressure arch, improved cohesion of material and support of discrete blocks [27], as illustrated in Fig 3.1.

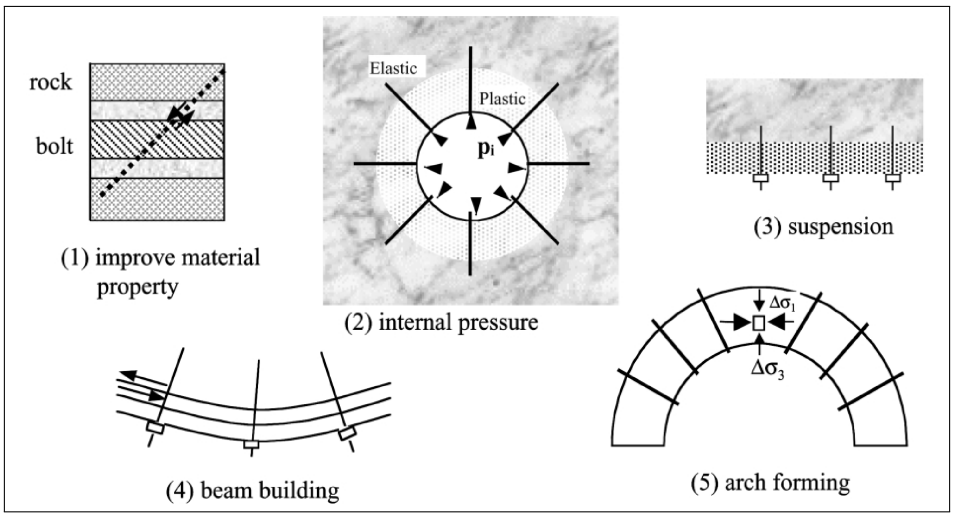

Figure 3.1: Different mechanisms of rock reinforcement by steel rock bolts; [28].

Based on the anchoring mechanism, all conventional rock bolts can be classified into three types; two-point anchored mechanical bolts (e.g. expansion shell and slot and wedge type bolts), fully encapsulated rebar bolts (cement or resin grouted rock bolts), and frictional bolts (e.g. split set and swellex) [29]. New developments in the bolt types

and rock bolting techniques cover the possible range of applications for different ground conditions. Modern rock bolt systems allow projects to be built and maintained at a much lower cost than installing large steel sets or concrete retaining walls [30]. The use of shotcrete together with rock bolts further promotes the application of bolts as a main supporting method.

3.2 Rock bolts degradation

The long-term effectiveness of the rock bolt to perform the intended function for the designed life in a given hydrochemical environment is an important challenge for underground construction. One of the main problems associated with rock bolt decay underground is corrosion. The main reason for this problem is the presence of underground water, humidity and chemical interaction between the surrounding media and the steel. Strong acids are produced by water in contact with sulphur which readily reacts with steel bolts and causes severe damages to the bolt [31]. Low and medium steel bolts have high susceptibility to corrosion once they come in contact with sulphates, chlorides, salts, silicates and bicarbonates. [32]. Rock bolts generally fail in tension. The bolt failure may start with shear movement leading to rock bolt bending, necking and ultimately tensile failure. The combined effect of stress and corrosive environment leads to the progressive development and growth of cracks on the surface of steel rock bolt causing its premature failure. According to [33], stress corrosion cracking failures of rock bolts may occur whenever a rock bolt is subjected to high stresses in the presence of an aggressive environment. There is slow initiation and growth of crack in the beginning which turns into a fast fracture when the stress corrosion crack reaches a critical length, as determined by the applied stress and the fracture toughness of the steel. The critical crack length can be of the order of few millimeters for rock bolts. Subsequently there is a sudden fast fracture across the remaining section of the bolt. The findings of a series of tests on the rock bolts with different metallurgies have shown that stress corrosion cracking only occurred for environmental conditions which produce hydrogen on the sample surface, eventually leading to hydrogen embrittlement and stress corrosion cracking [34]. In particular environment the anchor material is also attacked by aerobic and anaerobic bacteria. This causes biocorrosion by an irregular distribution of bacteria on the metal surface producing varying degrees of aeration. The presence of bacteria also accelerate chemical processes, such as the formation of sulphuric acid from pyrite [35]. The electrochemical corrosion testing of the rock bolts demonstrated that corrosion rate increased with temperature. Severe degradation of rock bolts occurred at $90°C$ due to influence of chlorides and dissolved oxygen [36]. The amounts of alloying elements have strong influence on the corrosion resistance of stainless steel. The presence of metals like chromium, nickel and molybdenum as well as the type of microstructure determine the corrosion resistance. The uniform distribution of alloying elements within the microstructure is required to impart better anticorrosive properties to steel. Irregular distribution, e.g. due to precipitations, result in decreased corrosive resistance [37].

3.3 Testing of degraded rock bolts

3.4 General

Steel rock bolts/dowels from the different cross cuts of Ganzstein, Katschberg, Tanzenberg, Roppener and Bosruck tunnel sites were tested in the ÖGI (Österreichisches Gießereiinstitut), which is under the umbrella of Montan University Leoben. The rock bolt samples served for 30 years at the above mentioned tunnel sites in a highly stressed and corrosive environment. The names and specifications of the samples are summarized in Tab. 3.1. The purpose of testing was to clarify whether the external influences over a time had affected the strength properties, composition and working performance of steel. The exact types of steel were not known and were to be determined as far as possible in succession. From the surface appearance the samples seemed to be in good conditions. Nevertheless the samples suffered from local corrosive attack in addition to anchor sediments and partly massive deformations as shown in Fig. 3.2

Table 3.1: Overview of the rock bolts samples from different tunnels

Reference	Cross-cut	Sample ID
Ganzstein	EQ-01	1
Katschberg	GQ-07	3
Tanzenberg	EQ-02	8
Roppener	ASN-01	9
Bosruck	GQ-06	10

The detailed investigations of the samples included mechanical properties tests to determine tensile strength and hardness, chemical analysis for determination of material composition, metallographic examinations and microstructure analysis to investigate the structure of the steel bolts. In one separate investigation, a comparative study of two samples of steel bolts one representing the old corroded bolt from the Katschberg tunnel and the other one a new sample as a reference as shown in Fig 3.3, were conducted.

3.5 Mechanical properties

3.5.1 Tensile test

Tensile strength of the old Katschberg sample and new steel specimen were determined at room temperature following the DIN 50125 specifications in accordance with ISO 6892-1 standards. Required length of specimen marked for cutting and testing can be seen in Fig 3.4. Tests were conducted to determine the yield stress, tensile stress and behavior of old and new steel bar subjected to axial loading. In another analysis a tensile test was carried out for the degraded samples from the all five sites. The test specimens were subjected to an axial load increased in increments from zero to the point of fracture. The stress and strain were computed at each step and stress-strain curves were plotted.

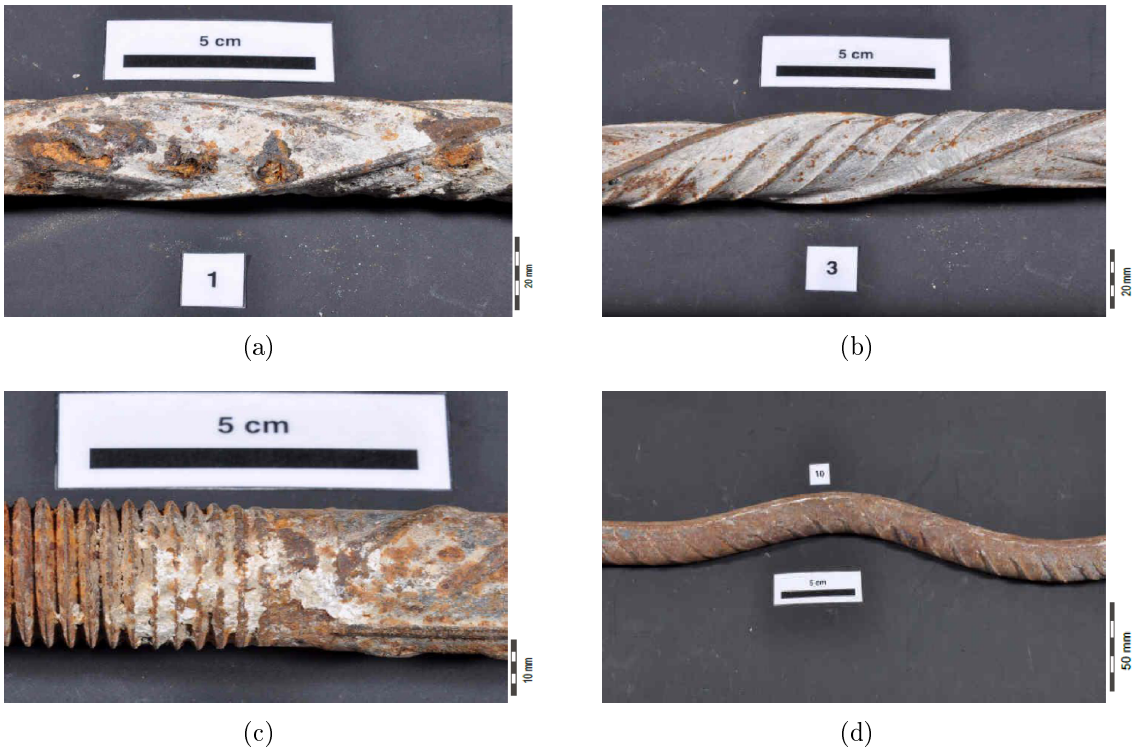

Figure 3.2: General condition of degraded anchors; (a) detail anchor 1 (b) detail anchor 3 (c) detail anchor 8 (d) detail anchor 10; [38]

Figure 3.3: New steel anchor (upper) and old (lower with plate); [39]

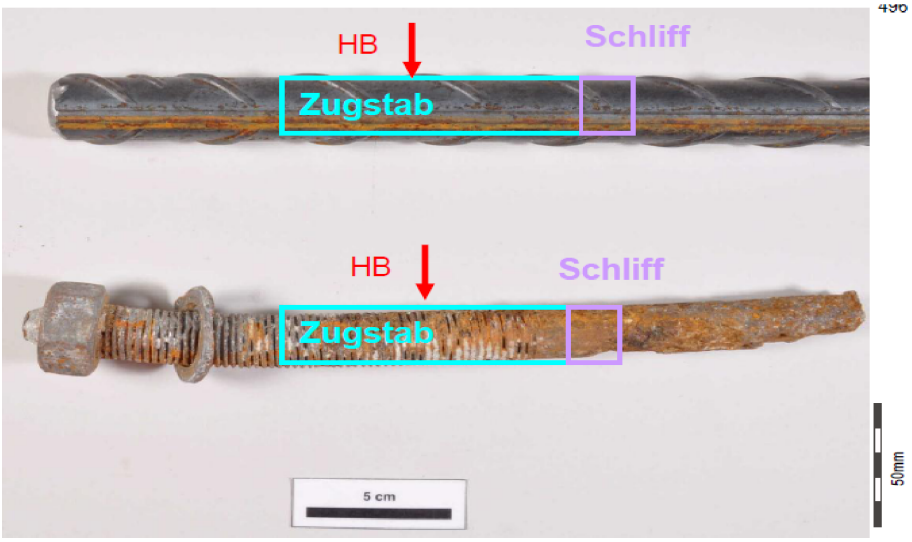

Figure 3.4: Details of sampling for new and old steel anchor; [39]

3.5.2 Hardness measurement

Hardness measurement of the old and new steel anchors was carried out using Brinell hardness test following DIN EN ISO 6506-1 standards. The Brinell test equipment is shown in Fig 3.5. Two sections of each sample one representing transverse and the other longitudinal section were cut from the steel anchors and subjected to testing after milling their edges. The Brinell hardness value of HV 10 was also determined on transverse and longitudinal surfaces (center) of the five tensile specimens according to DIN EN 6507-1.

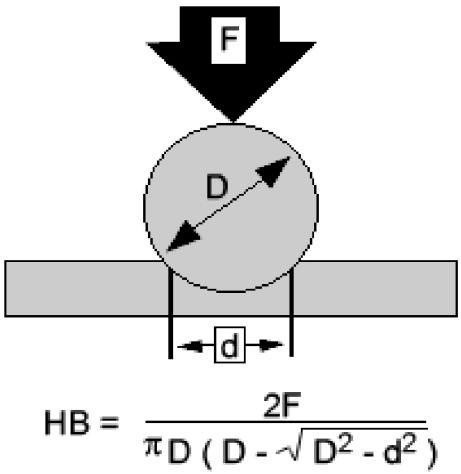

Figure 3.5: Schematic of the principle of the Brinell indenting process; [40]

3.6 Microstructure analysis using metallography and fracture pattern

Microstructure of the old and new steel anchors was studied by taking sample sections in the longitudinal and transverse directions as presented in Fig 3.6. For detailed investigation of the causes of corrosion and its effects at conspicuous areas, metallographic

cross-sections of all five samples were prepared. Microscopic study of the etched samples and fractured surfaces was performed using techniques like scanning electron microscopy and energy dispersive spectrometry (SEM/EDS) at different magnification.

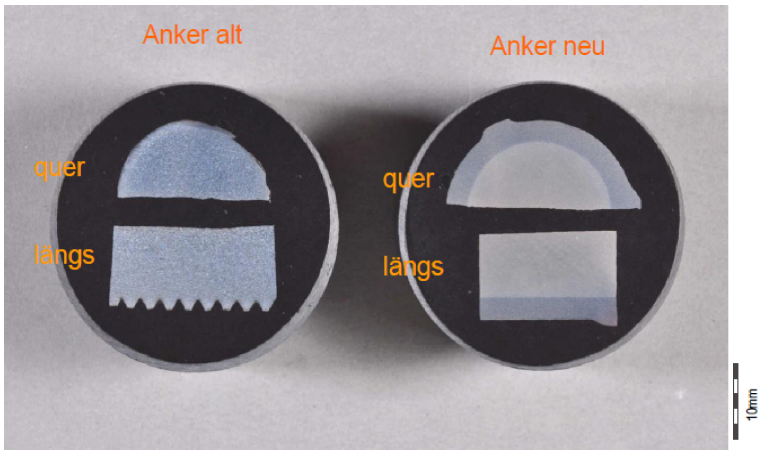

Figure 3.6: Cut view of old and new steel anchors; [39]

3.7 Chemical Analysis

Chemical analysis of the old and new steel anchor was conducted to determine the chemical composition and quantitative analysis of the constituent elements in the sample material.

3.8 Results and discussion

3.8.1 Tensile test

The stress-strain curve for the old and new steel anchor is shown in Fig 3.7, and the derived parameters yield stress Rp, ultimate stress Rm, failure strain A, and area reduction Z are given in Tab. 3.2.

Table 3.2: Results of tensile test for old and new steel anchor

Sample	d0 [mm]	Rp 0.2% [MPa]	Rm [MPa]	A [%]	Z [%]
Old-anchor	9.981	443	811	18.3	41
New-anchor	11.941	549	751	20.7	54

The strength characteristics were very similar on a first glance. The old anchor had a higher ultimate tensile strength but considerably lower yield strength than the new steel quality and lies in the 0.2% proof stress significantly lower than new anchor. This is due to the unfavorable ferrite grain boundary of the old anchor. The higher yield strength of new steel could be attributed to the induction of additional fine coating structure described

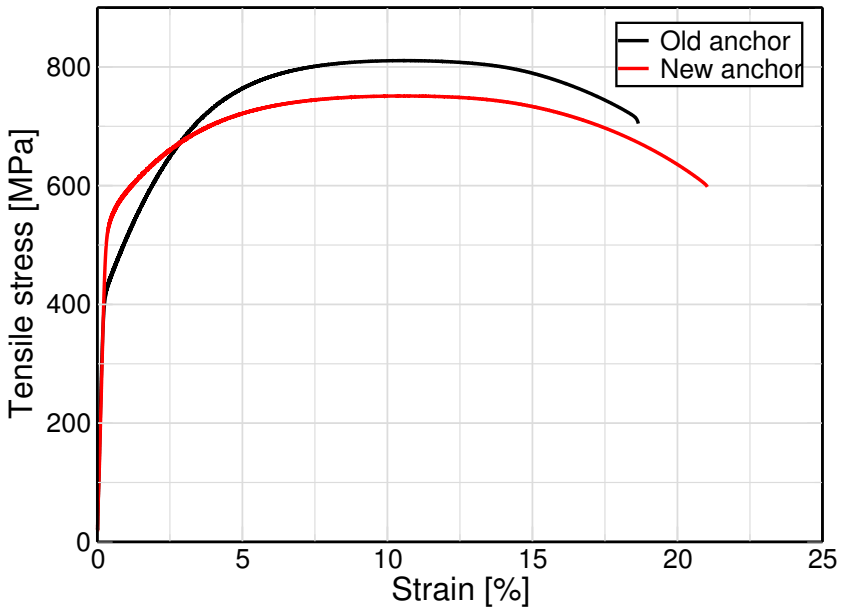

Figure 3.7: Stress-strain curve for the old and new steel anchor; [39]

in 3.8.3. The stress-strain curves for the five steel anchors are illustrated in Fig 3.8, and the derived parameters are listed in Tab. 3.3. The observations of the significantly higher hardness values HV10 for the anchor 9 is also confirmed in the tensile test. Anchor 9 shows differently high tensile strength. Furthermore, the anchor 1 and 3 and 8 and 10 to such an extent exhibit similar characteristics, that it likely involved identical types of steel in each sample. Whether the observed upper yield strength (ReH) for sample 8 is attributed to the respective steel specification or it is already part of the history due to changes, without accurate presence it may not clarify the steel specification.

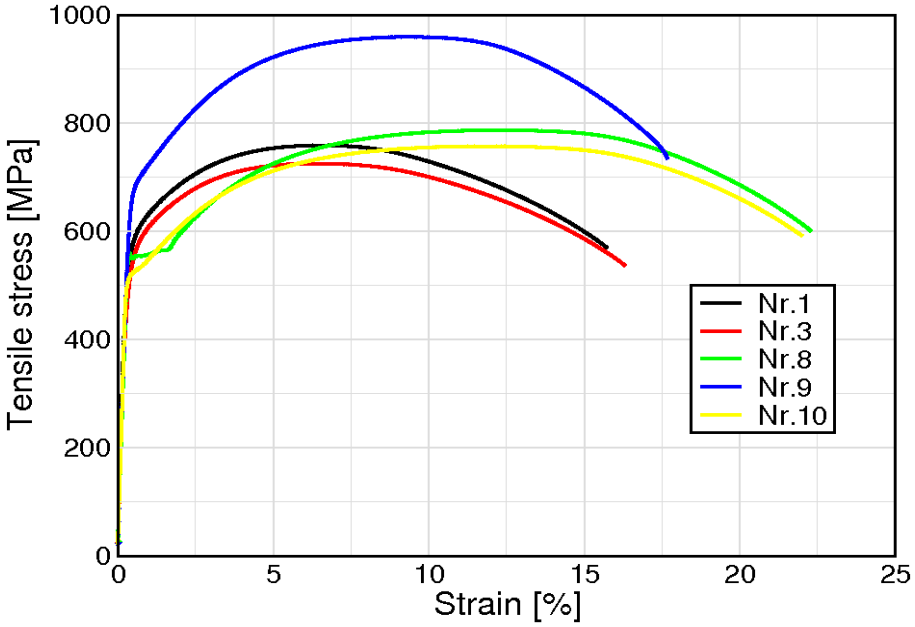

Figure 3.8: Stress-strain curves of the five tested anchors; [38]

Table 3.3: Results of tensile tests

Sample	ReH [MPa]	Rp 0.2% [MPa]	Rm [MPa]	A [%]	Z [%]
1		572	759	15.5	52
3		535	726	16.1	54
8	561	550	757	22.0	54
9		673	960	17.3	47
10		523	758	21.7	52

3.8.2 Hardness measurement

The results obtained from the old Katschberg sample and new reference sample are listed in Tab. 3.4. The hardness value is higher for the new steel anchor with a HB 290, than that of the old steel with a HB 242. This is due to the induction of supplementary coating material to new steel anchor. The higher HB values impart better elongation properties to steel. The Vicker hardness values for the outside and inside of the new steel anchor obtained from the pyramid indenter of diamond are given in Tab. 3.5. Hardness values determined for the five samples are presented in Tab. 3.6. All transverse and longitudinal impressions show relatively uniform values within the measurement inaccuracies. The values of anchor 9 are significantly increased, so this is likely to be a different type of steel or heat treatment.

Table 3.4: Brinell hardness values for the steel samples

Sample name	HBW10/3000			
	Value 1	Value 2	Value 3	Middle value
Steel anchors-old	244	243	239	242
Steel anchor-new	284	292	295	290

Table 3.5: Vicker hardness values for the new steel samples

Sample name	HV 50			
	Value 1	Value 2	Value 3	Mean value
New steel anchor-outside	340	341	339	340
New steel anchor-inside	235	238	243	239

Table 3.6: Brinell hardness values for the degraded steel samples

Sample name		HV 10			
		Value 1	Value 2	Value 3	Middle value
1	Longitudinal	234	191	226	217
	Transverse	233	196	236	222
3	Longitudinal	234	211	214	220
	Transverse	216	219	231	222
8	Longitudinal	227	226	216	223
	Transverse	219	226	228	224
9	Longitudinal	282	276	272	277
	Transverse	273	285	275	278
10	Longitudinal	213	246	214	224
	Transverse	230	233	216	226

3.8.3 Microstructure analysis using metallography and fracture pattern

Macro overview of the old rock bolts show a uniform structure of the entire cross section, while new bolts have a surface layer coating (dark stripes on the outer edge). The microstructure of the new steel anchor for the middle and outer sections are illustrated in Fig 3.9(a) and Fig 3.9(b) respectively. The microstructure consists of a continuous fine coating structure at the middle, with an additional inductive coating at the outer edge. The microstructure of the old steel anchor is depicted in Fig 3.9(c) and Fig 3.9(d). It shows a continuous uniform pearlitic structure with ferritic grain boundary. The micro structure composition has also shown the presence of sulfide rods in the old and new steel anchors. The distribution of the investigated sulfide in the steel anchors in longitudinal direction is illustrated in figure Fig 3.9(e) and Fig 3.9(f). For the old five anchors the overview pictures in stereo microscopic observation confirmed the observations from the continued strength measurements. Samples 1, 3, 8 and 10 show a nearly homogeneous fracture pattern in the plate-cup scheme, see Fig 3.10(a), Fig 3.10(b), Fig 3.10(c), and Fig 3.10(e). The fracture surfaces show slight differences between these two pairings. The fracture pattern of the test-9 also reflects the higher-strength behavior, see Fig 3.10(d). Metallographic overview at low magnification images shows the basic ferritic-pearlitic structure. While sample 1 and 3 again show a relatively coarse primary structure, see cross-sectional views in Fig 3.11(a) and Fig 3.11(b), the basic structure of the samples 8 and 10 is much finer, compare Fig 3.11(c) and Fig 3.11(e). This is already confirmed from the observed higher tensile strength coupled with higher elongation. Qualitatively distinct ferritic border zones can be detected in sample 3 and 10 (Fig 3.11(b) and Fig 3.11(e)). Sample 9, Fig 3.11(d), stands out again, because here is change from the ferritic-pearlitic basic structure to significantly higher pearlite. Thus here is already confirmed that it is a type of steel with correspondingly higher carbon content. Longitudinal sections of the samples show in addition to the basic crystalline structures, non-metallic inclusions such as manganese sulfides (only at high magnifications clearly visible).

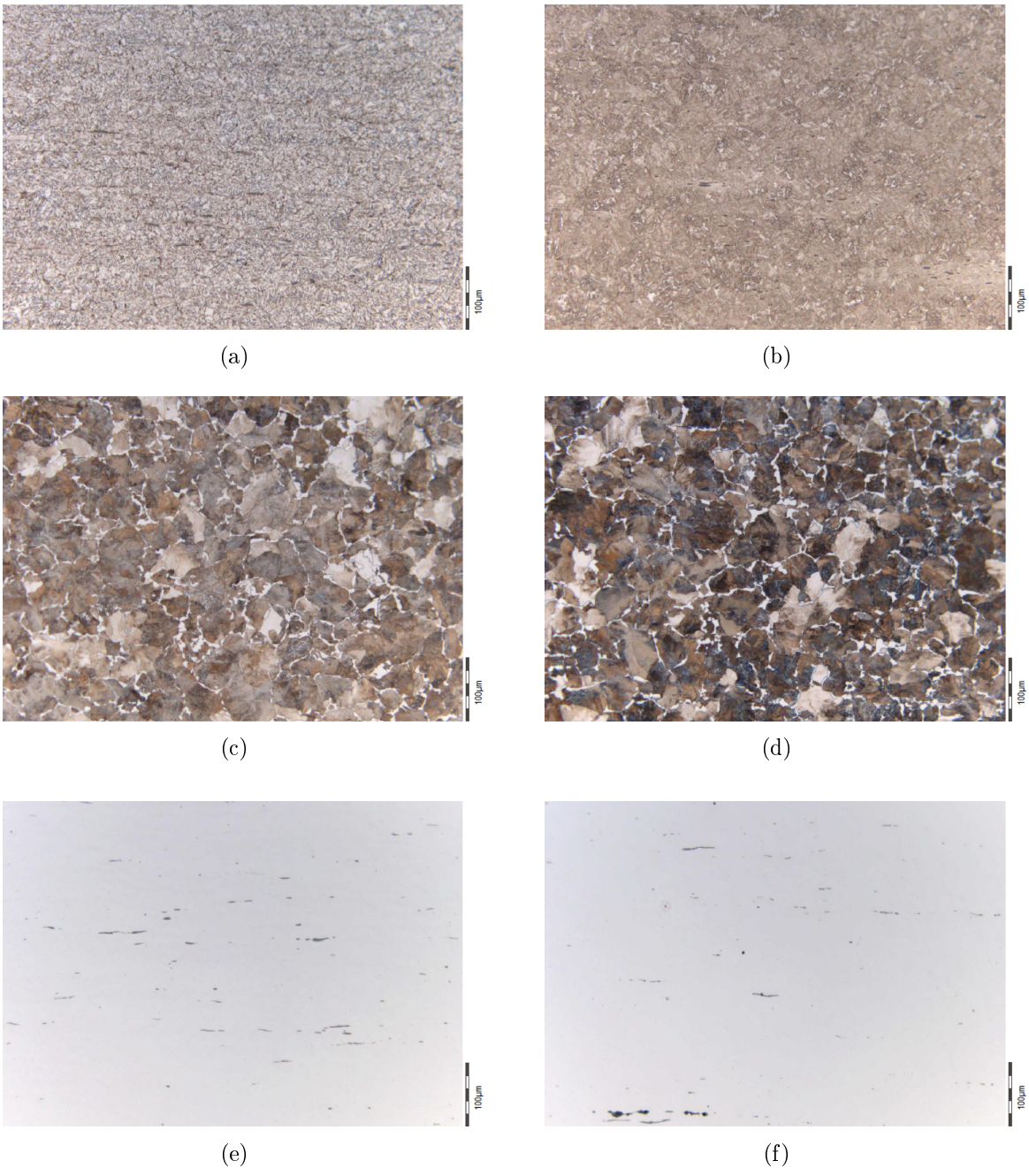

Figure 3.9: Microstructure of steel anchors; (a) coating structure at the middle section of a new steel anchor (b) coating structure at the outer section of a new steel anchor (c) Transverse section of the old steel anchor showing pearlitic structure with ferrite grain boundary (d) Longitudinal section of the old steel anchor showing pearlitic structure with ferrite grain boundary (e) sulfide grains distribution in the new steel anchor (f) sulfide grains distribution in the old steel anchor; [39]

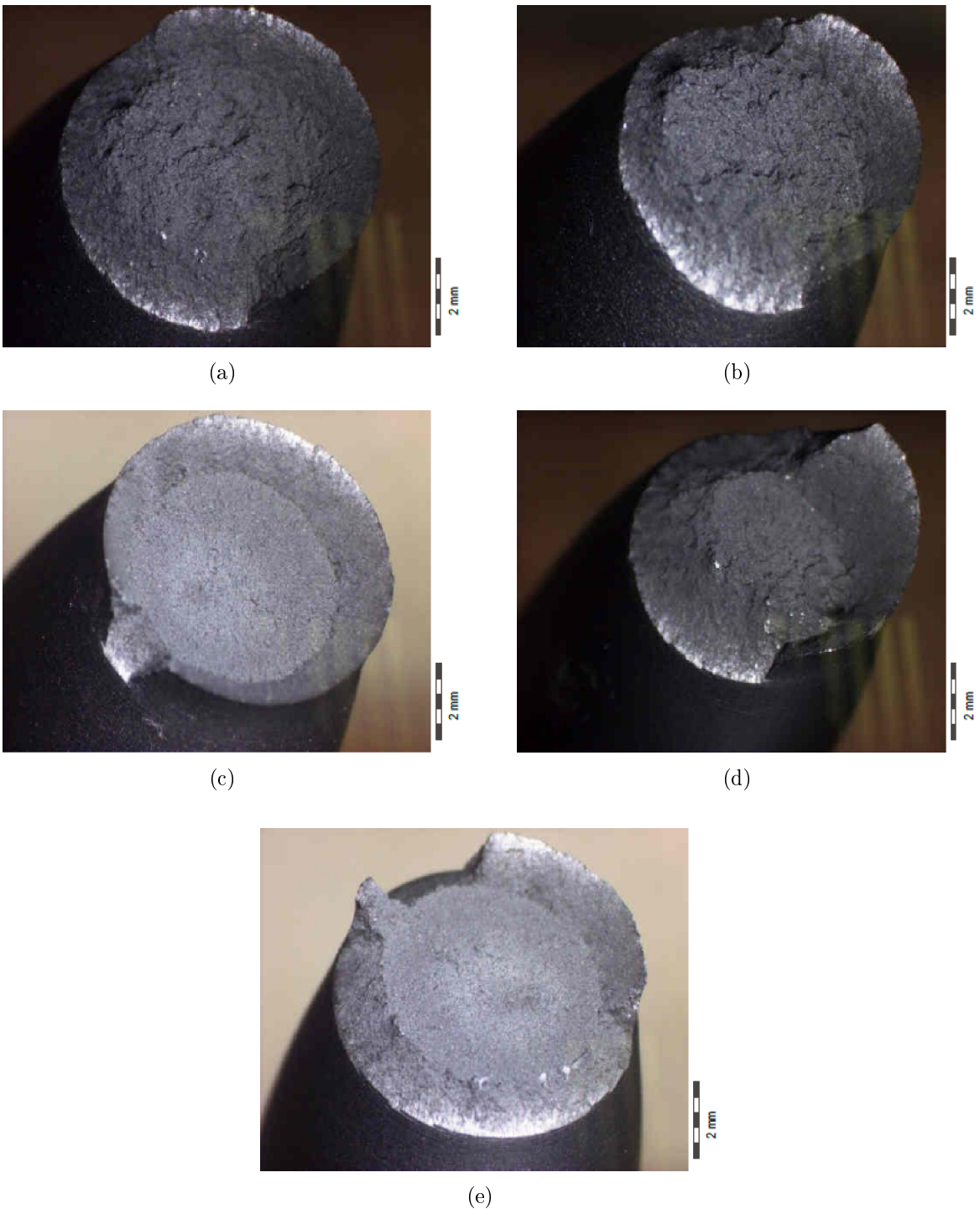

(a) (b) (c) (d) (e)

Figure 3.10: (a) overview of the fracture surface sample 1 in stereomicroscope, 11× (b) overview of the fracture surface sample 3 in stereomicroscope, 11× (c) overview of the fracture surface sample 8 in stereomicroscope, 11× (d) overview of the fracture surface sample 9 in stereomicroscope, 11× (e) overview of the fracture surface sample 10 in stereomicroscope, 11×; [38]

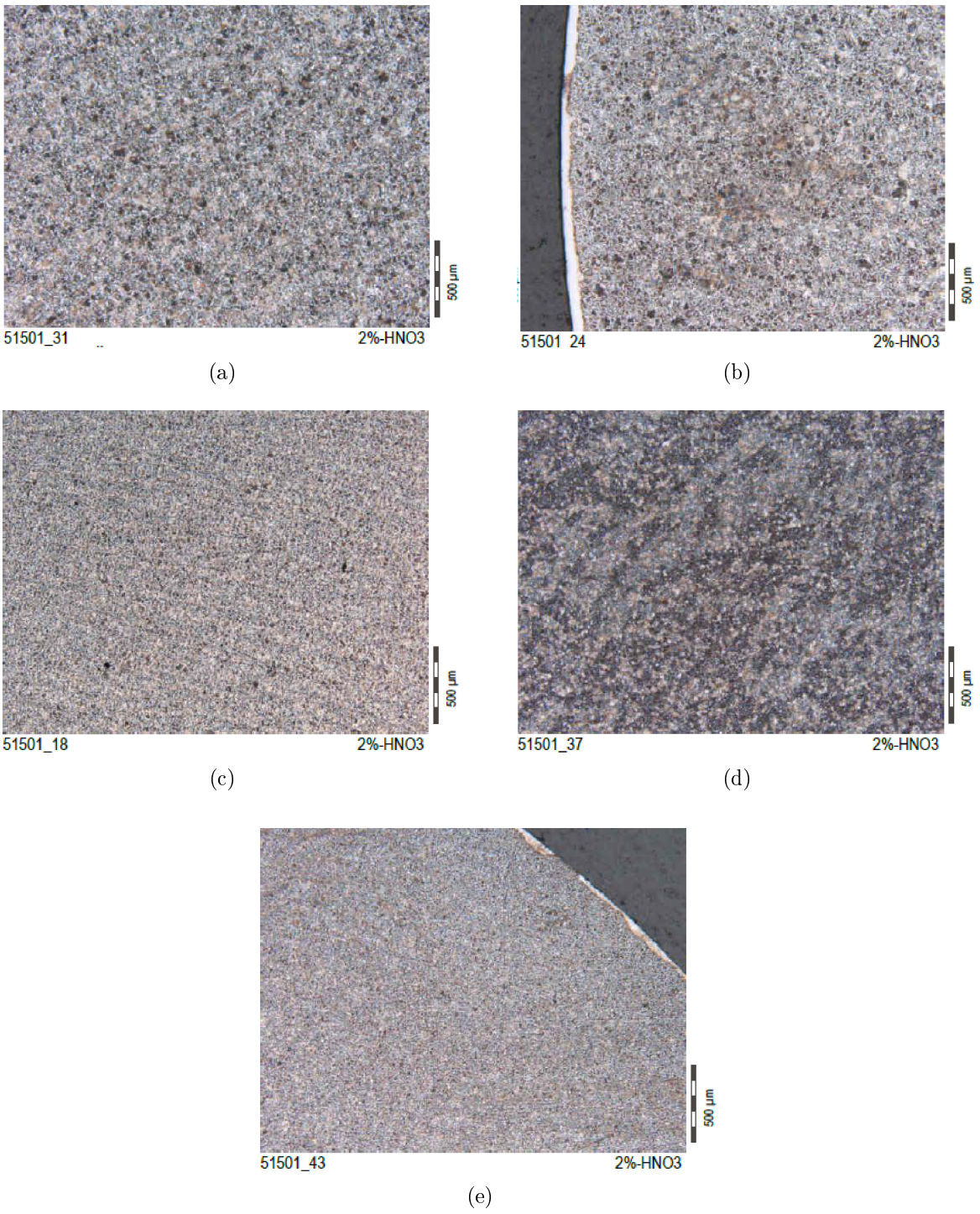

Figure 3.11: (a) Cross-sectional overview of an etched sample 1 centre, 50× (b) Cross-sectional overview of an etched sample 3 boundary area, 50× (c) Cross-sectional overview of an etched sample 8 centre, 50× (d) Cross-sectional overview of an etched sample 9 centre, 50× (e) Cross-sectional overview of an etched sample 10 boundary area, 50×; [38]

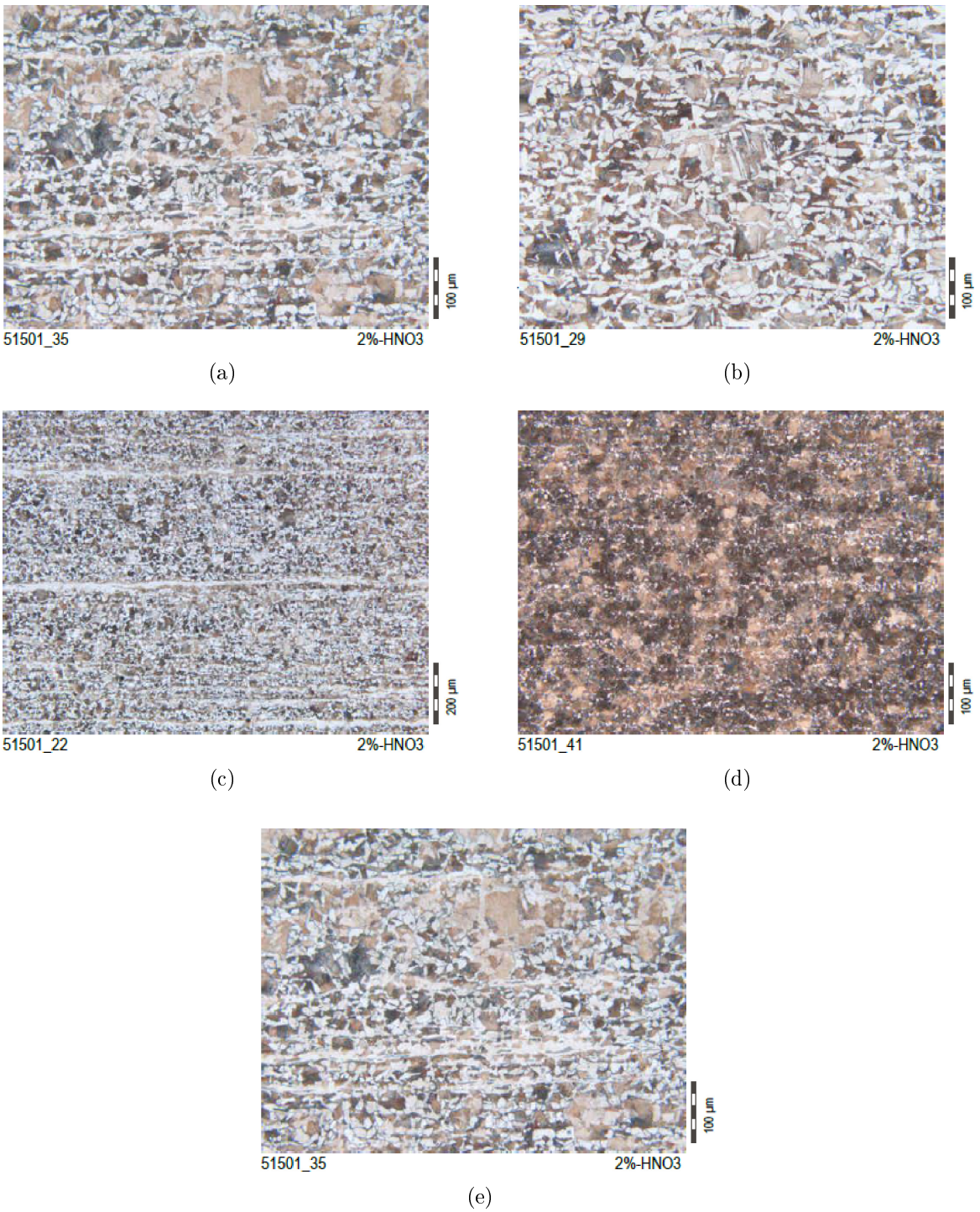

Figure 3.12: (a) Detail of the longitudinal section of an etched sample 1 centre, 200× (b) Detail of the longitudinal section of an etched sample 3 centre, 200× (c) Detail of the longitudinal section of an etched sample 8 centre, 200× (d) Detail of the longitudinal section of an etched sample 9 centre, 200× (e) Detail of the longitudinal section of an etched sample 8 centre, 200×; [38]

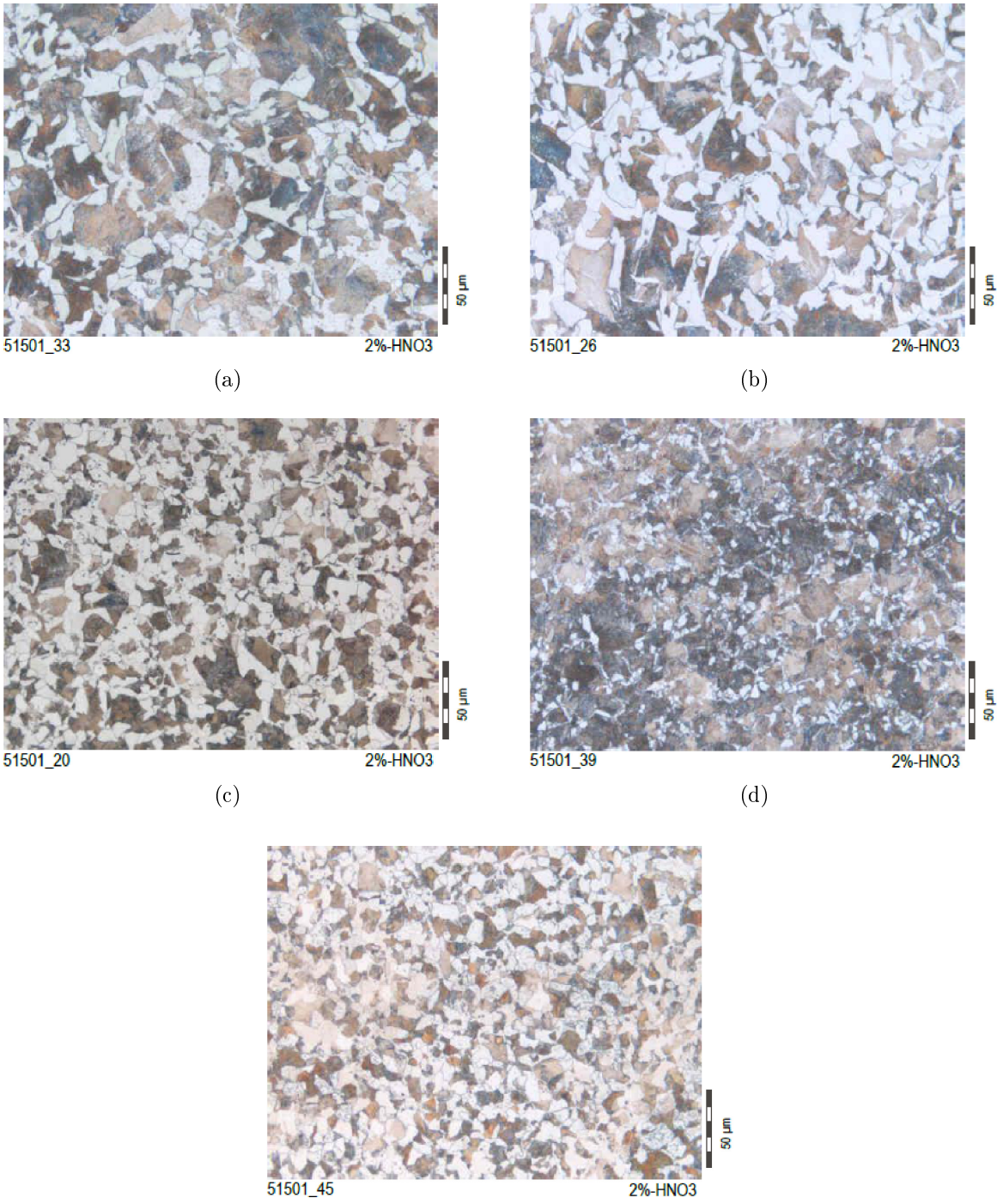

Figure 3.13: (a) Cross-sectional overview of an etched sample 1 centre, 500× (b) Cross-sectional overview of an etched sample 3 boundary area, 500× (c) Cross-sectional overview of an etched sample 8 centre, 500× (d) Cross-sectional overview of an etched sample 9 centre, 500× (e) Cross-sectional overview of an etched sample 10 boundary area, 500×; [38]

These are well developed with the exception of anchor 9 according to the available steel quality, compare Fig 3.12(a),(b),(c),(d),(e). Exemplary detailed pictures of the cross sections at high magnification underline the summary observations now more apparent. Samples 1 and 3 show a relatively coarse ferritic-pearlitic structure with estimated about 0.3-0.5% C, see Fig 3.13(a) and Fig 3.13(b). Samples 8 and 10 show a slightly higher proportion of ferrite and thus approximately 0.2-0.4% C, but at a much smaller grain sizes, see Fig 3.13(c) and Fig 3.13(e). Sample 9 shows a higher pearlite content in accordance with the estimated C content of the steel grade of approximately 0.6-0.8%, compare Fig 3.13(d). An exact assignment of grades alone from the tensile characteristics and structures is not possible. For this purpose a detailed chemical analysis was carried out. Because of the observed strength and hardness values as well as investigations of the structure, it is not currently expected that the samples were significantly affected by the external corrosive attacks. Detailed statements are not possible without exact knowledge of the used steel.

3.8.4 Chemical Analysis

Chemical analysis of the old and new steel anchor was conducted to determine the chemical composition of the sample material. These results are comparable to the results of a similar analysis conducted for determination of the chemical composition and metallurgies of the rock bolts as presented in Tab. 3.7 [33, 34]. Steel 10M30 represented old rock bolt grade. The chemical analysis results for the old Katschberg sample and new rock bolt sample are presented in Tab. 3.8. The analysis demonstrated that the old anchor consisted of pure, unalloyed carbon steel with 0.55% C. The strength was generated by almost fully pearlitic structure. The carbon content and tensile strength were in accordance with the type of steel C55, Material no. 1. 1203. The new steel anchor consisted of low-alloy carbon steel with 0.23% C, 1.31% Mn, 0.55% Cu, and tenth% share of Cr and Ni. These alloy components from the rolling heat lead to the formation of a coating structure. The composition is similar to 20Mn6, material no. 1. 1170. In the present case, the edge region has been firmed in terms of strength by an additional inductive coating process. The comparison of old and new steel anchors pointed to a fundamental difference in the chemical composition which led to subsequent variations in mechanical properties.

Table 3.7: Chemical composition of the commercial rock bolt steels (wt%)

Grade		C	Si	Mn	P	S	Ni	Cr	Mo	Al	V
1355	A	0.54	0.26	1.63	0.017	0.027	0.08	0.08	0.03	0.004	0.003
MA840B	B	0.37	1.05	1.46	0.013	0.009	0.01	0.02	0.01	0.004	0.043
MA810		0.36	1.00	1.40	0.021	0.013	0.01	0.02	0.01	0.005	0.040
MAC	C	0.25	0.36	1.32	0.016	0.027	0.07	0.05	0.01	0.005	0.210
10M30	AH	0.29	0.24	0.72	0.015	0.026	0.14	0.11	0.03	-	0.053
5152	D	0.54	0.10	0.90	0.015	0.025	0.35	0.90	0.10	-	-

Table 3.8: Percentage composition of constituent minerals in old and new steel anchors

Component	Steel anchors/Rock bolts	
	old	new
% C	0.55	0.23
% Si	0.34	0.34
% Mn	0.89	1.31
% P	0.013	0.013
% S	0.020	0.050
% Cr	0.04	0.14
% Ni	0.03	0.18
% Cu	0.07	0.55

3.9 Summary and conclusions

Five rock bolt samples one each from Ganzstein, Katschberg, Tanzenberg, Roppener and Bosruck tunnel sites were examined for their strength and integrity after being in service for about 30 years in the above mentioned tunnels. One set of additional investigations were conducted by comparing an old rock bolt from the Katschberg tunnel with a new reference steel sample. Although at the bolt surfaces local corrosive attacks could be observed, based on the acquired strength and hardness as well as the structural examinations it did not appear that the samples were significantly influenced by this corrosive attacks. It is very difficult to give detailed statements, however, without precise knowledge of the types of steel used and the respective manufacturing specifications. From the characteristic values and crystallized structures it is clear that the five bolts used had at least three different ferritic-pearlitic steel in structural steel design quality. The old bolts had a higher ultimate tensile strength but considerably lower yield strength than the new steel due to unfavorable ferrite grain boundary. The higher yield strength of new steel could be attributed to the induction of additional fine coating structure which was also corroborated in the hardness test. An exact classification of steel composition alone from the tensile characteristics and structures was not possible. For this purpose a detailed chemical analysis of the Katschberg sample and reference steel bolt was carried out which pointed to some fundamental differences in the constituent minerals of the two steel types. In general it could be concluded that under the given environmental circumstances the steel bolts performed satisfactorily and appeared to be in fairly good conditions after long period of service. The corrosive effects on the steel bolt 1 indicated the presence of water in the Ganzstein tunnel. The deformation of steel bolt 10 represented the localized shearing of the strata in Bosruck tunnel. Had the two phenomena transpired together at any cross cut, it might have resulted in stress corrosion cracking failure of the bolt. Use of corrosion resistant steel or subsequent measures to protect anchors for example grouting of epoxy coated bolts etc. could help in prolonging the service life of the steel bolts.

Chapter 4

Deterioration of Geomembrane

4.1 Introduction to Geomembrane

A geomembrane is defined as a very low permeability synthetic or reinforced bituminous sheet placed in contact with soil or concrete. They are extensively used in transportation application (tunnel), environmental applications (landfills and reservoirs) and geotechnical applications (dams) in substitution or in addition to compacted clay, concrete, steel and bituminous material [41]. They are used to contain or restrain gas and liquids movements. Geomembranes are manufactured in industrial plants and are shipped on site in rolls. The sheets are bonded together using welding or adhesive techniniques.
Geotextiles are permeable polymeric materials either woven or non-woven. Geotextiles help in the stabilization of structure by avoiding the concentration of applied loads at any single point of the soft substrate, filter subsurface water to flow into drains and mechanically protect geomembrane against abrasion and puncture.
Geomembranes are often used as a part of barrier system for modern landfills [42]. There are various types of geomembranes including polyvinyl chloride (PVC), polypropylene (PP), linear low-density polyethylene (LLDPE), medium-density polyethylene (MDPE), high density polyethylene (HDPE). In general, HDPE geomembranes consist of 96-97.5% of polyethylene resin, 2-3% of carbon black and 0.5-1.0% of other additives such as antioxidants and stabilizers. The density of finished geomembrane is defined as $\geq 0.940 g/cm^3$ for HDPE and $\leq 0.939 g/cm^3$ for LLDPE [43]. The distinguishing difference between HDPE and LLDPE geomembranes is the additional tensile elongation and puncture strength per unit area. LLDPE generally have 50% greater elongation properties with equivalent puncture strength per unit area in comparison to HDPE. For such reasons LLDPE is the best option for use in projects with the possibility to be subjected to high loads and differential settlements and deformations over time. The PVC geomembrane is one of the earliest geomembranes. Typical constituent of PVC (polyvinyl chloride) are 35% resin, 30-40% plasticizer, 25% filler, 5-10% pigments, 2-3% additives.

4.2 Geomembranes applications

Both geomembrane and geotextile are increasingly used in the environmental, geotechnical, and mining related areas. In some special applications the synthetic materials are required to perform services in environments exposed to extreme heat and ultra violet

(UV) radiations together with high mechanical loading and exposure to aggressive solutions and slurries [44]. Geosynthetic liners such as landfill caps are expected to have sufficient durability since they are intended to become permanent features of the landscape. Mining industry make extensive use of geomembranes in heap leach pads, solution ponds and evaporation ponds. According to [45] the other most common applications of geomembranes are their universal usage in landfill for solid and liquid municipal waste, industrial waste, discarded material from the construction and demolition as well as its applications in concrete protection work for concrete pipes, sever lines, waste water facilities, tunnels and manholes. Geomembranes are widely used in tunnel waterproofing against the aggressive attack of ground water. They are placed between the outer primary lining and permanent inner lining to prevent any seepage of water causing structural damage to inner lining. They are also used extensively in making structures for liquid containment like dams, canal lining, water and waste water storages, petro-chemicals etc. The selection of a particular geomembrane material is generally based on the overall performance and competence with respect to weathering resistance, chemical resistance, mechanical properties (elastic modulus, yield strength, puncture and tear resistance), UV resistance etc.

4.3 Properties of Geomembranes

The properties of geomembranes can be subdivided into physical, mechanical and endurance properties. The physical material properties of geomembranes include geomembrane thickness, density, water vapour transmission, and melt flow index.
The mechanical properties of polymers are controlled by the elastic parameters; the three moduli and the Poisson's ratio. Polymers are no purely elastic materials but are viscoelastic. They exhibit time and temperature dependence [46]. Mechanical properties of geomembranes play fundamental role in their applications as structural materials. Mechanical behavior involves the deformation of material under the influence of applied forces.
The thermal, chemical and biological properties can be categorized under the umbrella of endurance properties. These material properties explain how well the geomembrane liner will perform its intended function over a period of time. The geomembrane after installation will be subjected to the influence of different harmful agents under varied conditions. These agents can be such things as ultra violet (UV) rays from the sun, which break down the compounds in the geomembrane causing severe polymer damage. This is caused by short wavelength of UV light. The polymers should also confront chemicals and leachates. Hot and cold temperatures can also affect the mechanical and physical properties of geomembrane liners. In extreme cold environment the geomembranes become less flexible. The properties of polymeric geomembranes are governed by their polymer structure, molecular weight (i.e. the length of the chains) and the crystallinity [47]. The molecular weight of the polymer significantly affects the physical properties such as tensile strength, impact and rupture resistance, flexibility and long-term durability of the material under diverse conditions.

4.4 Aging and degradation of geomembranes

The designed life of a geomembrane will generally depend on the exposure conditions in which it has to serve. A well designed and installed intact geomembrane liner may suffer from some level of deterioration or aging with the passage of time that will lead eventually to its failure. The aging process of HDPE geomembranes can be considered as a combination of physical aging and chemical aging [42]. A geomembrane may be subjected to different types of degradations under the influence of different factors. The environmental exposure of a geomembrane can cause degradation mechanisms involving swelling, biological degradation, oxidative degradation and migration of plasticizer, UV degradation [48]. Liquid adsorption by geomembrane causes degradation by swelling resulting in change in physical and mechanical properties. Biological degradation attacks plasticizer and additives in the polymer and arises from the polymer being attacked by micro organism. PVC geomembranes due to their higher plasticizer content are more susceptible and conveniently affected by this type of degradation. Large scale degradation of geomembranes occurs due to the action of oxygen with the free radical present in the polymer resulting in chain breakage. UV degradation by the sensitive wavelengths causes bond scission in the polymer structure and free radicals are formed. The consequences of long term exposure include discolouration, surface cracks, and brittleness of the geomembrane. The UV degradation studies by [49] has shown that the HDPE geomembrane demonstrated more ductile behavior than fresh samples and the white HDPE were more resistant to the UV effects. The test results of a study conducted by [50] on unaged and about 30 years old HDPE geomembranes samples subjected to different environment demonstrated no significant changes in tensile properties, density, water adsorption properties and water extractable matter. After 15.5 years of service, only the impact resistance changed and reduced to half of its original value. The results of physical index tests (yield, elongation, tear and break properties) of samples of polyethylene liners in exposed and submerged conditions for 16 years by [51] showed a stiffning of geomembrane with time and a related decrease in elongation at break, but the effect was less assertive under unexposed conditions. The physical/mechanical damages of the geomembrane were more prominent than weathering/aging effects.

4.5 PVC geomembrane

Polyvinylchloride (PVC) is an amorphous thermoplastic material with a wide field of application. Unplasticized PVC (PVC-U) has hard and brittle characteristics and is typically used to produce pipes and profiles. An important characteristic of PVC polymers is the K value by Fikentscher [52] which characterizes the average molecular weight. Most commercial PVC polymers have K values within the range of 40 to 80 [53, 54]. Another important parameter for thermoplastic materials is the glass transition temperature T_{g} which describes the significant change of a hard and stiff (energy-elastic) material behavior to a more tough and soft one (entropy-elastic). This temperature is not a sharp point but more a region across some decades of temperature. For PVC-U the glass transition is at $T_{\mathrm{g}} = 80°C$. With the addition of plasticizers a modification of mechanical and thermomechanical properties is possible. With increasing content of plasticizers, which could be higher than 50%, the stiffness and the glass transition temperature can be reduced significantly [53, 55]. Typical plasticizers for PVC polymers are phthalate, and

di-(2 ethylhexyl) phthalate (DOP) is a frequently used representative of this group. The resistance against thermal degradation of PVC can be characterized by the temperature of dehydrochlorination (DHC). This temperature does not only depend on stabilizer systems and additives like plasticizers but also on premature stabilizer consumption. Typically published temperatures for DHC are in the range of 150 to 250°C [56, 57].

4.6 Investigation of used PVC geomembrane

Polyvinylchloride (PVC) is an amorphous thermoplastic material with a wide field of application.Geomembranes of plasticized polyvinyl chloride (PVC), which were in use for tunnel sealing over several years, were investigated in terms of their mechanical condition. Of particular interest was a possible aging of the material. Two samples from different cross-cuts within a tunnel site were selected. There were in total ten samples from five different tunnel sites available for testing. The names and specifications of the samples are summarized in the Tab. (4.1). Small strips of suitable size were cut from the individual sample for investigation.

Table 4.1: Summary of the investigated geomembranes.

Tunnel	Sample	Cross-cut
Tanzenberg	T8_EQ03_06	EQ03
	T8_EQ04_06	EQ04
Ganzstein	T1_EQ01_05	EQ01
	T1_EQ02_10	EQ02
Katschberg	T3_GQ12_01	GQ12
	T3_GQ14_01	GQ14
Roppener	T9_ASN5_01	ASN5
	T9_ASN7_01	ASN7
Bosruck	T10_GQ01_07	GQ01
	T10_GQ06_06	GQ01

Dimensional control:
Five strips of 50 mm × 10 mm dimensions were cut from each geomembrane, while areas with surface defects were preferred. The film thickness, t, was measured with a commercially available caliper. The irregularities in the film thickness were selectively measured. The total $n = 25$ individual measurements per geomembrane were calculated. The maximum film thickness $t_{\max}$, the minimum film thickness $t_{\min}$, the mean film thickness t_{x} and the standard deviation of the mean film thickness σt_{x} were evaluated.

Microscopy study:
Scanning electron microscopy (SEM) was conducted for selected specimens using a device of type Zeiss DSM 962 (Oberkochen, Germany). Specimens with 10 mm × 10 mm dimensions were cut with scissor before sputtered with a 15 to 20 nm thick gold layer.

Monotonic tensile test:
The determination of Young's modulus E, break stress σb, and tensile strain εb, were

based on DIN 527 using monotonous tensile test at room temperature. All tests were performed with strain rates of 1 mm/min (E) and 50 mm/min (all other parameters) on a standard tensile testing machine type Z010 (Zwick GmbH & Co. KG, Ulm, D). The deformations of the specimens were recorded with the associated test system of macro extensometer. The specimen fabrication was performed with a standard cutting die for tensile specimens. Seven individual measurements of each geomembrane were performed and the respective mean values, and standard deviations evaluated.

Thermal analysis:
The determination of the resistance of the geomembrane against dehydrochlorination (DHC) was performed on a differential scanning calorimetry (DSC) according to DIN 11 357 with a device of type DSC822 (Mettler Toledo GmbH, Schwerzenbach, CH). All tests started at a temperature of $23°C$ with a heating rate of 20 K/min under nitrogen atmosphere and were stopped manually at the onset of DHC. Recording of DHC-temperature marked the onset of material degradation. Due to the fact that low scattering orders NC.10.043 were measured from each geomembrane only one sample with a suitable punching iron with a diameter of about 5 mm was punched out.

Infrared spectroscopy:
For the analysis of chemical structure an infrared (IR) spectroscopy with a device type from the spectrum of GX (Perkin Elmer, Überlingen, Germany) was performed using the method of attenuated total reflection (ATR). The films were introduced by hand into the measuring unit. The evaluation of the IR spectograms (transmission as a function of wave number v) was accomplished.

4.7 Description of additional tests of Katschberg sample

An exhumed geomembrane made of polyvinylchloride (PVC) was characterized in terms of physical or chemical aging. The geomembrane was in service for approximately 30 years at the Katschberg tunnel. Chemical, mechanical and thermomechanical material properties of the old geomembrane were compared to a virgin geomembrane made of state-of-the-art PVC. Two sheets of PVC geomembranes, the old one from the Katschberg tunnel (old geomembrane) and a new one as a reference (new geomembrane), were prepared for testing as shown in Fig. 4.1. For both materials no datasheets with detailed information about mechanical or chemical properties were available.

The old geomembrane with a thickness of about 1.5 mm appears homogenous with yellow color. Several mechanical damages were observed which obviously occurred during the service or more likely during exhumation of the sheet. The new geomembrane with a thickness of about 2 mm consists of two layers, one turquoise and the other black. The K value was determined by viscosity measurements according to the standards in DIN EN ISO 1628-1:1998 and DIN EN ISO 1628-2:1999. The dilution of both materials contained insoluble components and especially in the old geomembrane jellied particles were detected which must be filtered with a 0.2 μm Teflon membrane, which is in contrast to DIN EN ISO 1628-2. Chromatography was carried out on the Thermo Electron LCQ Advantage MAX system equipped with vacuum degasser, quaternary pump, auto sampler (20 μL sample loop), and UV-vis diode array detector (all from Thermo Electron

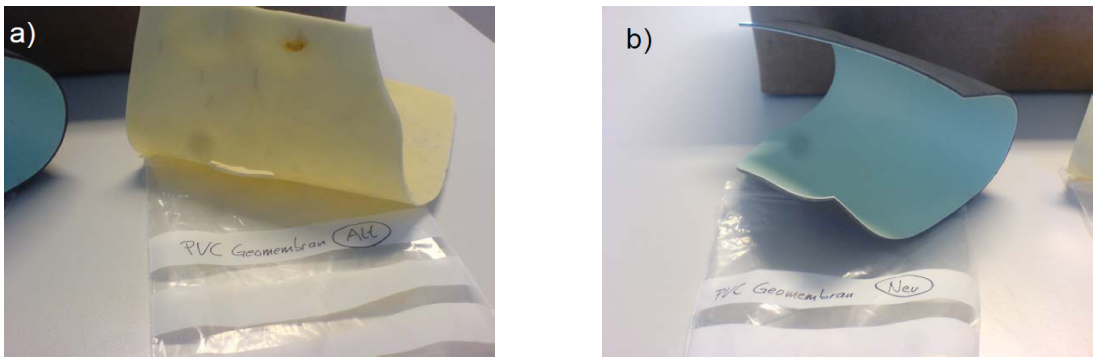

(a) (b)

Figure 4.1: (a) sample of old geomembrane (b) sample of new geomembrane; [58]

Corporation, Waltham, MA, USA). MS detection was performed on the Thermo Electron LCQ Advantage MAX LCMS/MS Ion Trap mass spectrometer equipped with an ESI (electro spray ionization) source. The separation column was a Hypersil Gold C18 (150 mm × 2.1 mm ID, 3 μm particle size) obtained from Thermo Electron.
– ESI Probe,
– Surveyor MS Pump Plus
– Surveyor Auto sampler Plus
– Surveyor PDA Detector
Following settings and parameters were used for the measurements:
MS-Settings:
– Sheath Gas Flow Rate: 20 a.u.(arbitrary unit)
– Spray Voltage: 6.5 kV
– Capillary Temperature: 200°C
– Capillary Voltage: 5 V
– Tube Lens Offset: 40 V
LC-Settings:
– Hypersil Gold C18 column, 150 $mm \times 2.1\ mm$, 3 μm + Guard column (Thermo Electron)
– Flow Rate: $200\mu L/min$
– Injected Volume: $10\mu L$
Different values used during the test are given in Tab. (4.2).

For the material analysis 5 g of each sample were shredded and extracted in a Soxhlet extractor for 8 h. During this procedure the DOP migrated into the ether phase while the PVC remained un-dissolved. The ether dilution was diluted by the factor 100 and afterwards injected into the LC-MS, which was previously calibrated with pure DOP. Tensile tests to detect the Young's modulus E, the failure stress σb and the failure strain εb were conducted according to DIN 527 at room temperature and with a strain rate of 50 mm/min. The specimens were punched out of the PVC sheets with a suitable tool to provide standardized and constant dimensions. Specimens of the old geomembrane were punched out under special consideration of the obviously destroyed regions of the sheet. The temperature dependent material stiffness was measured with dynamic mechanical analysis (DMA) according to DIN 6721. The storage modulus E' represents the stiffness of a visco-elastic material and corresponds approximately to the Young's modulus determined with the tensile test. The loss modulus E'' is proportional to the dissipated energy

Table 4.2: Values of different parameters used during analysis

No	min	ACN	MeOH
0	0	50	50
1	11	50	50
2	12	100	0
3	25	100	0
4	26	50	50
5	35	50	50

min: minute; ACN: Acrylonitrile; MeOH: Methyl hydroxide

during a loading cycle. The loss factor $tan\delta$ is the ratio of E'' and E' ($tan\delta = E''/E'$), which represents the mechanical damping of the material. Hence, a high $tan\delta$ is characteristically specific for a material with a high content of non-elastic deformation. For both materials E', E'' and $tan\delta$ as a function of the temperature were measured in displacement controlled ($30\mu m$) tensile mode between -60 and $120°C$ with a heating rate of 3 K/min and a frequency of 1 Hz. For specimen preparation again a punching tool for tensile test specimens was used to ensure constant dimensions. Specimens of the old geomembrane were punched out under special consideration of the obviously destroyed regions of the sheet. The DHC-temperature was measured with differential scanning calorimetry (DSC) according to DIN 11357 with a DSC of the Type DSC822 (Mettler Toledo GmbH, Schwerzenbach, CH) and heating rates of 10 and 20 K/min. All tests were started at $23°C$ under atmospheric environment and were stopped manually when DHC initiated.

4.8 Results and discussion

4.8.1 Dimensional control

The geomembranes from various tunnels showed different appearance, with little irregularities and scratches observed on the surface of samples from Katschberg and Roppener tunnels. Samples from the Tanzenberg tunnel had some significant damage or punctated impressions. In Fig. 4.2, are shown two examples of strip samples from Tanzenberg tunnel wherein the surfaces of items labeled 1 to 5, represented thickness measurements of the individual measuring points.The sample T8_EQ03_06 showed relatively homogeneous appearance whereas distinct impressions of the film were visible in the sample T8_EQ04_06. In the illustrated case, the measuring point 2 of the sample T8_EQ04_06 has a minimum thickness of $t = 0.40\ mm$. Fig. 4.3 demonstrated a sample T1_EQ01_05 in a vertical view with a thinnest point having thickness of $t = 0.49\ mm$. The mean values tx and standard deviations σtx from each $n = 25$ individual measurements of the various geomembranes are graphically shown in Fig. 4.4. For geomembranes from both cross-cuts of Katschberg and Roppener tunnel the matching tx and σtx were measured, whereas for all other samples higher values of σtx indicated large dispersion and high

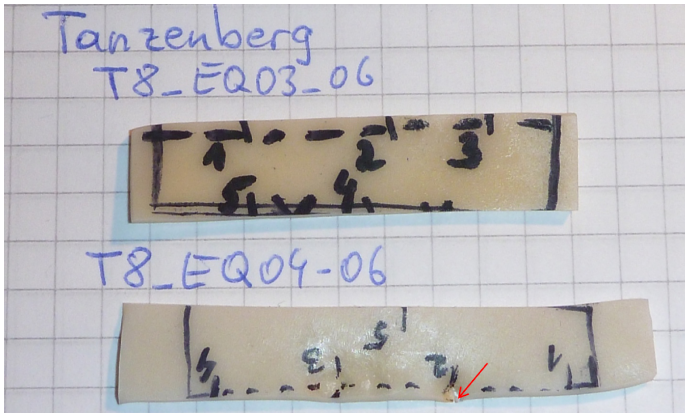

Figure 4.2: Exemplary representation of two strip samples T8_EQ03_06 and T8_EQ04_06 with measuring points 1 to 5 from Tanzenberg tunnel. The measuring point 2 of the sample (arrow) T8_EQ04_06 has a thickness of $t = 0.4\ mm$; [59]

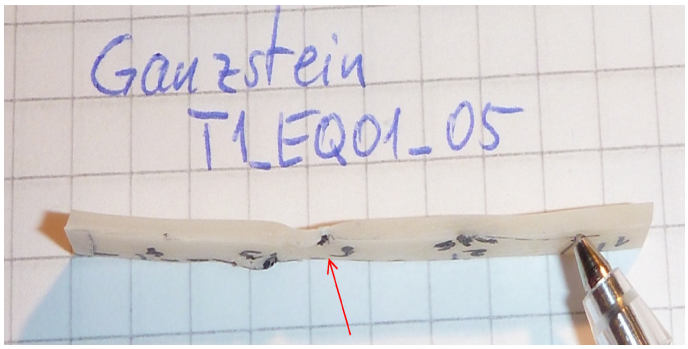

Figure 4.3: Exemplary representation of a strip sample T1_EQ01_05 of the Tanzenberg tunnel. The selected measurement point 5 of the sample (arrow) has a thickness of $t = 0.49\ mm$; [59]

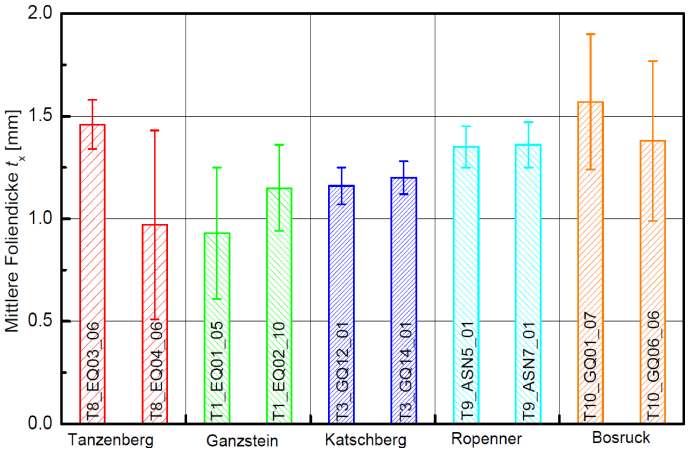

Figure 4.4: Mean film thickness tx and standard deviations of the mean film thickness σtx of the examined geomembrane; [59]

number of surface defects. The sample T8_EQ03_06 from the Tanzenberg had relatively small standard deviation as compared to T8_EQ04_06 due to difference in surface structure as a function of the transverse shock points. The increased standard deviation values of the geomembranes from Bosruck and Ganzstein compared to Katschberg and Roppener tunnel are due to more surface damage. In Tab. (4.3), $tmax$, $tmin$, tx and σtx of the geomembranes were examined together. The thinnest sample having thickness of $tmin = 0.2mm$ was T8_EQ04_06 from the Tanzenberg tunnel.

Table 4.3: Maximum film thickness $tmax$, minimum film thickness $tmin$, average film thickness tx and standard deviation of the average film thickness σtx of the investigated geomembranes.

Tunnel	Sample	$tmax$[mm]	$tmin$[mm]	tx[mm]	σtx[mm]
Tanzenberg	T8_EQ03_06	1.69	1.20	1.46	0.12
	T8_EQ04_06	1.51	0.20	0.97	0.46
Ganzstein	T1_EQ01_05	1.35	0.32	0.93	0.32
	T1_EQ02_10	1.38	0.50	1.15	0.21
Katschberg	T3_GQ12_01	1.31	0.97	1.16	0.09
	T3_GQ14_01	1.34	1.05	1.20	0.08
Roppener	T9_ASN5_01	1.57	1.10	1.35	0.10
	T9_ASN7_01	1.70	1.17	1.36	0.11
Bosruck	T10_GQ01_07	1.98	0.71	1.57	0.33
	T10_GQ06_06	1.90	0.61	1.38	0.39

4.8.2 Microscopic examinations

Fig. 4.5 shows the reflection electron microscopy (REM) image of the Ganzstein tunnel in 50 to 5000 times magnification. The surface of the sample T1_EQ01_05 reflected a clearly rougher appearance than the sample T1_EQ02_10. Assuming that same material was used in the two cross-cuts of the tunnel, the different surface characteristics of the geomembranes were the outcome of different conditions encountered with regard to the aging of the samples. The coarser texture of the sample T1_EQ01_05 may be related to the thermally induced aging of the material, resulting in sequence of further embrittlement of the material effect. In general the embrittlement of the plasticized PVC is related on the one hand with a loss of plasticizers by migration and on the other hand by a degradation of the polymer chains by thermal aging-induced dehydrochlorination [56, 57].

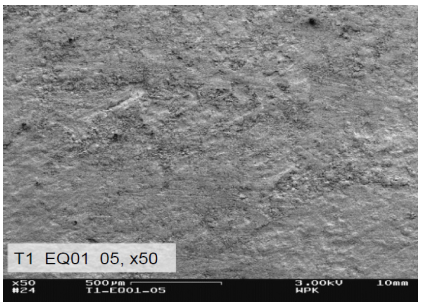

(a)

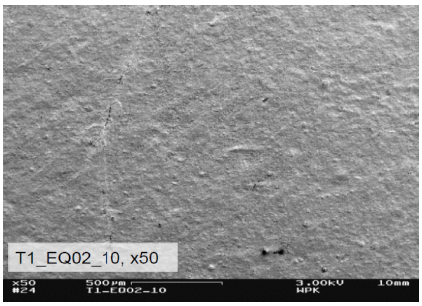

(b)

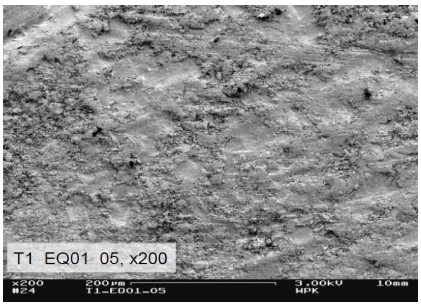

(c)

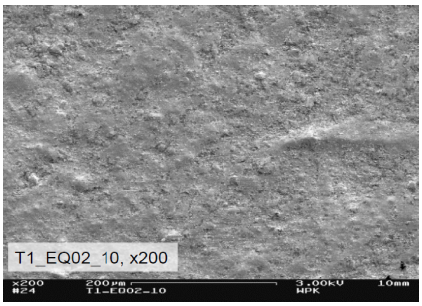

(d)

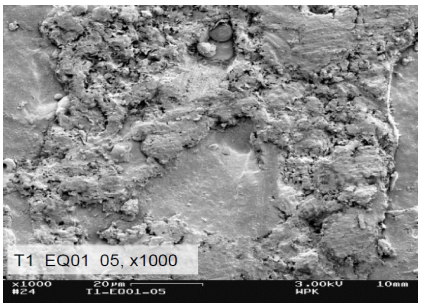

(e)

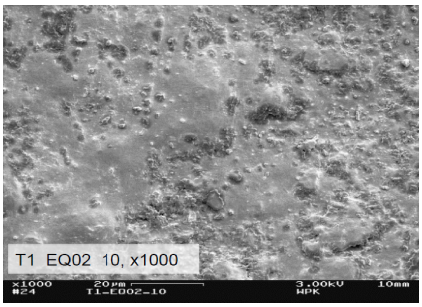

(f)

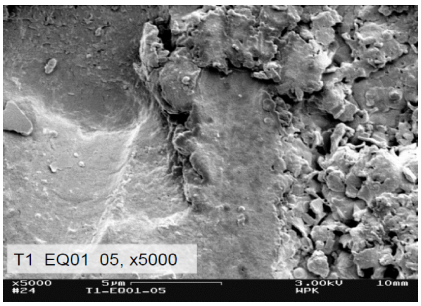

(g)

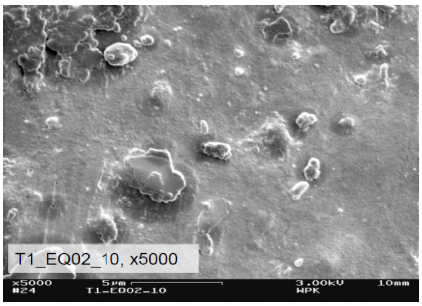

(h)

Figure 4.5: REM-Recording of the Ganzstein tunnel at different magnifications; Left: T1_EQ01_05; Right: T1_EQ02_10; [59]

4.8.3 Monotonic tensile test

The tensile test of the specific mean and standard deviation from $n = 7$ of the individual measurements of the elastic modulus E, failure stress σb and failure strain εb of the investigated geomembrane are summarized in Tab. (4.4).

Table 4.4: Young's modulus E, failure stress σb, and failure strain εb of the examined geomembrane; (Mean and standard deviation of $n = 7$ measurements)

Tunnel	Sample	E [MPa]	σb [MPa]	εb [%]
Tanzenberg	T8_EQ03_06	15.8 (±0.6)	18.7 (±0.7)	224 (±11)
	T8_EQ04_06	17.1 (±1.9)	17.8 (±0.4)	220 (±7)
Ganzstein	T1_EQ01_05	458 (±163	23.7 (±1.3)	131 (±12)
	T1_EQ02_10	21.3 (±2.5)	18.5 (±0.3)	203 (±11)
Katschberg	T3_GQ12_01	31.1 (±6.4)	14.3 (±0.3)	152 (±11)
	T3_GQ14_01	107 (±32)	16.0 (±1.0)	151 (±9)
Roppener	T9_ASN5_01	49.5 (±6.9)	18.2 (±1.2)	140 (±23)
	T9_ASN7_01	30.7 (±1.9)	19.1 (±0.9)	187 (±4)
Bosruck	T10_GQ01_07	14.0 (±0.6)	17.7 (±0.9)	203 (±18)
	T10_GQ06_06	12.5 (±0.8)	16.9 (±1.0)	210 (±15)

The individual curves of measurements for the samples from Tanzenberg, Ganzstein, Katschberg, Roppener and Bosruck are shown in Fig. 4.6 Fig. 4.7,Fig. 4.8,Fig. 4.9, and Fig. 4.10 respectively, wherein each graph shows the results of the failure stress and strain and the corresponding means and standard deviations from the two cross passages of a tunnel. The data of the two cross-cuts from the Tanzenberg tunnel differ only slightly from each other. A significant difference was detected between the two cross passages of the Ganzstein tunnel, in which case compared to the entire test program is by far the highest modulus of $E = 458$ MPa and the lowest elongation at break of about 131%

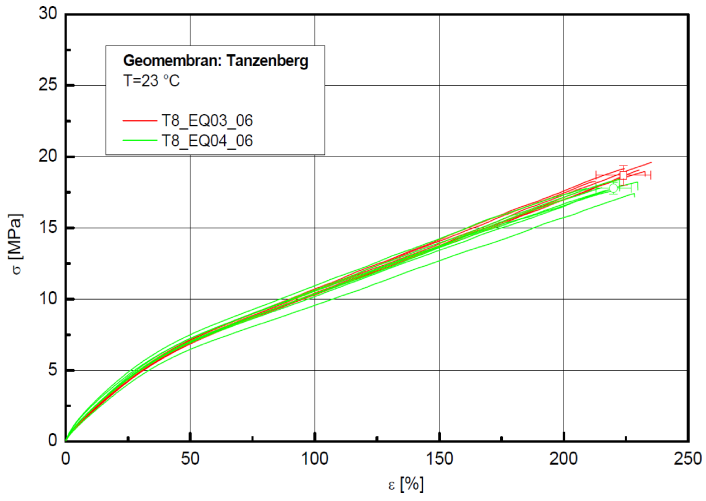

Figure 4.6: Stress-strain diagram of the Tanzenberg tunnel samples; [59]

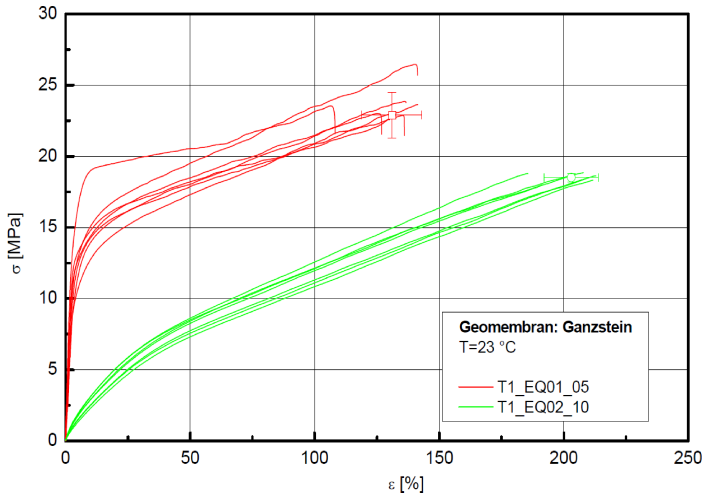

Figure 4.7: Stress-strain diagram of the Ganzstein tunnel samples; [59]

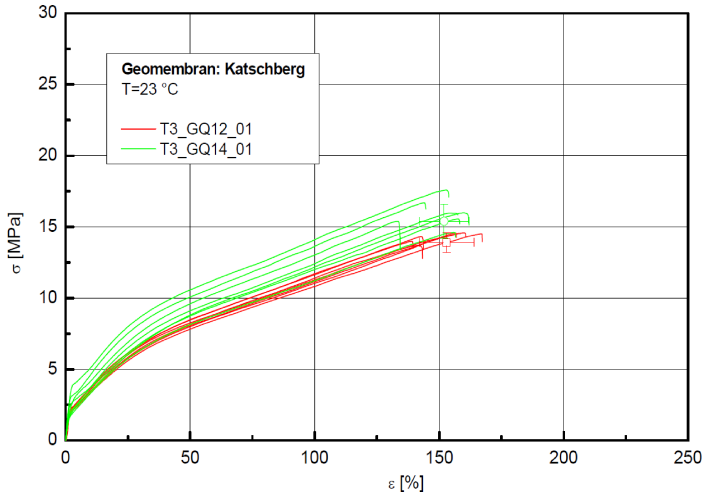

Figure 4.8: Stress-strain diagram of the Katschberg tunnel samples; [59]

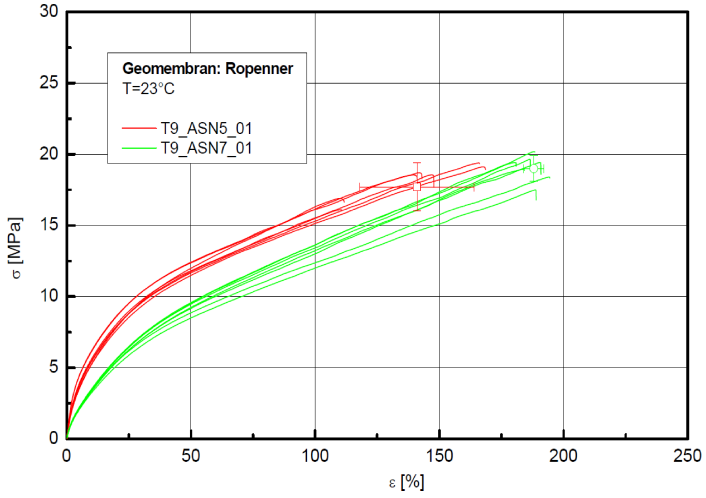

Figure 4.9: Stress-strain diagram of the Roppener tunnel samples; [59]

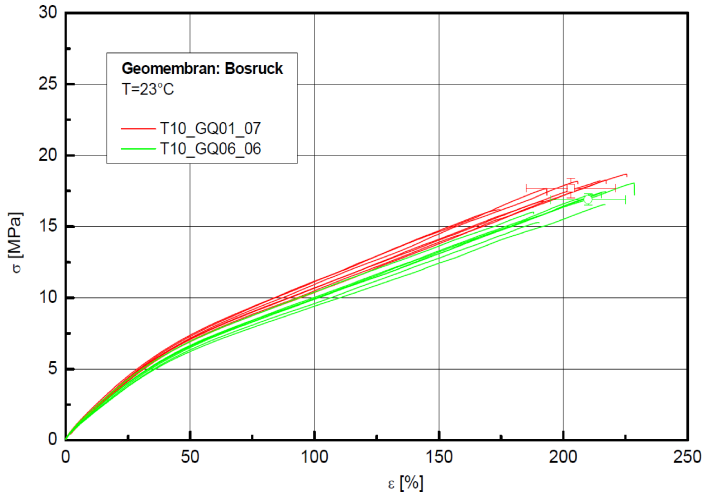

Figure 4.10: Stress-strain diagram of the Bosruck tunnel samples; [59]

representing pronounced embrittlement of the sample T1_EQ01_05. A similar although not so pronounced tendency was also observed in Katschberg tunnel wherein the sample T3_GQ14_01 had significantly higher modulus than the sample T3_GQ12_01, and Roppener tunnel with a slightly higher modulus and a slightly lower σB for T9_ASN5_01. The values of the two cross-cuts from Bosruck tunnel slightly differ from each other. The representative stress strain curves of the previously described measurements are summarized in Fig. 4.11. As a reference a measured curve of Project NC.10.043 representing a mint and unused geomembrane with the mean values of $E = 25.18$ ($\pm$ 2.3) MPa, $\sigma b = 16.3$ ($\pm$ 1.0) and $\varepsilon b = 242$ ($\pm$ 12) was inserted. In the present studied program all geomembranes showed lower elongation at break than the reference curve. The elastic moduli were both below and above the values of the reference curve NC.10.043. While the unaged sample from the previous considerations showed a similar reference curve, a shorter and higher elongation at break pointed to the embrittlement of the geomembrane marked by breakdown stresses for samples T1_EQ01_05 (Ganzstein) and T9_ASN5_01 (Roppener). The geomembranes from both cross-cuts of Katschberg tunnel showed matching shorter elongations with slightly higher breakdown stresses for T3_GQ14_01.

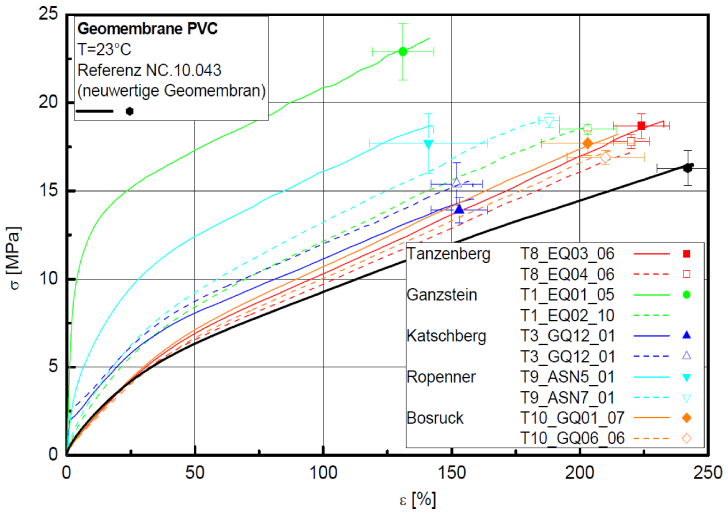

Figure 4.11: Summary of the stress-strain diagrams of the investigated geomembranes; [59]

Note that for the examined geomembrane the plasticizer content at this point was not known but with high probability it could be above 50%. The plasticizer content influences the mechanical and thermomechanical properties of PVC, wherein increasing plasticizer content e.g. significantly decreases the stiffness. Assuming that within a tunnel in two cross passages the same material was used, some of which have markedly different tensile tests results indicating that during the deployment of geomembrane the material properties altered differently. Mainly in the samples from Ganzstein and Roppener the observed embrittlement of the material showed different operating conditions of the geomembranes at the various cross-cuts.

4.8.4 Thermal analysis

The resistance of PVC against thermal aging can be characterized by the temperature of dehydrochlorination (DHC). The degradation depends on its stabilizer system and additives such as plasticizers, as well as on the consumption of the previous stabilizer. Typical temperatures for DHC are between $T_{DHC} = 150 - 250°C$ [56, 57].

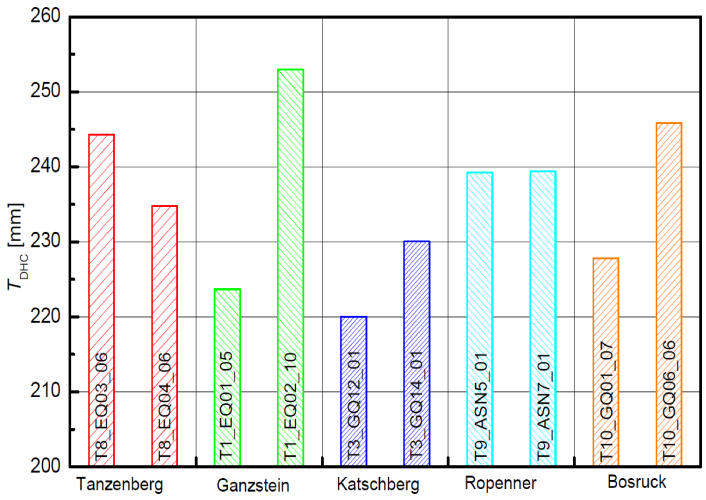

Figure 4.12: Dehydrochlorination temperature T_{DHC} of the investigated geomembranes; [59]

Fig. 4.12. illustrated the measured T_{DHC} of the geomembrane. All T_{DHC} measured were $220 - 253°C$ and thus comparable with the value of $228°C$ obtained for the already used project NC.10.043, and $259°C$ for a brand new geomembrane. Differences in the T_{DHC} were found between the cross-cuts for all samples except Roppener tunnel. Assuming same material used with identical stability in different cross-cuts of the same tunnel, the difference in T_{DHC} could be attributed to different operating conditions of geomembrane. Higher consumption of stabilizers is often associated with higher operating temperatures. Looking at the sample T1_EQ01_05 from Ganzstein, the much lower T_{DHC} could be the result of higher thermal stress or higher stabilizer consumption than for the sample T1_EQ02_10. This assumption for the sample T1_EQ01_05 was also reflected in the rougher surface characteristics Fig. 4.5 and the much more brittle material behavior in the tensile test Fig. 4.7. In Roppener samples the tensile tests reported significant difference in the results for different cross-cuts, however, comparable T_{DHC} values, so that the embrittlement of the sample T9_ASN5_01 would be in conjuction with other factors probably due to different plasticizer level.

4.8.5 Infrared (IR) spectroscopy

Fig. 4.13 illustrates the IR transmission spectra of investigated samples from the two cross-cuts of the Tanzenberg tunnel. It also describes the characteristics of PVC transmission bands with the associated binding pairs, which in all geomembranes have been investigated and the material of the tunnel liners was identified as PVC [60]. (ν....stretching, δ....deformation vibration, ρ....rocking vibration). Comparing the bands of the carbonyl groups as a measure of the content of plasticizer for the Ganzstein samples in Fig. 4.14, it seemed to fall as much smaller peak occurred for T1_EQ02_10 as compared to T1_EQ05_05. The results indicated that the observed embrittlement at T1_EQ01_05 is associated with the considerable loss of plastizicer. The characteristics of PVC C-Cl bonds at a wave number $v = 615\ cm^{-1}$ were not visible and therefore outside the detection limit of IR analysis (4000-650 cm^{-1}). Since the sample from Katschberg was composed of two layers Fig. 4.15, the IR transmission spectra illustrated both sides. The prominent display detected at wave numbers between 1700-1740 cm^{-1} in all the samples were due to vibrations of carbonyl ($C = 0$), phthalates such as diethyl hexyl phthalates ($DEHP$) and dioctyl point (DOP) as plasticizer.

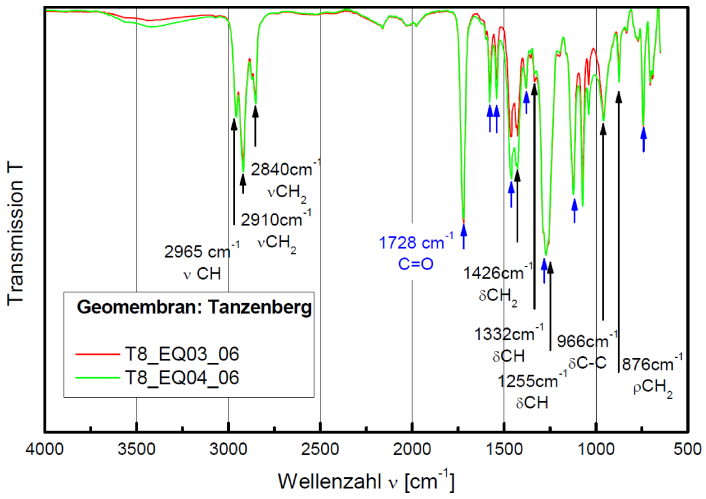

Figure 4.13: IR transmission spectrum for the Tanzenberg samples; [59]

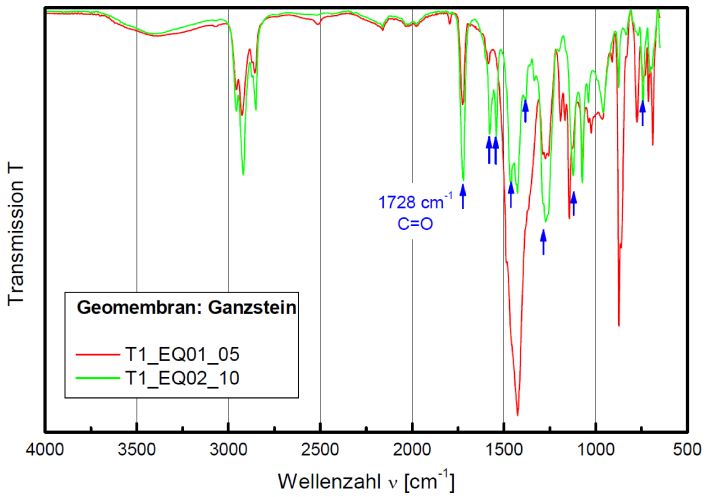

Figure 4.14: IR transmission spectrum for the Ganzstein samples; [59]

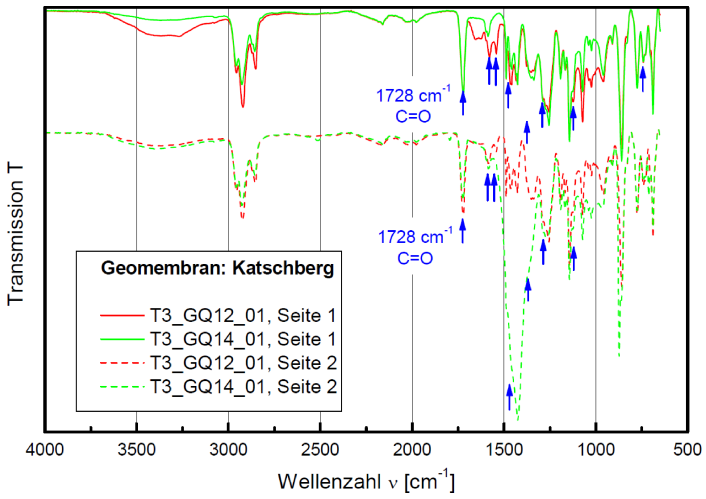

Figure 4.15: IR transmission spectrum for the Katschberg samples; [59]

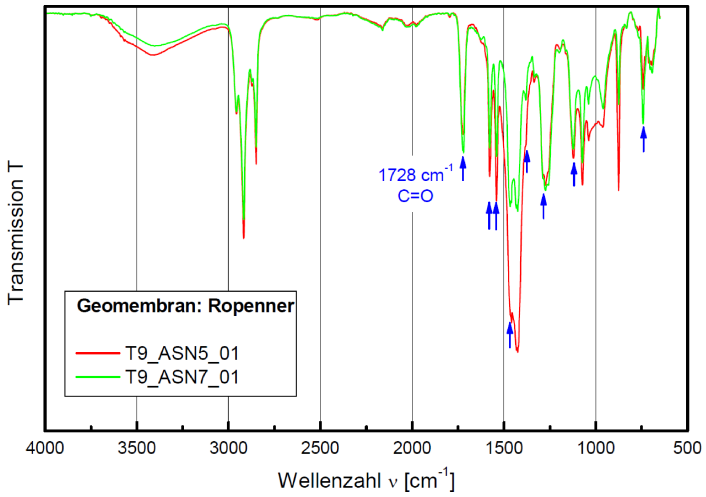

Figure 4.16: IR transmission spectrum for the Roppener samples; [59]

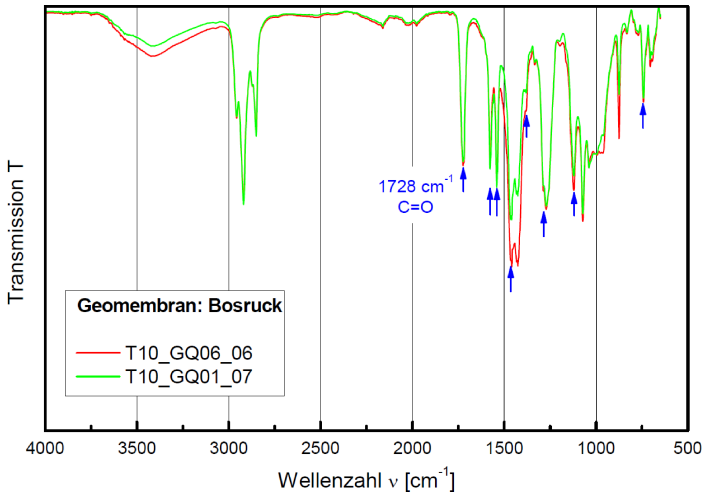

Figure 4.17: IR transmission spectrum for the Bosruck samples; [59]

Other plasticizers attributable to softener are marked with a blue arrow. Among samples of the other tunnels Fig. 4.16 and Fig. 4.17 only small difference was observed in the area of carbonyl groups. However, in general some significant difference in plasticizer content was found between samples from different cross-cuts. Assuming that for various cross-cuts of the tunnel, the same material with the same plasticizer content was used, some of the geomembranes exhibited significant differences in the softening of relevant bands on different states. It can not be excluded that different environmental conditions in the cross passages led to differences in the chemical structure of the geomembrane. With the exception of the Tanzenberg samples, all geomembranes showed transmission bands at wavenumbers of 2512, 1795 and 1450 cm^{-1}, the later sometimes quite intensively pronounced. This indicated the presence of lime stone ($CaCO_3$) in the vicinity. The exact origin of the lime can be identified from the available information about the sites. On the other hand chalk is often used as a filler material in PVC. Under acidic conditions the slow leaching of the filler chalk can not be ruled out. On the other hand it could be attributed to the fact that for being in contact with calcareous formation over many years, the surrounding mountain water has entered the geomembrane.

4.8.6 Viscosity measurement (K value)

The results of the viscosity measurements of the two PVC sheets are summarized in Tab. (4.5), where average values of the concentration of dilution c and the reduced viscosity RV are listed. The concentration of pvc was reduced by diluting with a thinner. Reduced viscosity RV also called viscosity number refers to the specific viscosity divided by the concentration, expressed in $[ml/g]$.

Table 4.5: Dilution concentration c and reduced viscosity RV of the old and new geomembrane (average value of the two measurements)

c[g/ml]		RV[ml/g]	
old	new	old	new
0.00941	0.00821	91.4888	83.8678
0.00766	0.00672	89.2325	79.6413
0.00586	0.00548	84.7933	77.0298
0.0047	0.00431	83.3533	74.1410
0.00405	0.00375	81.4170	73.0475
0.00214	0.00202	76.6819	67.9612

Fig. 4.18 shows the data RV as a function of c graphically. The RV of both materials decreases with decreasing c. For the old geomembrane higher viscosities were measured than for the new geomembrane. An extrapolation of the data to a concentration of $c = 0\ [g/ml]$ provides the intrinsic viscosity IV which was determined to IV $old = 73.0\ [ml/g]$ for the old geomembrane and IV $new = 63.2\ [ml/g]$ for the new geomembrane. The intrinsic viscosity reflects the capability of a polymer in solution to enhance the viscosity of a solution and is related to the molecular weight or degree of polymerization. According to DIN EN ISO 1628-2 the IV's are equivalent to K values of 54.7 for the old geomembrane and 50.9 for the new geomembrane, which is a difference of about 7%.

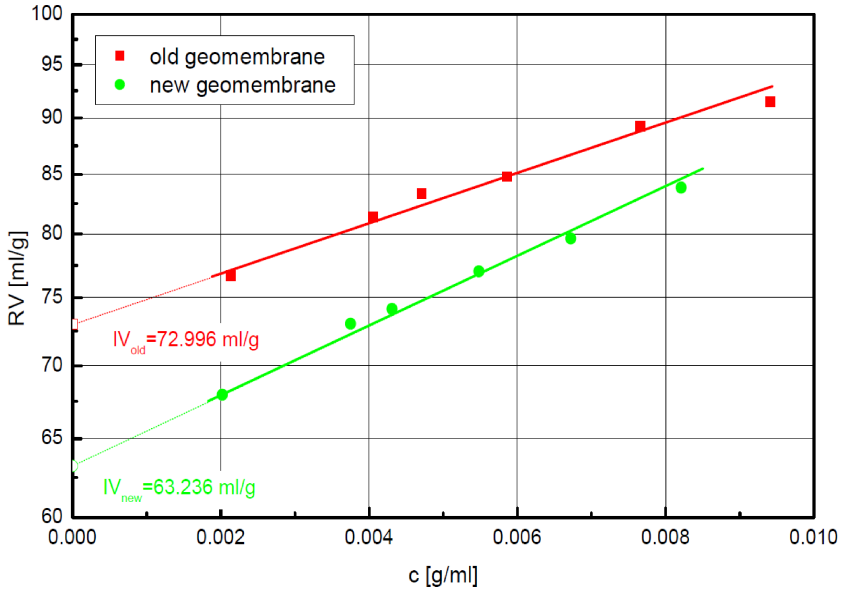

Figure 4.18: Reduced viscosity RV as a function of the dilution concentration c for the old and new PVC-geomembrane. The intrinsic viscosity IV was determined by an extrapolation to $c = 0$ $[g/ml]$; [58]

4.8.7 Content of plasticizers

For the old geomembrane as well as for the new geomembrane DOP was clearly identified as plasticizer by a retention time of 20.20 min, which was compared to the calibration with pure DOP, and by the m/z-signal of 391. The m/z denotes mass to charge ratio of an ion in mass spectrometry analysis. The quantitative analysis resulted in a DOP content of 27.8% for the old geomembrane and 42.3% for the new geomembrane which is a difference of 14.5%.

4.8.8 Mechanical properties

Standard tensile tests at room temperature were conducted to determine mechanical properties of the PVC geomembranes. The stress-strain curves are summarized in Fig. 4.19.

Tab. (4.6)lists the main results of the tensile tests. For all properties somewhat higher values were measured for the new geomembrane. The Young's modulus E for the old geomembrane is about 20% lower than for the new geomembrane and also the failure stress σb (-7%) and the failure strain εb (-15%) are lower for the old geomembrane.

Table 4.6: Young's modulus E, failure stress σb and failure strain εb for the old and new PVC-geomembrane

Parameter	Old geomembrane	New geomembrane
E [MPa]	20.2 ($\pm$ 0.9)	25.1 ($\pm$ 2.3)
σb [MPa]	15.2 ($\pm$ 0.6)	16.3 ($\pm$ 1.0)
εb [%]	206 ($\pm$ 15)	242 ($\pm$ 12)

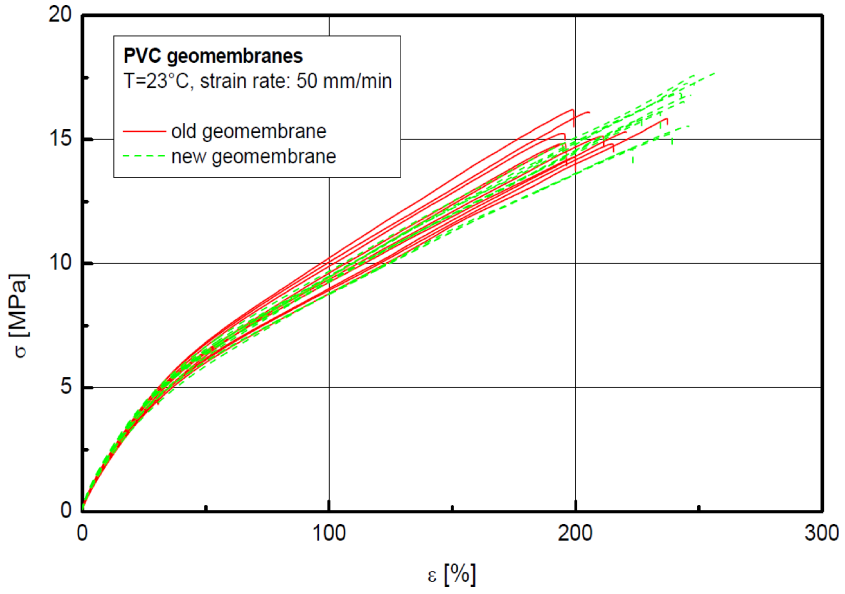

Figure 4.19: Stress-strain curves for the old and new geomembranes; [58]

4.8.9 Theromechanical properties

Fig. 4.20 shows the storage modulus E', the loss modulus E'' and the loss factor $tan\delta$ as a function of the temperature T. The storage modulus E' is measure of the stiffness of a viscoelastic material and is proportional to the energy stored during a loading cycle. It is roughly equal to the elastic modulus for a single, rapid stress and reversible deformation. The loss modulus E'' represents the energy dissipated during one loading cycle for example energy lost as heat or vibrational energy. The loss factor $tan\delta$ is the ratio of loss modulus to storage modulus (E''/E'). It represents mechanical damping or internal friction in a viscoelastic material. At $T < -40°C$ both materials are in the glassy state and show a very stiff behavior which is expressed by the relatively high values for E' and E'' and the low $tan\delta$. Between -40 and $80°C$ the glass transition for both PVC geomembranes was detected. The glass transition temperature indicates the relaxation in a polymer where it changes from a glass to a rubber or undergoes a transition from a rubbery, viscous amorphous liquid, to a brittle, glassy amorphous solid. It is brought about by changing the degree of branching or crosslinking in a polymer or addition of plasticizer. The glass transition temperature T_g can be determined in different ways and for the measured data T_g was taken from the tangential onset of $E'(T_g(E'))$ and the maximum of $E''(T_g(E''))$. For the new geomembrane $T_g(E') = -28°C$ is about 8 K lower than for the old geomembrane with $T_g(E') = -20°C$. A similar tendency was detected for the second method, where $T_g(E'') = -33°C$ of the new geomembrane is about 5 K lower than for the old geomembrane with $T_g(E'') = -28°C$. With both evaluation methods a lower T_g was determined for the new PVC geomembrane, which is an indication of the higher content of plasticizers. Comparable literature values for theT_g of plasticized PVC were found for plasticizer contents between 30 and 40% [55]. The curves for the loss factor $tan\delta$ show no significant differences between the old and the new geomembrane. The maximum for $tan\delta$ was detected in the range of $10 - 20°C$ which may be relatively close to the practical application temperature of the geomembranes.

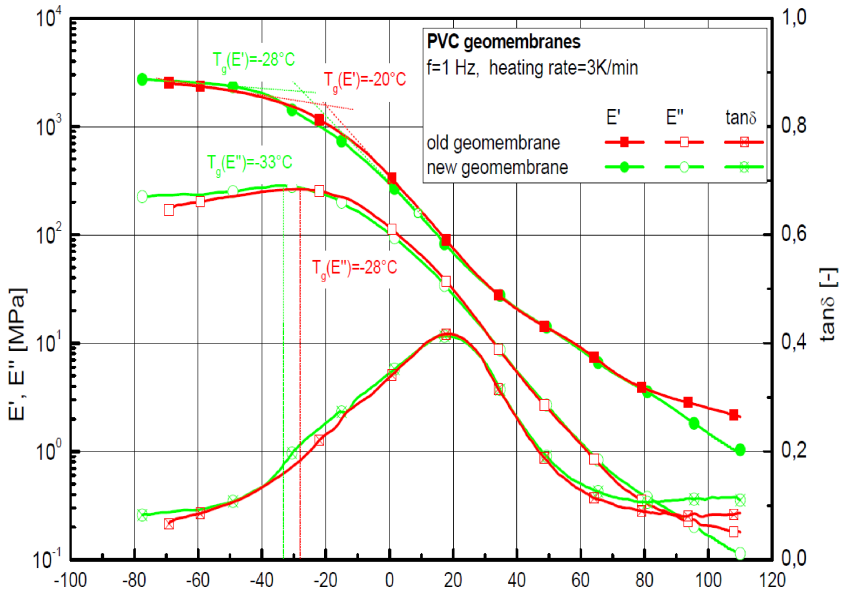

Figure 4.20: Storage modulus E', loss modulus E'' and loss factor $tan\delta$ as a function of the temperature T for the old and new PVC-geomembrane, measured in tensile mode (displacement controlled, $30\mu m$) at a heating rate of 3 K/min; [58]

4.8.10 Dehydrochlorination

During the DSC measurements with a heating rate of 10 K/min relatively noisy data were recorded for both materials. Hence, the measurements were repeated with a heating rate of 20 K/min. Anyway, at both heating rates the onset for DHC could be determined. For both experiments the DHC-temperatures are summarized in Tab. (4.7) and Tab. (4.8). At 10 K/min the DHC-temperature of the old geomembrane with 213°C shows a 14% lower value than the new geomembrane with 249°C. At 20 K/min the difference in the DHC-temperature of the old geomembrane with 228°C and the new geomembrane with 259.4°C is about 12%. The somewhat higher values at higher heating rates are typical. Generally, the DHC-temperatures for both tested materials are in a typical range [56, 57].

Table 4.7: Dehydrochlorination- (DHC) temperature of the old and new PVC-geomembrane at a heating rate of 10 K/min

dT/dt [K/min]	DHC-temperature [°C]	
	old geomembrane	new geomembrane
10	230.5	258.1
10	227.7	260.4
10	224.8	259.8
	$\bar{x} = 227.7$	$\bar{x} = 259.4$
	$\sigma_x = 2.9$	$\sigma_x = 1.2$

As no information about the exact stabilizer packages were available and moreover no comparison of the old geomembrane to its virgin condition is possible, the lower DHC-temperature of the old geomembrane may not necessarily be a result of material aging, but may also be an effect of different stabilizer packages.

Table 4.8: Dehydrochlorination- (DHC) temperature of the old and new PVC-geomembrane at a heating rate of 20 K/min

dT/dt $[K/\text{min}]$	DHC-temperature [°C]	
	old geomembrane	new geomembrane
20	230.5	258.1
20	227.7	260.4
20	224.8	259.8
	$\bar{x} = 227.7$	$\bar{x} = 259.4$
	$\sigma_x = 2.9$	$\sigma_x = 1.2$

4.9 Conclusion

In the present research a characterization of Polyvinyl chloride (PVC) geomembranes was carried out, which were in service for the purpose of waterproofing in tunnels for about 30 years. Two samples were analysed from the various cross-cuts of each five tunnels. A one-dimensional analysis with particular reference to surface damage showed that in some samples (Tanzenberg T8_EQ04_06) quite a high probability existed for leaks in the form of point-like holes and penetrations. The samples of Ganzstein tunnel were additionally investigated by SEM due to their obviously different behavior which in sample T1_EQ01_05 found indications of a material deterioration. The tensile tests showed some significant differences in the measured parameters between the cross-cuts. A specially designed optical examination test results for the sample T1_EQ01_05 from the Ganzstein demonstrated definite impressions of embrittlement of the geomembrane. General differences reflected in the tensile tests and in the determination of the DHC-temperature and IR spectroscopy. A brittle material behavior was brought together with the aging of material, usually with a lower DHC-temperature (= higher consumption of stabilizers) or a difference in the plasticizer content in compound. Assuming that uniform geomembranes were used in the tunnel, the study results strongly suggest that different aging mechanisms encountered during the life time in various cross-cuts. Of particular importance was when to critically question the marked embrittlement of the material of Ganzstein and Roppener samples. Changes in the DHC temperature interpret it more in the direction of a higher thermal load, while differences in the plasticizers content rather suggest to migration of plasticizers possibly in combination with ambient media. Combination of two mechanisms would in practice be probably responsible for the observed changes in material.

Most measured values of the old geomembrane from Katschberg tunnel were in typical ranges for PVC-P and were also comparable to the reference values of the new geomembrane. A clear difference exists in the content of DOP which was detected as plasticizer in both materials. The 14.5% lower content of DOP in the old Katschberg sample may be responsible for a 5-8 K higher glass transition. It can not be clearly determined, if some amount of DOP was leached out during the service time or if originally a lower content of DOP was used for the old geomembrane. Generally, an increasing content of plasticizer reduces the stiffness of the material. However, for the Katschberg sample a 20% lower Young's modulus was measured than for the new geomembrane which is in

contrast to the expectations related to the content of plasticizers. Hence, the low Young's modulus of the old geomembrane may not necessarily be related to the content of plasticizers. Only minor differences were found in stress and strain at break. Surprisingly, the difference in the stiffness was not observed with the DMA, where the storage modulus at room temperature was almost the same for both materials. The approximately 7% higher K value of the Katschberg sample indicates a somewhat higher average molecular weight. It can not be verified if a higher molecular weight was originally used to produce the Katschberg specimen, or if potentially cross-linking led to an increase. Anyway, the K values for both materials are in a typical range for PVC. For both materials typical DHC-temperatures were measured which indicate a sufficient stabilization against thermal degradation. It can not be verified, if different stabilizer packages are responsible for the somewhat shorter DHC-temperatures of the old geomembrane or if a consumption of stabilizers during the service time led to a lower thermal resistance. The test results show that the detected values for the Katschberg sample are still in typical ranges for plasticized PVC. Based on the conducted methods no significant indications for a considerable degradation of material properties were detected so that it can be concluded, that the Katschberg sample is still in good condition.

Chapter 5

Numerical Simulation of the tunnel linings

5.1 Introduction to the shotcrete support system

Shotcrete as a support measure is a major part of the New Austrian Tunnelling Method (NATM) [61]. NATM is essentially an empirical approach, which evolved from the practical rock tunnelling experience, where the strength of the surrounding ground is deliberately mobilized to the maximum possible extent in combination with a thin flexible shotcrete lining, to provide an early stage of stability, which represent an equilibrium between the support and the rock mass [62]. After the excavation step the shotcrete support is immediately applied to the exposed surface of the tunnel. The installed tunnel lining is loaded from the beginning by the excavation work and the associated stress redistribution in the ground. The tunnel convergence and stress distribution inside the shotcrete shell strongly depends on a lot of parameters like the construction parameters such as excavation sequence, rate of advance, shell thickness, geometry of the tunnel cross section, ring closure time/distance and shotcrete mix-design. The evaluation and interpretation of stresses in shotcrete linings will help in predicting the lining behavior. Thus monitoring is also a very important part of the NATM. The excavation of a tunnel changes the primary stress field into a three-dimensional pattern at the tunnel face. The volume of rock squeezing into the opening creates deformations around and above the tunnel, which cannot be simulated directly in 2D finite element (FE) analysis. About two diameters behind the tunnel face, the stress field turns into an essentially two-dimensional system. Hence, common structural design models consider two-dimensional plane strain FE analysis after adopting assumptions, which take into account volume loss, percentage of theoretical tunnel volume, and deformations prior to introduction of structural support elements. The behavior of shotcrete and concrete linings of a subway tunnel using progressive softening analysis by employing two-dimensional finite elements coupled with the boundary element method to investigate the distribution and progress of cracks in the inner lining and the depth of a compression zone was studied by [63]. The use of 3D models is on the increase where the nature of problem is more complex or to deal with the exact evaluation of the effects of excavation processes. Three-dimensional analysis was conducted by [64], to simulate the excavation process of shallow and deep tunnels using soil nails and temporary linings. The results show the influence of the soil properties and excavation procedure on face deformation and ground settlements. The effects of tun-

nelling on the existing support system (*i.e.* shotcrete lining and rock bolts) of an adjacent tunnel by means of a full 3D finite element model using a Mohr-Coulomb elastoplastic constitutive law with a non-associated flow rule were examined by [65]. The results show that the effect of tunnelling on the existing support system is strongly dependent on the position between the existing and new tunnels as well as on the proximity of the two tunnels.

This study deals with three-dimensional numerical analysis of stresses in the shotcrete lining of a deep tunnel after the installation as well as long-term behaviour of the shotcrete support after deterioration and its impact on the overall stability of the tunnel support system consisting of rock mass, shotcrete and the inner lining. More specifically, the study will determine the mechanical behaviour of shotcrete support subjected to stresses during the advance of the excavation face, stress distribution upon gradual deterioration of shotcrete support and its subsequent response on the inner lining regarding the residual forces acting on it after the degradation of the shotcrete support. The excavation process according to the principles of NATM is divided into top-heading, bench and invert advance. The simulations have been implemented with the finite element code-ABAQUS 6.10.1.

5.2 New Austrain Tunnelling Method- (NATM) Basic Approach For Numerical Simulation

The construction of tunnels and the development of tunnelling methods in a country are strongly influenced by the Geographical situation, topography, infrastructure, environment, hydrology and many more subjects. The NATM comprises a lot of information and different thematic areas. This basic approach can just present a small amount of fundamental information which is needed for the understanding of the structure of the model and the numerical simulation. Further information about the NATM can be found in [66], and [67]. In terms of tunnelling, the geology in Austria is generally difficult and tends to change rapidly along the tunnel route. Tunnel construction in the Alps means facing a high overburden and, in some places heavily squeezing rock conditions and further more tunnelling in urban environments is gaining importance. After the mid-fifties Austria had a number of brilliant engineers like Rabcevicz, Müller, Pacher, Lauffer, Seeber, et.al. who greatly influenced and promoted the development of tunnelling in Austria by innovative ideas. Most important was the development of NATM (New Austrian Tunnelling Method), which introduced the observational approach in tunnelling. The theoretical basis for NATM is to conceive the ground around the tunnel not just as a load, but works also as a load-bearing element of support. In combination with the time-dependent development of ground reactions as a result of tunnel excavation, the type and quantity of the support elements required is systematically adjusted. The ground reactions, taking the form of lining deformations and lining pressures, are measured and the stability of the excavation is confirmed by frequent monitoring. Depending on the project conditions (e.g. shallow soft ground tunnel, deep rock tunnel) and the results of the geotechnical measurements, the requirements for a specific support are determined. Adjustable contractual arrangements always leave room for the most economical type and amount of support in the tunnel. The typical support elements in NATM are the systematic application of shotcrete and rock anchors to allow controllable deformation

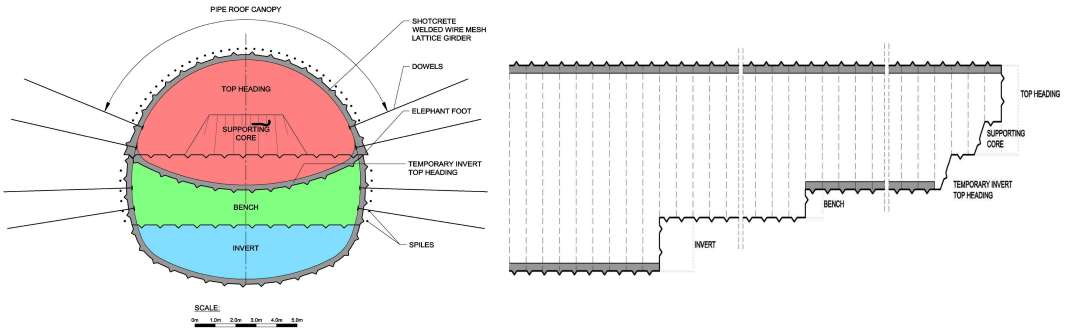

Figure 5.1: Construction sequence including an invert arch; after [68].

of the rock mass. Steel ribs or lattice girders provide limited early support before the shotcrete hardens and ensure correct profile geometry. If the ground conditions require any support at the tunnel face or ahead of the excavation face bolts, sealing shotcrete, spiles or pipe canopies can be installed. The subdivision of the excavation cross-section into top heading, bench and invert depends on geological conditions as well as on logistical requirements to facilitate the use of standard plant and machinery in tunnelling. Side drift galleries are provided to limit the size of large excavation faces and the associated surface settlements. With the increasing demand to construct road and railway tunnels with cross-sections up to 150 m^2, the construction techniques were further developed and standardised. If favourable rock conditions are expected to be encountered, the top half of the tunnel cross-section is usually advanced by drill and blast techniques. A few hundred meters behind the excavation face, the bench is excavated simultaneously, always leaving a ramp on one half of the cross-section for access to the top heading. Behind the bench excavation, the invert is prepared. Fig. 5.1 shows the principal excavation sequences in a typical NATM excavation process.

An invert arch is only provided, if required by ground conditions and is normally excavated in two halves to maintain access to the excavation at the front. Different aspects require different methods of conventional tunnel excavation and support. In deep rock tunnels subjected to squeezing ground conditions, the shotcrete lining thickness shall not further be increased. The main support elements are long rock anchors. The shotcrete lining is slotted and steel ribs slide along locks to allow controlled deformation. Once the rock pressure is significantly reduced and stabilisation of the ground pressure is confirmed by monitoring, the slots in the lining are closed with shotcrete.

5.3 Numerical model

A three-dimensional (3D) model was developed in this study using finite element package ABAQUS 6.10.1. The particular features and different parts of the model are described below. Construction of a three-dimensional geometry of the model assembly, mesh generation, boundary condition, defining material properties and material behavior, contact formulations etc. have been comprehensively dealt with to provide basic information about the numerical analysis.

The second part of the analysis deals with the excavation of the tunnel in stages, starting with excavation of the top heading, bench and invert with simultaneous installation of primary shotcrete support in the respective areas to achieve initial stability of the

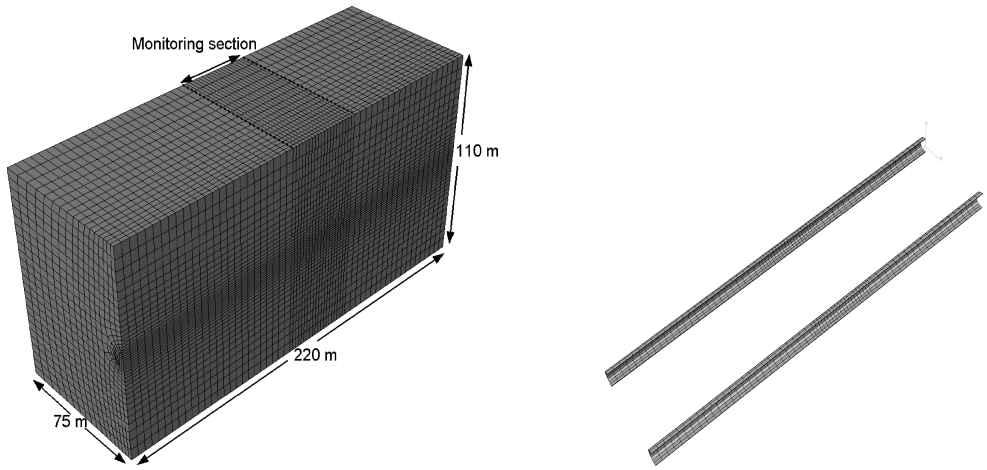

Figure 5.2: Three-dimensional finite element mesh of the model;(a) Rock model (b) Shotcrete and Liner element

structure. The permanent inner liner was installed after complete excavation of the tunnel. The last part, the deterioration of shotcrete takes into account the long-time degradation of the strength properties to simulate the deterioration of the shotcrete shell. The progressive increase of stresses in the inner lining and stress dissipation into the surrounding rock with the degradation of shotcrete support shows the interaction between the shotcrete shell and the inner liner.

5.4 Finite element model and design

Fig. 5.2 represents the design and different components of the finite element model. The modeled domain is 220 m in length, 75 m in width and 110 m in depth. The tunnel is having a polycentric cross-section and the diameter of arch in the top heading of the tunnel is $2R = 10\,\mathrm{m}$ and constructed at a depth of 250 m below the ground surface. The ground is assumed to be marl and is idealized homogeneous and isotropic with a unit weight of $\gamma = 27\,\mathrm{kN/m^3}$. The horizontal ground stress is obtained assuming Poisson's ratio of $\nu = 0.4$. The outer boundaries are located far away from the tunnel so that there are no influences from the boundary conditions to the tunnel. This is the case when the horizontal mesh length is 4 to 5 times the tunnel diameter [69].

By taking advantage of the homogeneity and isotropy of the material and the symmetry of the geometry and loading conditions into account only half of the tunnel is modeled. The coarse elements at both ends of the model served to isolate the central finer mesh from the boundary effects and to decrease the calculation steps. Results from the central mesh with a length of 40 m, will be used in the analysis. The excavation (round) length in the coarser area of the mesh was 4 m which reduced to 2 m in the central finer mesh region for better evaluation. The tunnel face is advanced using the top heading, bench and invert excavation techniques with simultaneous installation of shotcrete initial support. The shotcrete lining has a thickness of 200 mm and is constrained to move with the exposed tunnel surface after the excavation to model the interaction between the shotcrete lining and the surrounding rock mass. Thus, the shotcrete lining is tied to the exposed tunnel

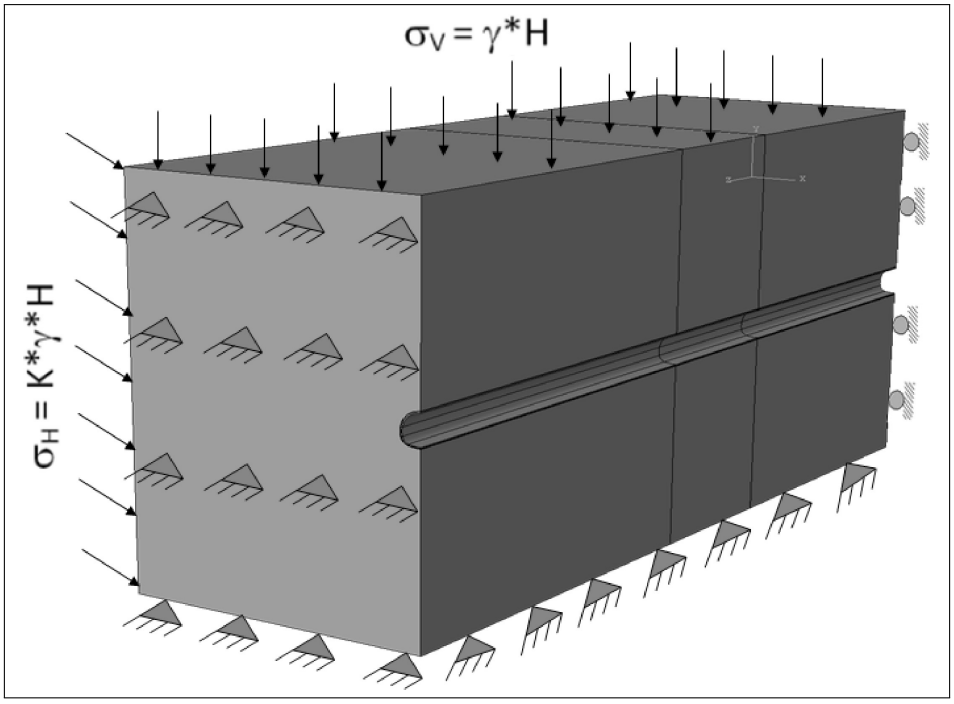

Figure 5.3: Schematic representation of model boundary conditions and loads

surface during the subsequent simulation so that the shotcrete lining follows the motion of the exposed tunnel surface. The thickness of the inner liner is 300 mm. As usual in NATM tunneling, the inner lining is installed after the full excavation of the tunnel, supported initially only by reinforced shotcrete.

5.4.1 Boundary conditions

The boundary conditions applied to the model can be seen in Fig. 5.3. The model is fixed from the front and rear side, and the bottom part of the model has been pinned. The right vertical side of the model representing a plane of symmetry has been bounded by roller supports. The vertical earth-pressure is applied on the top side and horizontal earth-pressure is applied on the left vertical side of the model.

5.4.2 Description of continuum elements mesh, nodes and elements

Three-dimensional solid continuum elements used in the model consisted of first-order linear interpolation hexahedral brick elements as shown in Fig. 5.4. The finite element mesh consisted of 32695 eight-node isoparametric hexahedral elements with reduced integration points and hourglass controls (C3D8R) to represent the rock mass. The shotcrete shell and liner consisted of 650 and 1300 eight-node elements respectively, of the type (C3D8R). The shotcrete shell and liner meshes were also generated using three-dimensional eight-node full integration elements (C3D8) for having possibility of stress and displacement calculation at multiple integration points within an element like in case of bending moments and normal forces. The reduced integration scheme is based on the "uniform strain formulation" where an average strain is calculated over the element volume. Uniformly

reduced-integration rules are appealing computationally because a substantial reduction in the number of function evaluation is achieved. Reduced integration has a series of drawbacks of mesh instability commonly known as "hourglassing" (ABAQUS). Kinematic zero-energy modes are present in reduced integration elements formulations so that, if the mesh is geometrically consistent with a global pattern of such modes, a singular stiffness matrix is obtained and the element is rendered ineffective. The expression "full integration" refers to the number of Gauss points required to integrate the polynomial terms in an element stiffness matrix. Full integration linear elements use two integration points in each direction. Thus the three-dimensional element C3D8 uses a 2 array of integration points in the elements. Another advantage of full integrated solid elements is that they do not suffer from volumetric locking because of constant volume strain generation in these elements. Thus, they can be safely used in plasticity problems.

The mesh control tool in ABAQUS uses so called FREE, STRUCTURED, and SWEEP techniques to generate a required mesh type. The SWEEP technique using medial axis algorithm was selected as a best fit to the model geometry as shown in Fig. 5.5 and Fig. 5.6.

5.5 Constitutive model used in the numerical analysis

The numerical model consists of different components:

1. Ground
2. Shotcrete shell (reinforced sprayed concrete)
3. Inner liner (concrete)

The behavior of the surrounding ground and shotcrete was assumed to be governed by an elasto-plastic constitutive relation based on the Mohr-Coulomb criterion. The behavior of the inner liner was governed by linear elastic relationship. Plastic strains are produced during a loading process. [71]. The direction and magnitude of the plastic

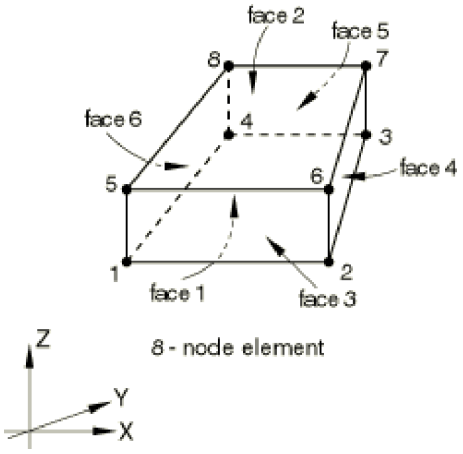

Figure 5.4: Three-dimensional eight-node reduced integration (C3D8R) brick element; [70].

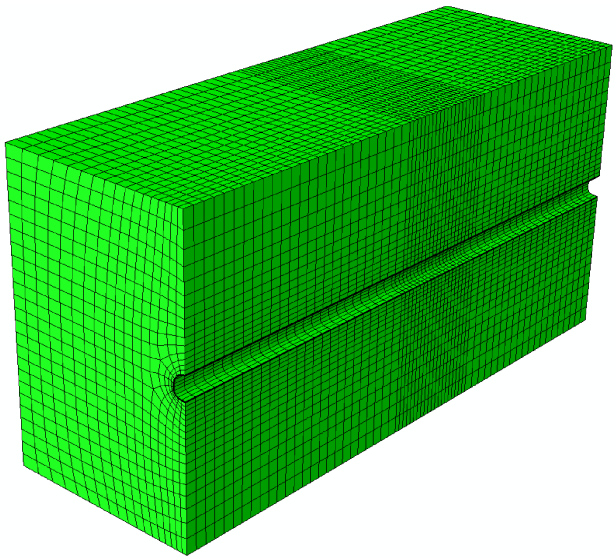

Figure 5.5: FE mesh of the model with (C3D8R) brick element

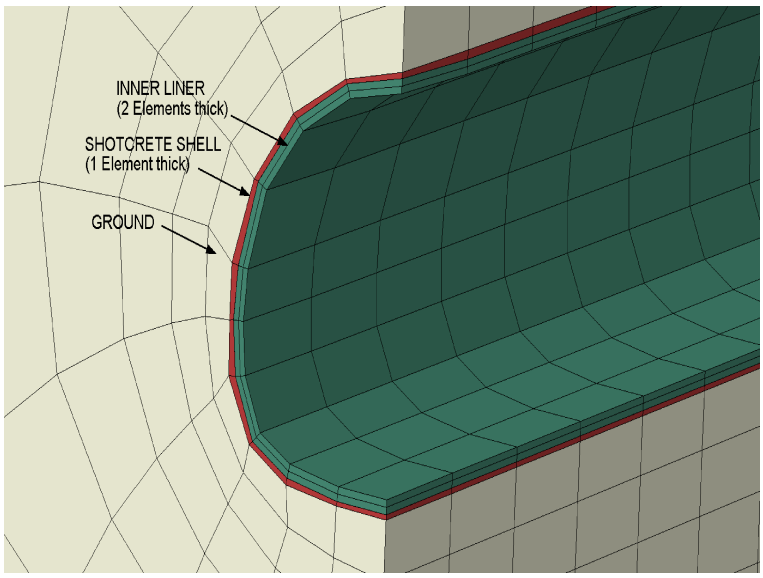

Figure 5.6: Close view of the FE mesh used in the model

strain increment vectors is defined by the flow rule. Using the concept of plastic potential function g in the fluid-flow, we define the flow rule as

$$d\varepsilon_{ij}^{p} = d\lambda \frac{\partial g}{\partial \sigma_{ij}} \tag{5.1}$$

where $d\lambda$ is a non-negative scalar function and gradient vector $\partial g/\partial \sigma_{ij}$ defines the direction of the plastic strain increment vector $d\varepsilon_{ij}^{p}$, *i.e.*, normal to the potential surface $g = 0$ at the current stress point. Due to this the rule is also called normality condition. The flow rule is termed associated if the plastic potential surface has the same shape as the yield surface, *i.e.*, $g = f$ and the flow rule is given by

$$d\varepsilon_{ij}^{p} = d\lambda \frac{\partial f}{\partial \sigma_{ij}}, \tag{5.2}$$

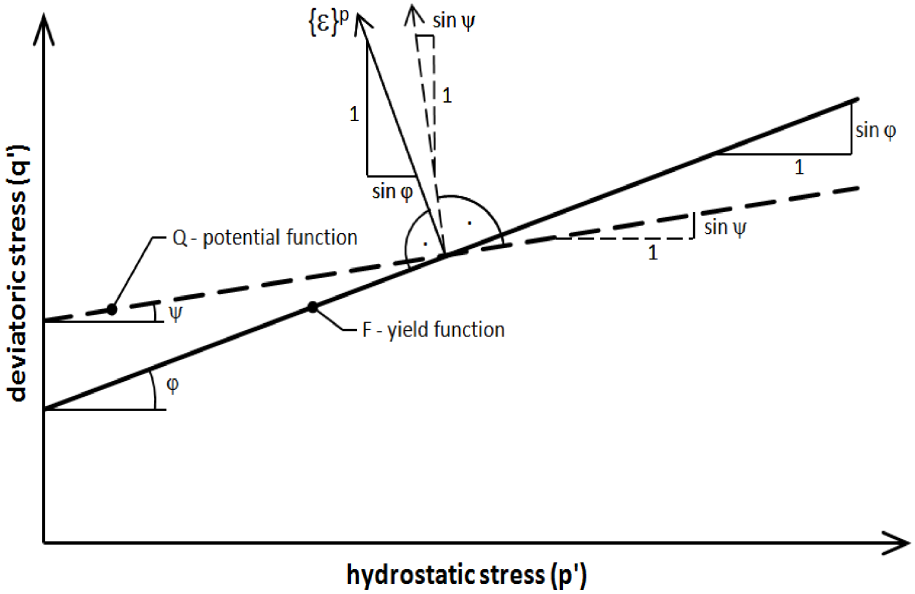

Figure 5.7: Basic principle of non-associated flow rule; after [8].

In this case plastic strain develops along the normal to the loading surface. Associated flow rule with a coulomb yield function leads to an overestimation of dilation in soil and concrete. A frictional material for which the plastic strain rate vector at a point on the yield surface is not in general normal to the surface are said to follow non-associated flow rule using Coulomb criterion as shown in Fig. 5.7.

The loading criteria for a plastic material requires that the stress increment vector $d\sigma_{ij}$ be tangent to the yield surface, whereas the flow rule requires that the plastic strain increment vector $d\varepsilon^p_{ij}$ be normal to the plastic potential surface. The total strain increment is assumed to be the sum of the elastic strain increment and the plastic strain increment:

$$d\varepsilon_{ij} = d\varepsilon^e_{ij} + d\varepsilon^p_{ij}. \tag{5.3}$$

The stress increment and the elastic strain increment are related through Hooke's law:

$$d\sigma_{ij} = C_{ijkl} d\varepsilon^e_{kl} \tag{5.4}$$

Where C_{ijkl} is the tensor of elastic stiffness. Using equation (5.1), the stress-strain relations for an elasto-plastic material are expressed as

$$d\sigma_{ij} = C_{ijkl}\left[d\varepsilon_{kl} - d\lambda \frac{\partial g}{\partial \sigma_{kl}}\right] \tag{5.5}$$

The plastic deformation of Coulomb material is accompanied by an increase in volume called dilation if ($\psi \neq 0$). Clays (regardless of over-consolidated layers) are characterized by a very low amount of dilation ($\psi \approx 0$). The dilation angle (ψ) is related to the friction angle (ϕ) and angle of internal friction (ϕ_i) by [72] as;

$$\phi = \phi_i + \psi \tag{5.6}$$

For non-cohesive soils (sand, gravel) with the angle of friction $\phi > 30°$ the value of dilation angle can be estimated as

$$\psi = \phi - 30° \tag{5.7}$$

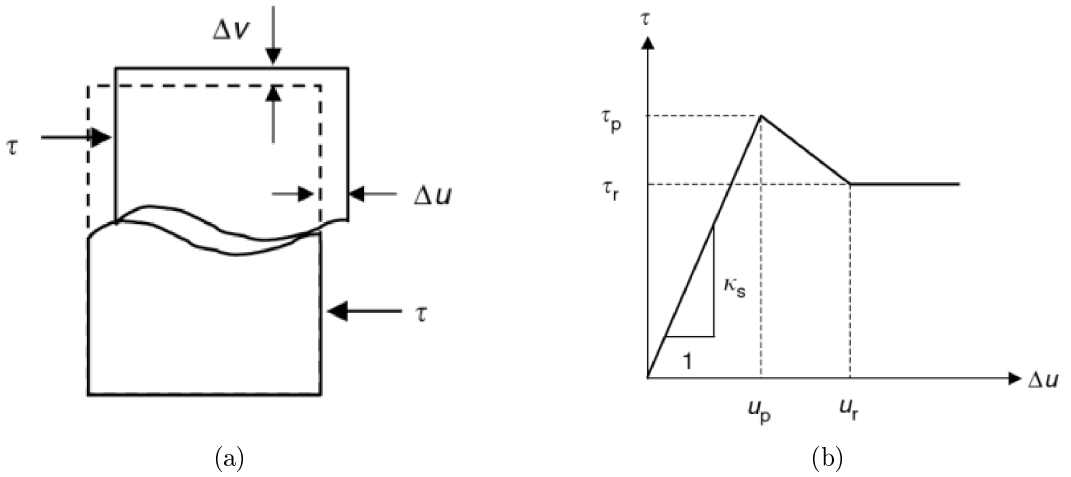

(a) (b)

Figure 5.8: (a) Schematic diagram of a fracture sheared under constant normal stress. (b) Shear stress as a function of shear displacement; adapted from [74].

Dilation angle is assumed to be zero for the values of friction angle less than 30°. Shear deformation causes normal and shear displacements to occur in rock and soil in the form of dilation because the asperities of one fracture surface ride up those of the other [73]. Displacement parallel to the nominal fracture plane is the shear displacement denoted by Δu, whereas that perpendicular to the fracture surface is the dilation denoted by Δv. A plot of shear stress and shear displacement with shear stiffness, ks can be seen in Fig. 5.8.

The change in the volume during the failure is not considered in this study and therefore the dilation angle is taken as $\psi = 0$.

5.6 Material parameter and Material Model

The main physical-mechanical parameters used in the analysis included the Young's modulus E, the Poisson's ratio ν, the cohesion c, the friction angle ϕ, and the dilation angle ψ. The rock mass and support elements were assumed to be homogenous and isotropic. The material parameters of the shotcrete used in the analysis were determined by a series of uniaxial and triaxial tests performed in the laboratory of the Chair of Subsurface Engineering at Montan University. The concrete samples were tested at the Institute of Rock Mechanics and Tunneling of the Technical University Graz. (See Chapter 2 Deterioration of Tunnel Lining). Tab. (5.1), summarizes the main physical-mechanical properties of the surrounding rock mass, the shotcrete shell and the inner liner used in the numerical simulation.

5.7 Contact formulations

In the numerical model suitable contact conditions were defined between interacting surfaces as shown in Fig. 5.9. The specific regions of the model and different components of the assembly that can potentially come into contact with each other include;

1. Ground and shotcrete shell

Table 5.1: Material parameters used in the finite simulations

Parameters	Rock	Shotcrete	Liner (concrete)
Construction model	Mohr-Coulomb	Mohr-Coulomb	Elastic
Unit weight γ (kN/m^3)	27.00	23.64	25.02
Young's modulus E (MN/m^2)	500	10000	30500
Poisson's ratio ν	0.4	0.2	0.2
Cohesion c (kN/m^2)	3000	9000	–
Friction angle ϕ (°)	35	36	–
Dilation angle ψ (°)	0	0	0

2. Shotcrete shell and inner liner

5.7.1 Interaction between shotcrete lining and surrounding ground

The shotcrete liner and ground were fused together using tie constraint for a rigid body that allows one to constrain the motion of regions of the assembly to the motion of a reference point. The shotcrete shell is constrained to move with the exposed tunnel surface after the excavation to model the interaction between the shotcrete lining and the surrounding rock mass throughout the simulation. No slippage is allowed between the interacting surfaces.

5.7.2 Contact formulations between shotcrete shell and inner liner

When surfaces are in contact they usually transmit shear as well as normal forces across their interface. To provide waterproofing characteristics, a PVC geomembrane was placed between the shotcrete shell and the inner liner. The contact between the shotcrete shell and the inner liner was then modeled using the following interaction behavior;

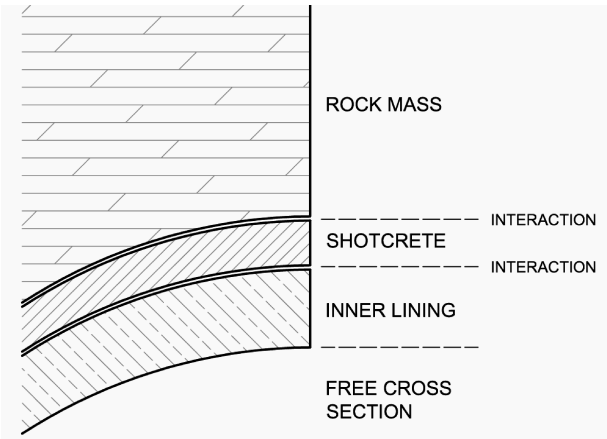

Figure 5.9: Model design showing interaction between different interacting surfaces; after [68].

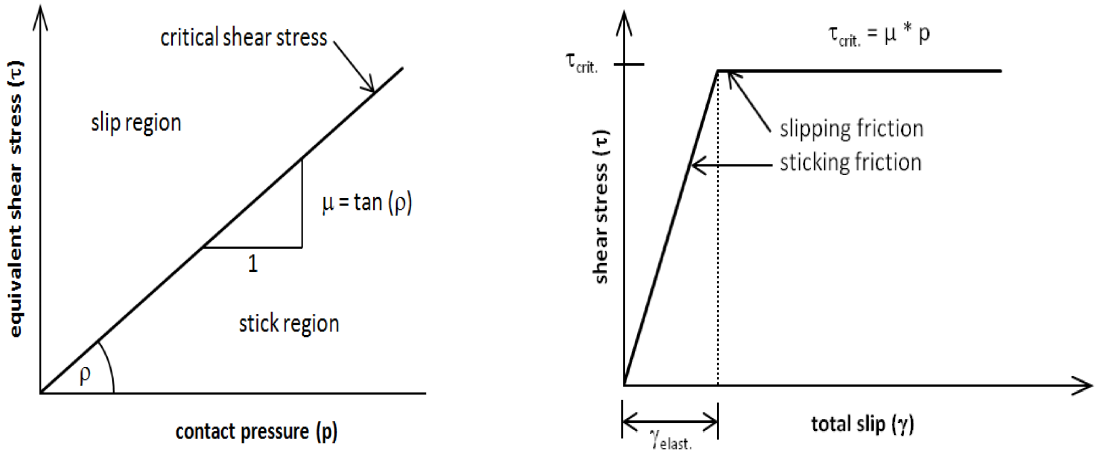

(a) (b)

Figure 5.10: (a) Coulomb friction law. (b) and elastic slip behavior; [70].

Tangential behavior:

- In defining the tangential behavior between the interacting surfaces the basic Coulomb friction law was invoked with a friction coefficient of $\mu = 1$ and no cohesion to provide the possibility for finite sliding/slippage as shown in Fig. 5.10.

- The Coulomb friction model defines the critical shear stress, τ_{crit}, at which sliding of the surfaces starts as a function of the contact pressure, P, between the surfaces.

$$\tau_{crit} = \mu * P \tag{5.8}$$

- To achieve numerical convergence, an elastic slip of $\gamma_{\text{elast}} = 1$ mm is defined. In other words, the maximum transferable shear stress τ_{crit} is reached after a displacement of 1 mm.

Normal behavior:

- Separation of the two surfaces was allowed once contact had been established between the contacting surfaces. This eliminates the possibility for transfer of tensile stresses.

- To ensure numerical convergence a so called "hard contact" as shown in Fig. 5.11, is implemented. After the clearance between the two surfaces is closed a transfer of normal stresses-contact pressure is possible.

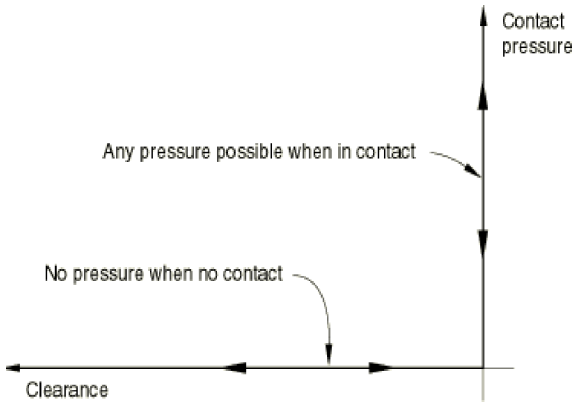

Figure 5.11: Contact normal behavior "hard contact"; [70].

5.8 Numerical implementation of rock bolting

The effect of bolting was included in the simulation by means of increased soil cohesion in the reinforced volume. Rock bolt can transfer normal forces, shear forces and bending moments to the grid. The original failure envelope is thereby shifted upwards, indicating an improvement of the apparent strength parameters (σ_c, ϕ), as represented by the Mohr-Coulomb diagram in Fig. 5.12. The support expansion pressure is defined by the following equations;

$$p_A = \sigma_3 = \frac{F_A}{A} \tag{5.9}$$

$$A = \frac{r_0 + k \cdot l_a}{r_0} \cdot A_0, \tag{5.10}$$

where F_A is the tensile strength or yield point of anchor, A is the associated surface of the anchor effect, r_0 is the tunnel radius, k is the geometric factor, l_a is the anchor length, and A_0 is the assigned area of the anchor effect on the cavity.

Passive approach:
According to this approach unconfined compressive strength of rock increases with nailing. An increase in the cohesion value of the rock in the plastic field (residual cohesion) on the basis of equation (5.11) was suggested by [75]. For straight raised vertical fracture, the increased cohesion is given by;

$$\Delta c_P = \sigma_3 \cdot \frac{1 + \sin\phi}{2\cos\phi}, \tag{5.11}$$

where σ is the confinement produced by the action of rock bolt.

Active approach:
Active approach dictates that horizontal displacement of the axis is caused due to increased compressive strength by the confinement

$$\Delta c_P = \sigma_3 \cdot \tan\phi. \tag{5.12}$$

5.9 Sources of nonlinearities

All physical structures are nonlinear in that the structure's stiffness changes as it deforms. There are three types of nonlinearities in structural mechanics simulations:

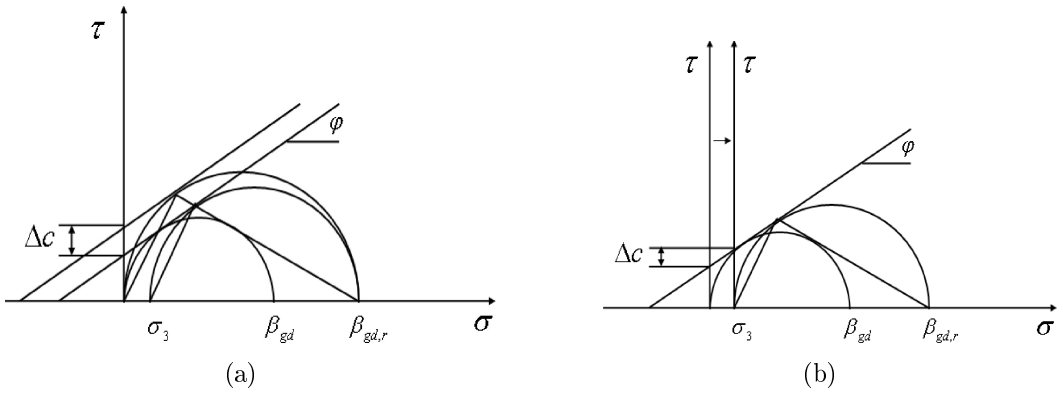

Figure 5.12: Effect of rock anchoring on the failure envelope; (a); passive approach of increasing cohesion in 2D Mohr-Coulomb diagram, (b); active approach of increasing cohesion in 2D Mohr-Coulomb diagram, after [76].

1. Material nonlinearity
2. Geometric nonlinearity
3. Boundary nonlinearity

1. Material nonlinearity:

Material nonlinearity depends on current deformation state and possibly past history of the deformation. Other constitutive variables (temperature, prestress, moisture, time etc.) may be involved. In fact all materials show a nonlinear behavior. Material nonlinearities may give rise to very complex phenomenon such as path dependence, localization, fatigue, shake down and progressive failure. In the category of material nonlinearity, elasto-plasticity and creep are major issues analyzed using generally the strain incremental theory. Materials exhibiting nonlinear behavior include rubber or polymers, nonlinear plasticity or viscoplasticity in concrete or bitumen. In this study mostly elastic material behavior was considered. Nevertheless due to time dependency of elastic parameters, additional schemes mingled with solutions for nonlinear elasto-plastic material were implemented. Nonlinear simulations were broken into a suitable number of load increments steps and approximate equilibrium configurations were found at the end of each load increment.

2. Geometric nonlinearity:

This type of nonlinearity is introduced by change in geometry as a result of large displacements. Change in geometry as the structure deforms is taken into account in setting up the strain-displacement and equilibrium equations. The structure responds to the applied load in under going through large deflections or changes in structure stiffness as the load increases. In the present study geometric nonlinearity may be entailed by the excavation of tunnel, where large displacements are expected.

3. Boundary nonlinearity:

Boundary nonlinearity occurs if the boundary conditions undergo any change during analysis. This type of nonlinearity is extremely discontinuous. When contact between different flexible components, or structural assemblies are established as a result of progressive displacement during simulation, there is large and immediate change in the response of the structure. In boundary condition or "contact" nonlinearity the stiffness of

the structure or assembly may change considerably when two or more parts either contact or separate from initial contact. Nonlinearities may arise at the constrained contact interface between shotcrete shell and the ground as well as between shotcrete shell and the inner liner due to friction and contact pressure. For obtaining solutions for FE nonlinear problems, ABAQUS make use of the Newton-Raphson methods in which load is applied incrementally and for each increment, iteration is performed until convergence is achieved. In the analysis, a step takes place over a finite period of "time". One has to specify the initial time-increment, $\Delta T_{\text{initial}}$, and the total time, T_{total}. The ratio of the initial time increment to the step time gives the proportion of load applied in the first increment. The initial load increment is given by $\Delta T_{\text{initial}}/T_{\text{total}} \times Load$.

Considering linear analysis one step can be calculated using one increment. In nonlinear analysis one has to select optimum initial increment size so that if simulation may encounter trouble in obtaining a solution using too large load increment, perhaps because the model may undergo plastic deformation, increment size has to be reduced.

5.10 Simulation of tunnel excavation and support phases

Considering the widely recognized fact that the tunnel excavation process induces a typically 3D stress and strain field, a three-dimensional numerical model was used in the simulation. The significant amount of disturbance induced ahead of the excavation front produces pre-convergence and surface displacements before the passage of excavation. Using 3D simulation with elastic model, pre-convergence values of about 27% of the final displacement were reported by [77]. Excavation and lining cases studied in this work are referred to the highway tunnel profile with polycentric cross-section. The tunnel was constructed following a top heading, bench and invert excavation sequence. Bench excavation started after advancing the top heading for 40 m and excavation of invert initiated after the bench advanced for 60 m. Excavation and lining phases are simulated through 186 different analysis steps using a step-by-step approach by successive removal of continuum elements in front of the tunnel face while successively installing shotcrete lining behind the tunnel face. For an excavated element, just prior to the excavation step, the forces that the element to be excavated is exerting on the remaining part of the model at the nodes on the boundary between them are stored. The effect of the excavated elements on the rest of the model is then calculated. The excavated elements remain inactive during subsequent analysis steps. It should be noted that just after the reactivation of support elements, the newly added shotcrete lining in the current analysis step carried no stress as it was installed after the deformation of rock mass caused by the excavation in the previous step, i.e, it was a passive support. The detailed analysis procedures employed during this sequential excavation model is as follows:

1. Step 1: Introducing the initial stress state to reach equilibrium before tunnel excavation begins. The representative elements of shotcrete lining and inner lining are deactivated, as there is no lining at the beginning of the analysis Fig. 5.13.

2. Step 2: Excavation of the top heading is achieved using the model change option in the ABAQUS. This option has been intensively used throughout the analysis to perform the removal and reactivation of lining elements.

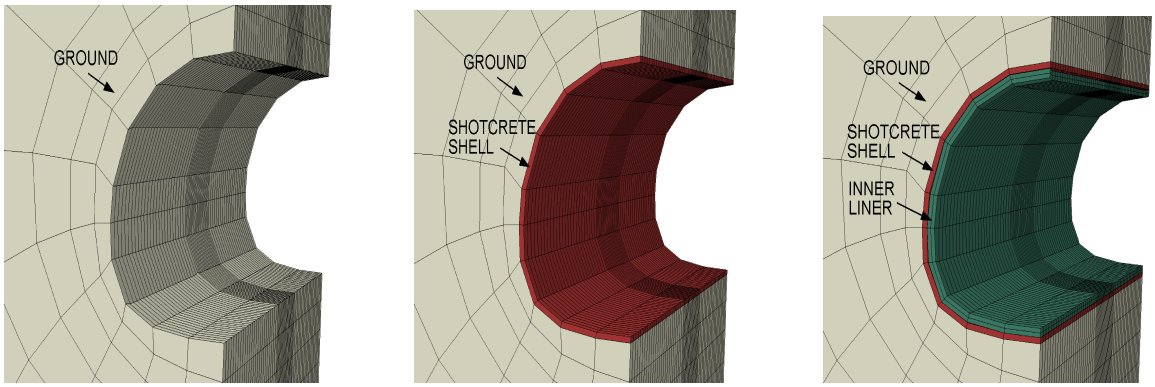

(a) (b) (c)

Figure 5.13: (a); shotcrete and liner deactivated, (b); shotcrete activated, (c); liner activated.

3. Step 3: The beam elements representing the shotcrete support in the top heading area are activated to provide initial support to the excavated surface.

4. Step 4: The excavation of continuum elements deactivation in the top heading, bench and invert area followed by activation of shotcrete lining elements in the respective area is continued until completion of the tunnel excavation at step 167.

5. Step 5: The inner lining elements are activated in segments of 12 m starting from step 168 till completion at step 186.

6. Step 6: The deterioration of shotcrete properties simulated from step 187 till 195, the last step for completion of analysis.

The detailed configuration of excavation and support installation phases in the top heading, bench and invert area are depicted in Fig. 5.14.

5.11 Simulation of shotcrete lining deterioration

Deterioration process of shotcrete shell was simulated using C3D8R and C3D8 types of elements in the shotcrete and inner liner. The degradation of material properties of the shotcrete shell was simulated using the user subroutine USER DEFINED FIELD (USDFLD). This subroutine provided the facility to define field variables for a material as function of time. The material properties were linked to the field variables and supposed to change in the particular calculation step defined in the analysis. The complete break up of the simulation takes the following configuration;
STEP 1 to STEP 167: Simulation of tunnel construction
STEP 168 to STEP 186: Simulation of inner lining construction
STEP 187 to STEP 195: Simulation of the shotcrete shell deterioration
The deterioration of shotcrete was assumed to be linear. The material properties were reduced by 10% in each calculation step beginning with STEP 187, till 90% of its initial value in STEP 195. The purpose was to see the effect of this reduction on the stresses in the shotcrete liner as well as its dissipation into the inner liner or surrounding ground. To investigate the deterioration of material properties the following parameters were reduced separately and in different combinations in the simulation;

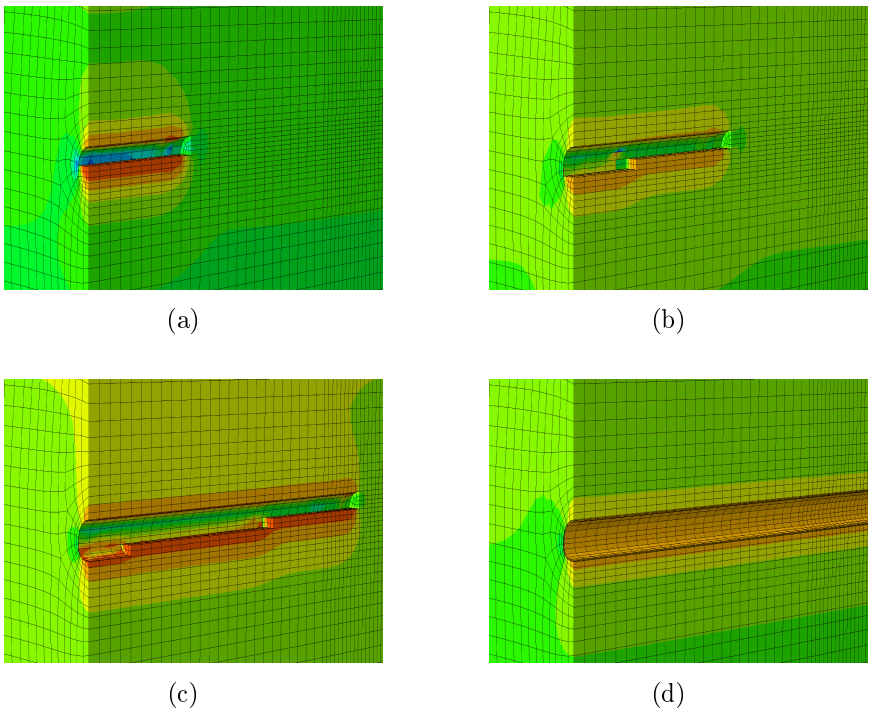

Figure 5.14: Visualization of the tunnel excavation and support process. Vertical stresses around the tunnel are shown, (a); top-heading excavation, (b); top-heading followed by bench, (c); incl. invert, (d); installation of the inner lining after the excavation is finished.

- Young's modulus (E)
- Cohesion (c)
- Friction angle (ϕ °)
- Young's modulus plus cohesion (E and c) simultaneously
- Young's modulus plus cohesion plus friction angle (E and c and (ϕ °)) simultaneously

The strength values for the above mentioned parameters related to various calculation steps are presented in Tab. 5.2. One calculation was run with 99.99% reduced values of Young's modulus, cohesion and friction angle of the shotcrete to see the effect of this magnificent reduction on the support system.

5.12 Results and discussion

The detailed discussion and interpretation of the observed results of numerical calculation are presented in this chapter. In this study a three-dimensional model was adopted to simulate a sequential excavation method of tunnel construction and support. The effect of stresses and deformations in the surrounding ground and initial shotcrete support during the excavation of top heading bench and invert were investigated. The evolution of stress fields of the rock mass and shotcrete lining is depicted in Fig. 5.14. First part of the results

deals with the evaluation of stresses (and deformations) produced during construction of the tunnel. It also considers stresses (if any) acting on the inner lining during its installation. The second part of this research was focused on the investigation of stresses and radial displacements in the inner liner that were induced during the deterioration of shotcrete shell. A rigorous numerical analysis of the support degradation problem was a complicated task because of the presence of several types of materials and their interaction and the 3D nature. Separate cases were considered to see the effects of deterioration of strength properties of the shotcrete shell on the entire support system comprising of surrounding rock mass, shotcrete lining and permanent inner lining. The effect of particular element types used in the simulation was also observed. Some abbreviations were also used for the purpose of convenience inside the text or in the figures. All such abbreviations could be found in the list of abbreviations. The most commonly used ones included;

SHOT numerical model of the shotcrete shell
LINER numerical model of the inner liner

5.13 Tunnel construction

The primary stress in the initials state was 6.8 MPa in the position of the tunnel axis. Through the sequential excavation of top-heading, bench and invert the stress pattern changes during the whole process. The numerical values were extracted from the excavation step chosen in the middle section of the model, where a finer mesh generation was used for better numerical accuracy. Fig. 5.15, shows radial displacement of the tunnel and shotcrete shell in the crown area. The displacement value of 8 cm resulting from top heading excavation progressively increased during excavation of the bench. It reached to its maximum level of 9.2 cm with the invert excavation, and thereafter no further displacement was observed when the invert closure was completed, so that the final steady state settlement occurred at some point of invert. Thus the expedient invert closure will help to reduce settlement. Shotcrete support was applied after 2.2 cm displacement of the rock mass had already been happened. Obviously shotcrete support did not inhibit further displacement of the tunnel perimeter altogether, nevertheless it helped in slowly

Table 5.2: Deterioration of Young's modulus, cohesion and friction angle of shotcrete

Step	Deterioration	E(GPa)	c(MPa)	(ϕ (°))
Step 186	0%	10.0	9.0	36.0
Step 187	10%	9.0	8.0	35.0
Step 188	20%	8.0	7.0	34.0
Step 189	30%	7.0	6.0	33.0
Step 190	40%	6.0	5.0	32.0
Step 191	50%	5.0	4.0	31.0
Step 192	60%	4.0	3.0	30.0
Step 193	70%	3.0	2.0	29.0
Step 194	80%	2.0	1.0	28.0
Step 195	90%	1.0	0.5	27.0

bringing the system towards stability. The results illustrated that most of the displacement took place during excavation of the top heading. In situations where strict control of the displacements is mandatory, alternate means e.g. fore-poles will produce satisfactory results.

The tangential stresses in the shotcrete shell are illustrated in Fig. 5.16. The stresses were calculated using C3D8R (8-node linear brick reduced integration) and C3D8 (8-node linear brick) types of elements exhibiting linear elasto-plastic material behavior based on the Coulomb failure criterion. The tangential stress in the spring line of the shotcrete shell calculated in the middle finer mesh region of the model using C3D8R type of elements was 16.5 MPa initially when only top heading excavation was implemented. The stress value increased further with the advancing of bench to 22.7 MPa and finally reached a maximum value of 24.9 MPa with the excavation of invert. Generally a very similar stress distribution was observed using C3D8 type of elements in the shotcrete shell. The stress values selected for plotting represented the highest of all integration points in the element. The tangential stress values calculated at the same locations in the shotcrete shell amounted to 14.7 MPa with the excavation of top heading. It increased to 22.7 and 25.5 MPa with the bench and invert excavation respectively. The stress pattern showed that using C3D8 elements, comparatively low level of stress was developed during excavation of top heading only, whereas same quantity of stress was generated for both types of elements during excavation of bench and invert. As shown in Fig. 5.15, young shotcrete allowed sufficient deformation to take place which would otherwise break due to high stresses during excavation of the top heading. The shotcrete got hardened to withstand stresses during subsequent phases of bench and invert excavation. The installation of the inner lining started when the tunnel was fully excavated and shotcrete shell installed, and deformations of the systems were down to zero. At this point there was already a state of equilibrium between the rock mass and the sthotcrete shell, and there would be no further displacement in the shell as long as primary support elements

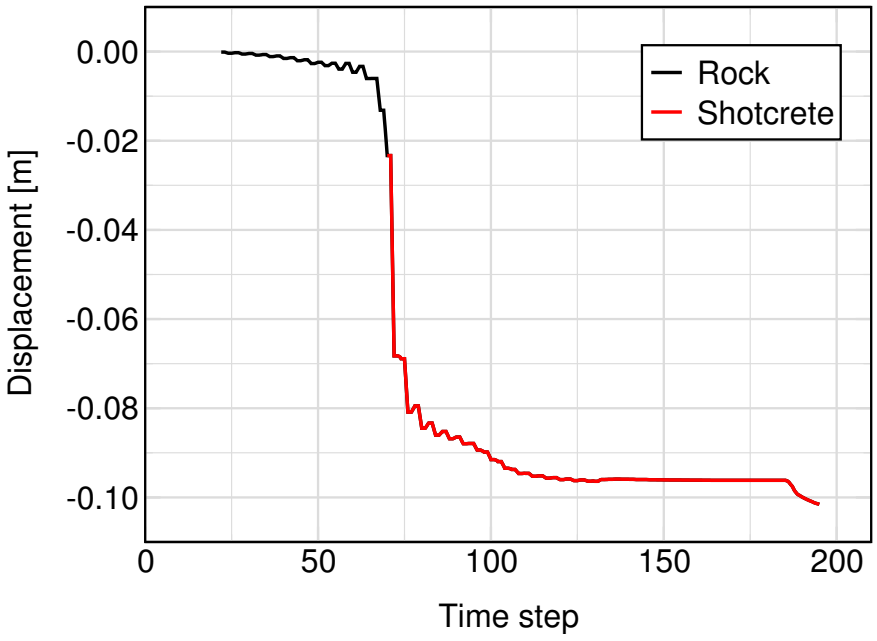

Figure 5.15: Overview of radial displacements of the rock and shotcrete liner obtained at the crown

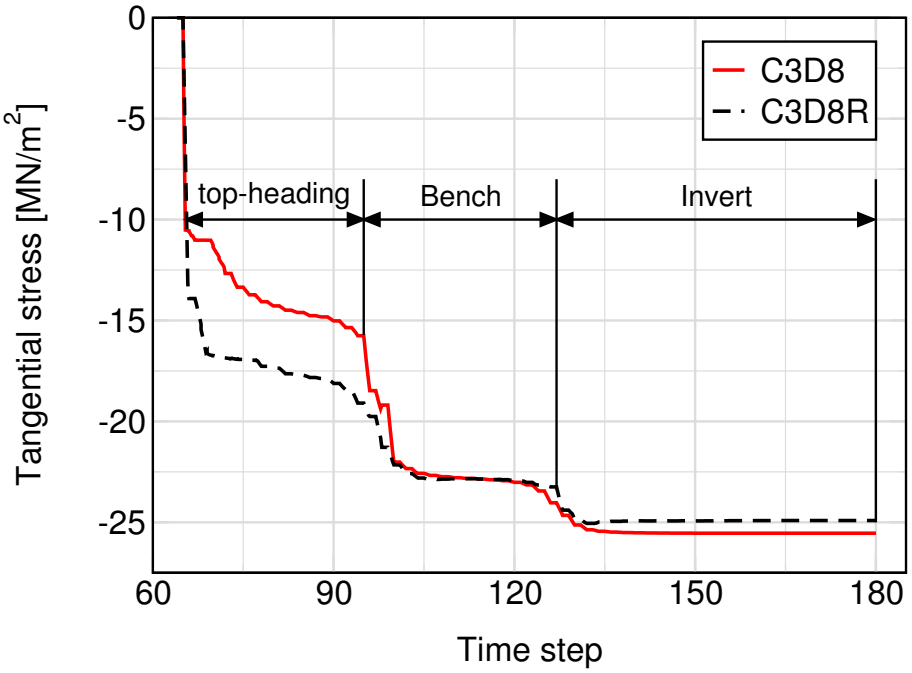

Figure 5.16: Tangential stress at the spring-line in the shotcrete shell. Comparison of stresses for the two element types (C3D8R and C3D8)

kept their full strength. Ideally the inner liner should be free of stresses at installation. As can be seen in Fig. 5.17, the inner liner was having zero stresses at its installation. It remained stress free till the time when shotcrete properties were degraded to simulate shotcrete deterioration. The numerical results also demonstrated the spreading of small plastic zone at the immediate vicinity of the side wall of the excavation face as shown in Fig. 5.18. The magnitude of plastic strain increased with the increase of stresses in the surrounding ground as a result of shotcrete shell deterioration and is illustrated in Fig. 5.19.

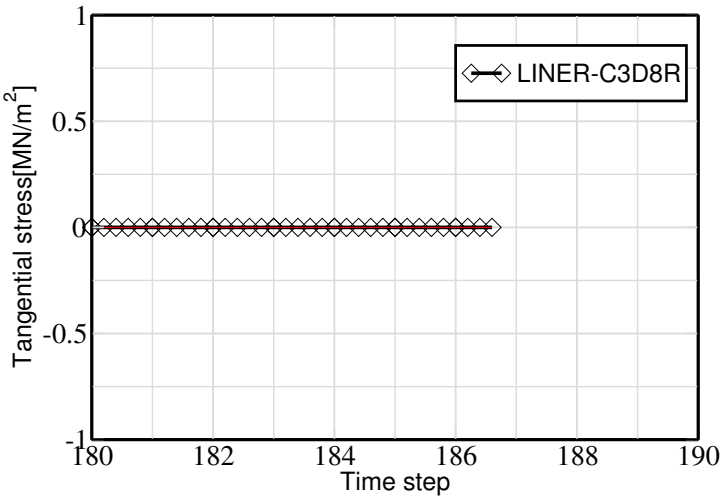

Figure 5.17: Tangential stress at the spring-line in the inner liner

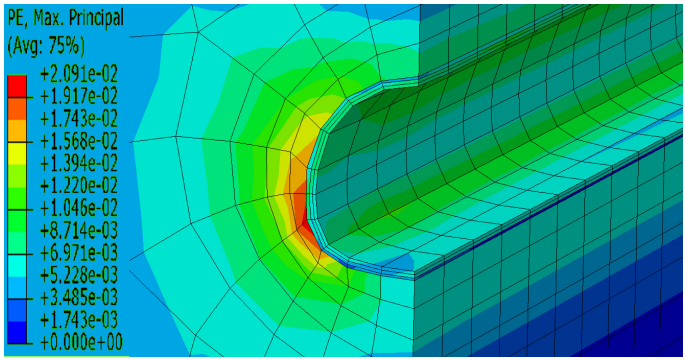

Figure 5.18: Plastic zone generated at the side wall of the tunnel

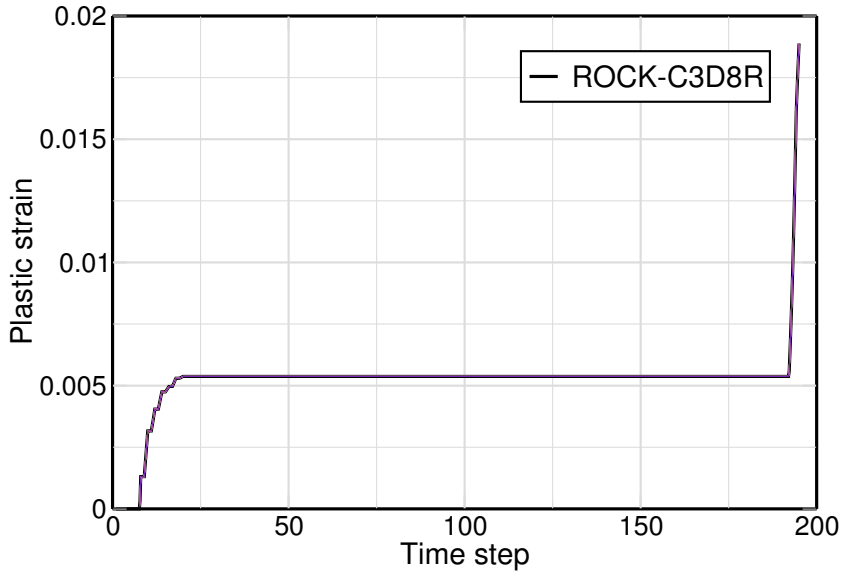

Figure 5.19: Equivalent plastic strain (PEEQ) in the ground; strain value increased with shotcrete shell deterioration at step 186 till end of analysis at step 195

5.14 Deterioration of shotcrete shell

The assessment of the shotcrete deterioration incorporated;

- Evaluation of stress transfer from the shotcrete shell to the inner liner during deterioration of shotcrete support
- Determination of the effects of using different element types (C3D8R, C3D8) on the stresses in the linings
- Investigation of the effects of different deterioration processes of shotcrete shell by lowering strength parameters individually or in different combinations shown in table 6.2.

Two cases were considered to include the effects of particular element type used in the numerical analysis. Both types of elements use Mohr-Coulomb elasto-plastic material behavior;

- Case A: Eight-node hexahedral elements with reduced integration (C3D8R)

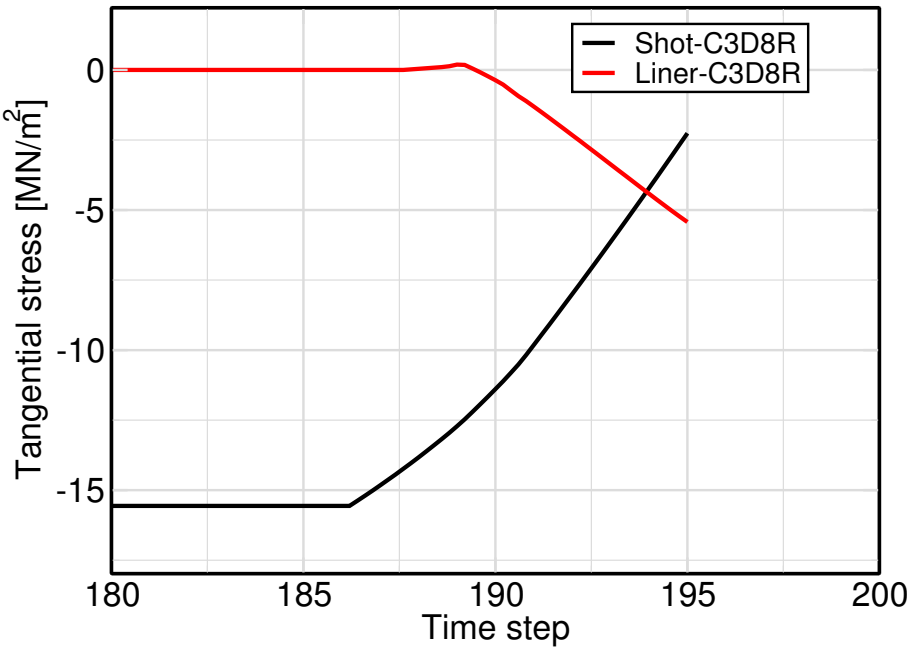

Figure 5.20: Transfer of tangential stresses between shotcrete shell and the inner liner during deterioration of shotcrete; stresses at spring-line; deterioration caused by degradation of Young's modulus; results based on (Case A)

- Case B: Eight-node hexahedral elements with full integration (C3D8)

The special requirement for usage of C3D8 type of elements was realized while multiple integration points were needed for calculation of normal stresses in the slender shotcrete shell modeled with single element thickness. The inner liner was having two elements regarding the thickness and modeled with both types of elements. The results obtained were utilized in calculation of normal forces and bending moments in the lining. Fig. 5.20 illustrates the stress distribution in the shotcrete shell and in the inner liner during deterioration of the shotcrete shell.

The deterioration was simulated by the degradation of the Young's modulus of the shotcrete shell using eight-node hexahedral elements with reduced integration (Case A).

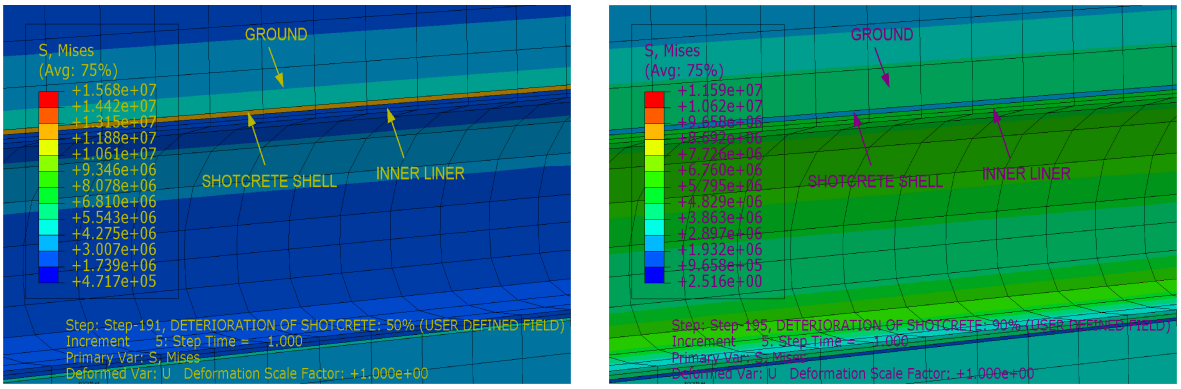

(a) (b)

Figure 5.21: (a) Distribution of stresses in the shotcrete, liner and ground at 50% degradation of shotcrete shell; (b) Stress pattern changed at 90% deterioration of shotcrete shell.

The phenomenon of stress release associated with the deterioration of shotcrete shell and redistribution of the released stress into the inner liner and surrounding ground is shown in Fig. 5.21. The stress states in the shotcrete shell and inner liner during degradation were represented by a set of different curves (black, red) for the analysis step-number 180 till 195. The results depicted that the stresses in the shotcrete shell had stabilized after reaching a steady state value of 15.2 MPa. This value of stress began to drop in a non-linear way with the onset of shotcrete degradation at step 187. The Tangential stresses at the spring line in the shotcrete shell dropped to 2.26 MPa, with the 90% degradation of shotcrete Young's modulus in the analysis step 195. The shotcrete shell had relieved of sizable quantity of stresses with deterioration. Conversely the inner liner which was initially completely stress free had started to load with the commencement of shotcrete deterioration. Tangential stresses at the spring line in the inner liner gradually started to increase and reached as high as 5.43 MPa in the last analysis step. As shown, the stresses in the shotcrete shell decreased more than the stresses in the inner liner increased. Obviously, the stress dissipation as a consequence of shotcrete support degradation did not necessarily transfer exclusively into the inner liner but the surrounding ground had to cater for the lingering stresses. As degradation process proceeded the shotcrete shell gradually liberated of the stresses it inhibited. Fig.5.22 illustrates the stress distribution in the shotcrete shell and inner liner during deterioration of the shotcrete shell.

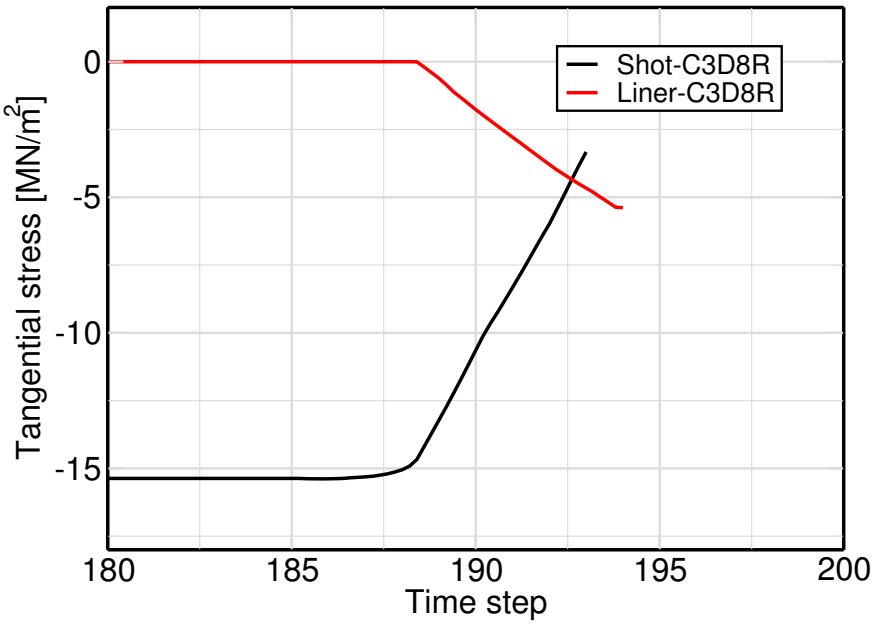

Figure 5.22: Transfer of tangential stresses between shotcrete shell and the inner liner during deterioration of shotcrete; stresses at spring-line; deterioration caused by degradation of shotcrete cohesion; results based on Case A.

The deterioration was simulated by the degradation of the cohesion of the shotcrete shell using eight-node hexahedral elements with reduced integration (Case A). The stress state changed in the system with deterioration of shotcrete lining. Tangential stress at the spring line in the shotcrete shell reduced from 15.2 MPa to 3.44 MPa with 90% degradation of shotcrete cohesion.

On the other hand the tangential stress at the spring-line in the liner raised to 5.38 MPa. This showed that Young's modulus had comparatively more prominent influence on the stress transition than cohesion did. The effects of simulating shotcrete deterioration by

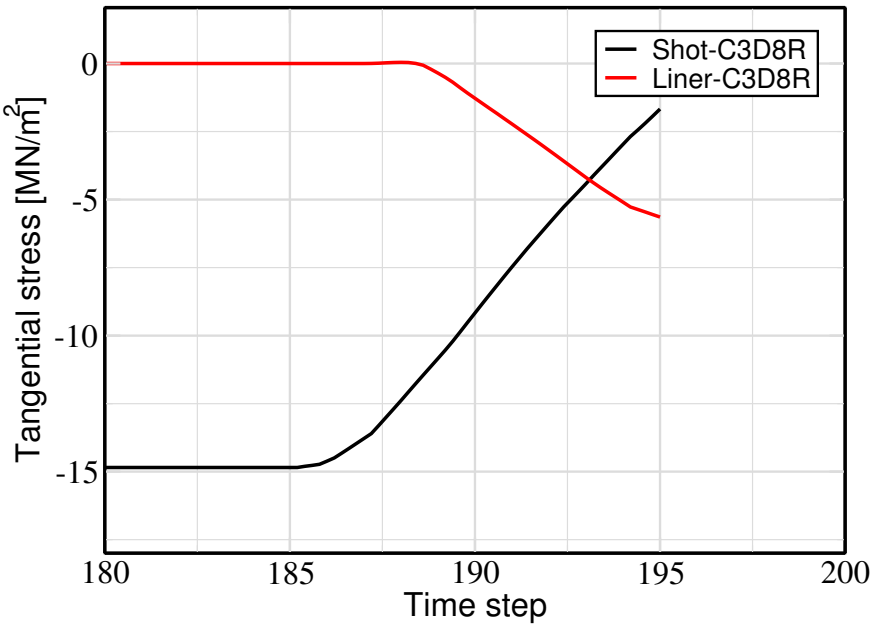

Figure 5.23: Transfer of tangential stresses between shotcrete shell and the inner liner during deterioration of shotcrete; stresses at spring-line; deterioration caused by degradation of shotcrete Young's modulus and cohesion; results based on Case A.

degrading Young's modulus and cohesion of the shotcrete simultaneously could be seen in Fig. 5.23. The tangential stresses in the shotcrete shell reduced to 1.67 MPa with shotcrete deterioration. There seemed to be enormous decrease in the strength characteristics with lowering Young's modulus and cohesion of the shotcrete support. The devastative action was amplified when these factors operated in combination. Consequently the inner liner had to sustain the supplementary load generated due to sufficiently damaged shotcrete shell. This fact led to as high as 5.64 MPa tangential stress value in the spring-line area of the inner liner. To observe the joint effect of reducing Young's modulus, cohesion and friction angle on the shotcrete deterioration, a simulation was run by degrading their values simultaneously using eight-node hexahedral elements with reduced integration (Case A). The tangential stresses in the shotcrete shell reduced to 1.47 MPa with shotcrete deterioration as depicted in Fig. 5.24. Reducing values of all shear strength parameters substantially affected shotcrete deterioration as observed in the analysis. The shotcrete shell was damaged to the extent that it hardly supported any significant quantity of stresses it subsisted. The transfer of stresses from the shotcrete to the inner liner increased during this particular simulation and reached a level of 5.91 MPa. This finding signified the fact that the inner liner was intersected by a considerable magnitude of stresses in case of depletion of shotcrete support. In a separate simulation administered to observe the influence of only reducing friction angle on the stresses, it was found that there occurred no alteration in the position of stresses. Nevertheless, in combination with Young's modulus and cohesion, friction angle materialized to participate in modifying stresses. Up untill now primary support has been assumed not to contribute to the permanent support of the tunnel and that depending on the conditions, it totally deteriorate after several years of its installation.

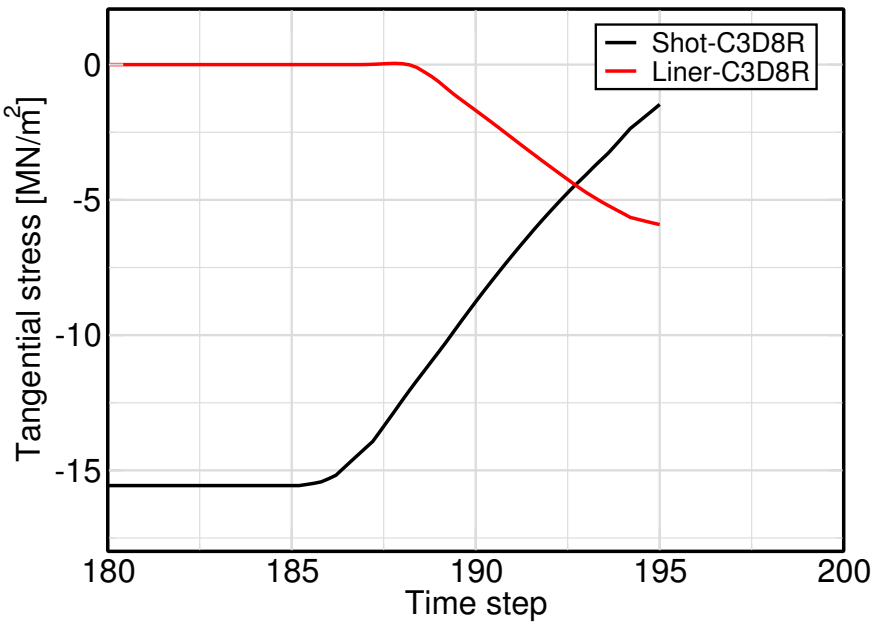

Figure 5.24: Transfer of tangential stresses between shotcrete shell and the inner liner during deterioration of shotcrete; stresses at spring-line; deterioration caused by degradation of shotcrete Young's modulus, cohesion and friction angle; results based on Case A.

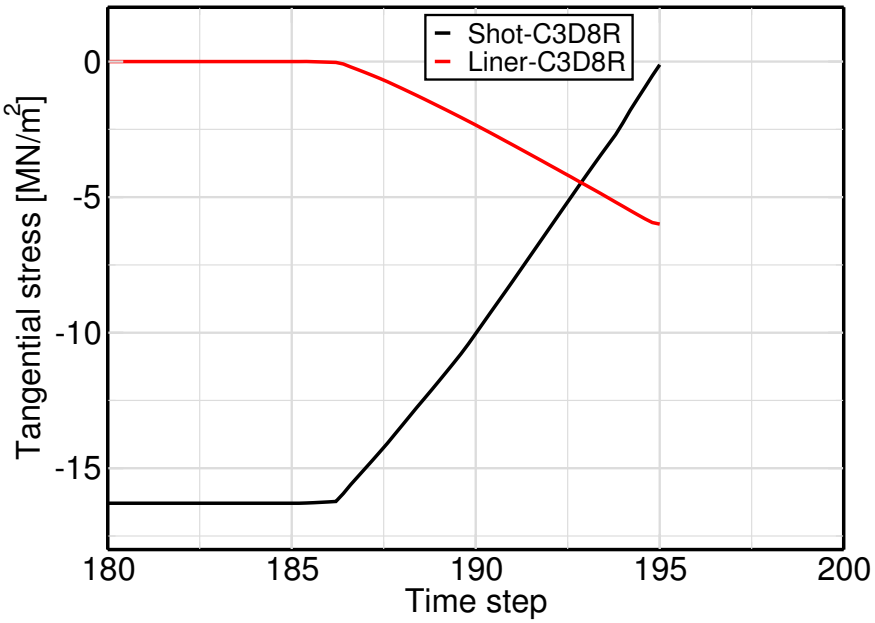

Figure 5.25: Transfer of tangential stresses between shotcrete shell and the inner liner during deterioration of shotcrete; stresses at spring-line; deterioration caused by 99% degradation of shotcrete Young's modulus, cohesion and friction angle; results based on Case B.

In order to discuss a situation by almost complete elimination of shotcrete shell to function as a support member a special case was considered by running a simulation with 99% reduction of the actual properties of the Young's modulus, cohesion and friction angle of the shotcrete using eight-node hexahedral elements with full integration (Case B) as illustrated in Fig. 5.25. There appeared a tremendous amount of decrease in stresses and the shotcrete shell apparently liberated of maximum of the stresses it was holding. The tangential stresses at the spring line in the shotcrete shell reduced to 0.12 MPa. The stress transfer from the shotcrete to the inner liner further increased during this special simulation and reached a level of 6.00 MPa. This high level of stress is crucial to be considered in the design calculation for inner liner, particularly in dealing with long-term stability of support elements under aggressive environments. The outcome of such computations dictates that a full contribution to load bearing of the shotcrete lining during the whole life time may generally be ruled out due to the above mentioned effects. The results also predicted that using Young's modulus as a deterioration factor of the shotcrete, the load transfer started earlier but at a slow rate as compared to that of cohesion, in which case the load transfer started later but at a comparatively faster rate. The elements type (C3D8R, C3D8) had a minor effect on the stresses and displacements in the support elements.

5.15 Normal Forces and Bending Moments

Based on the stress distributions along the shotcrete shell and inner liner, the normal forces and moments along the circumference of the inner liner were investigated. The deterioration levels adopted for calculating normal forces and bending moment were 10%, 30%, 50%, 80% and 90% degradation of shotcrete Young's modulus, cohesion and friction angle separately or in various combinations. The normal forces acting on the inner lining with degradation of shotcrete Young's modulus alone are illustrated in Fig. 5.26. The normal forces increased, as expected, in the final lining by decreasing the material properties of the shotcrete. Generally, the normal forces in the liner seemed to be evenly distributed around the circumference with lower deterioration levels of shotcrete support. Normal force in the liner at the spring-line reached a value of 367 kN/m with 30% degradation of shotcrete. It is also shown that the normal force in the liner reached a maximal value of 1433 kN/m at the spring-line with 90% deterioration of shotcrete. Comparatively lower values of structural forces were obtained at the tunnel crown and invert.

The normal forces in the inner lining with degradation of shotcrete cohesion alone are depicted in Fig. 5.27. The normal forces obtained shows similar distributions but with smaller magnitudes. The normal force at the spring-line reached as high as 1068 kN/m with the deterioration of 80% of shotcrete cohesion. By just decreasing the angle of friction in one of the simulations, no stresses were induced in the inner lining. This is because the angle of friction was decreased between 36° and 25° only and due to this reduction, the stress in the shotcrete shell was still smaller than the compressive strength. Much lower values of friction angle, from the authors view are not realistic.

The normal forces in the inner lining with degradation of shotcrete Young's modulus, cohesion and friction angle are shown in Fig. 5.28. With the decrease of all parameters of the shotcrete support, there was enormous increase in the normal forces acting on the

inner liner. The circumferential axial force in the spring-line region was calculated to be 415 kN/m with 30% degradation of shotcrete. This value kept on increasing with the increase in deterioration level of shotcrete. At 90% deterioration of shotcrete the normal force in the liner reached to 1580 kN/m at the spring-line, indicating the highest value anywhere along the circumference. The normal force values at this deterioration level, calculated at the crown and bottom of the liner were 1440 kN/m and 840 kN/m respectively.

The bending moments in the inner lining with degradation of shotcrete Young's modulus alone are illustrated in Fig. 5.29. The bending moment increased with the degradation of shotcrete. There was slight inward moment at the crown area which diminished while moving towards the spring-line. There is pronounced outward moment in the spring-line and invert, whereas inward moment was observed at the side wall. The negative bending moment at the side wall reached an absolute value of 4.5 kNm/m with the 90% deterioratin of shotcrete. The maximum value of positive bending moment was observed at the invert to be 6.5 kNm/m. The bending moment value increased at the bottom as compared to that at the crown with the increase in degradation level of the shotcrete.

The bending moments in the inner lining with degradation of shotcrete cohesion alone are portrayed in Fig. 5.30. The bending moment had shown similar behavior with the decrease in cohesion value as observed in case of shotcrete Young's modulus degradation but with the reduced magnitude. The maximum positive bending moment observed at the invert had a value of 3.4 kNm/m at 80% degradation of shotcrete.

The bending moments in the inner lining with degradation of shotcrete Young's modulus, cohesion and friction angle are illustrated in Fig. 5.31. The bending moment increased with the degradation of shotcrete. There was remarkable outward moment in the spring-line and invert, whereas inward moment was observed at the side wall. The negative bending moment at the side wall reached an absolute value of 7.6 kNm/m with the 90% deterioratin of shotcrete. The maximum value of positive bending moment was observed at the invert to be 7.8 kNm/m. The bending moment value increased at the bottom as compared to that at the crown with the increase in degradation level of the shotcrete. The higher values of bending moment at the side wall should be given due consideration. The inner side of the lining in the side wall area will be under tension but still within the limit of both compressive failure and tensile cracking in the concrete. At other locations, the loads were also within the limit of concrete capacity. The moderately high values of thrust may counter the effect of bending at the invert.

The normal force and bending moments in the inner lining with 99% degradation of shotcrete Young's modulus, cohesion and friction angle are illustrated in Fig. 5.32. Normal forces and bending moments in the liner were substantially increased after almost full deterioration of shotcrete. The normal force reached an absolut values of 1628 kN/m at the spring-line and relatively low values were obtained at the crown and invert. The bending moment reached a positive value of 8.3 kNm/m at the invert, and the negative bending moment at the sidewall increased to 7.7 kNm/m.

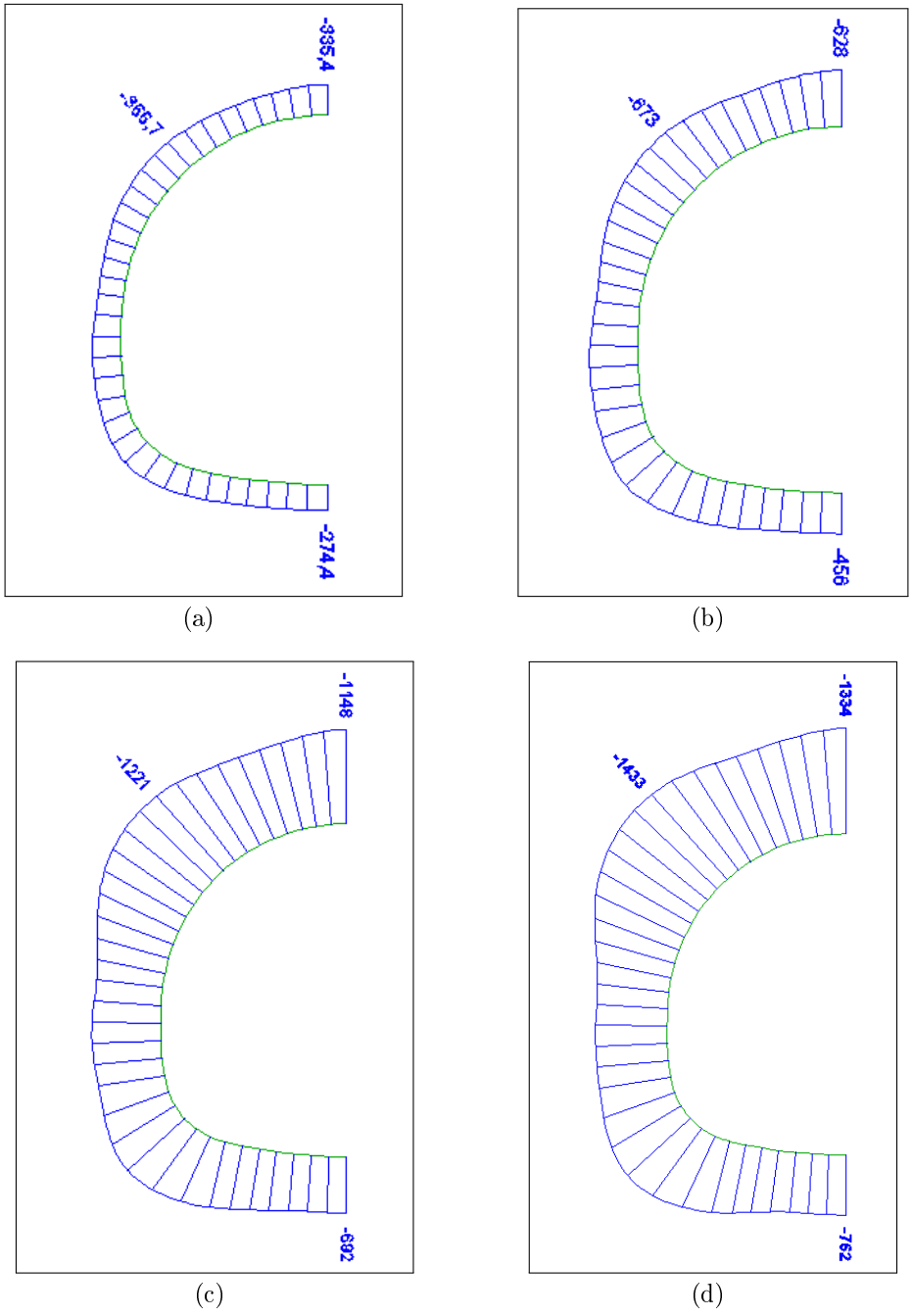

Figure 5.26: The normal forces (kN/m) in the inner lining with degradation of shotcrete Young's modulus, (a); 30% degradation of shotcrete, (b); 50% degradation of shotcrete, (c); 80% degradation of shotcrete , (d); 90% degradation of shotcrete.

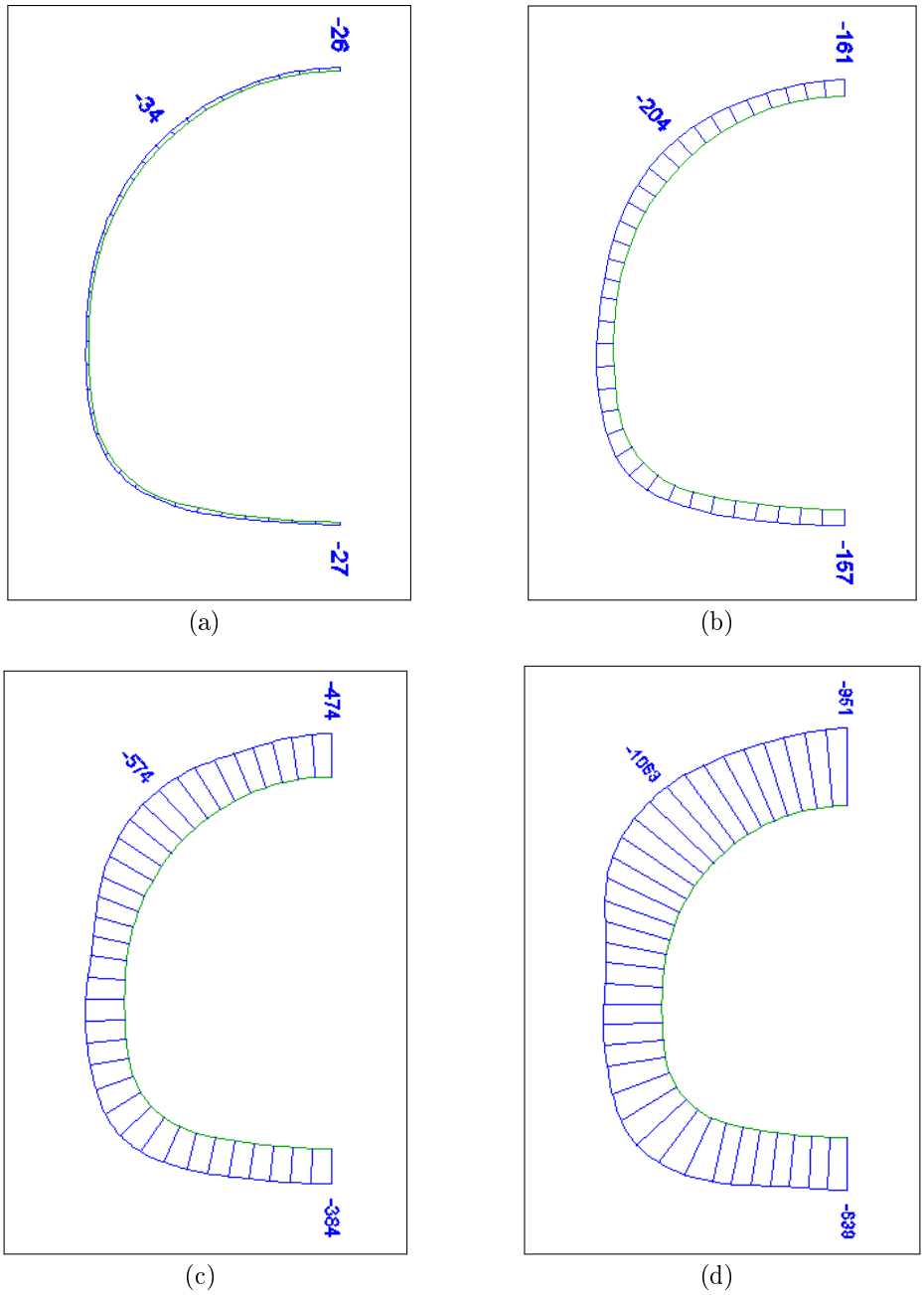

Figure 5.27: The normal forces (kN/m) in the inner lining with degradation of shotcrete cohesion, (a); 10% degradation of shotcrete, (b); 30% degradation of shotcrete, (c); 50% degradation of shotcrete , (d); 80% degradation of shotcrete.

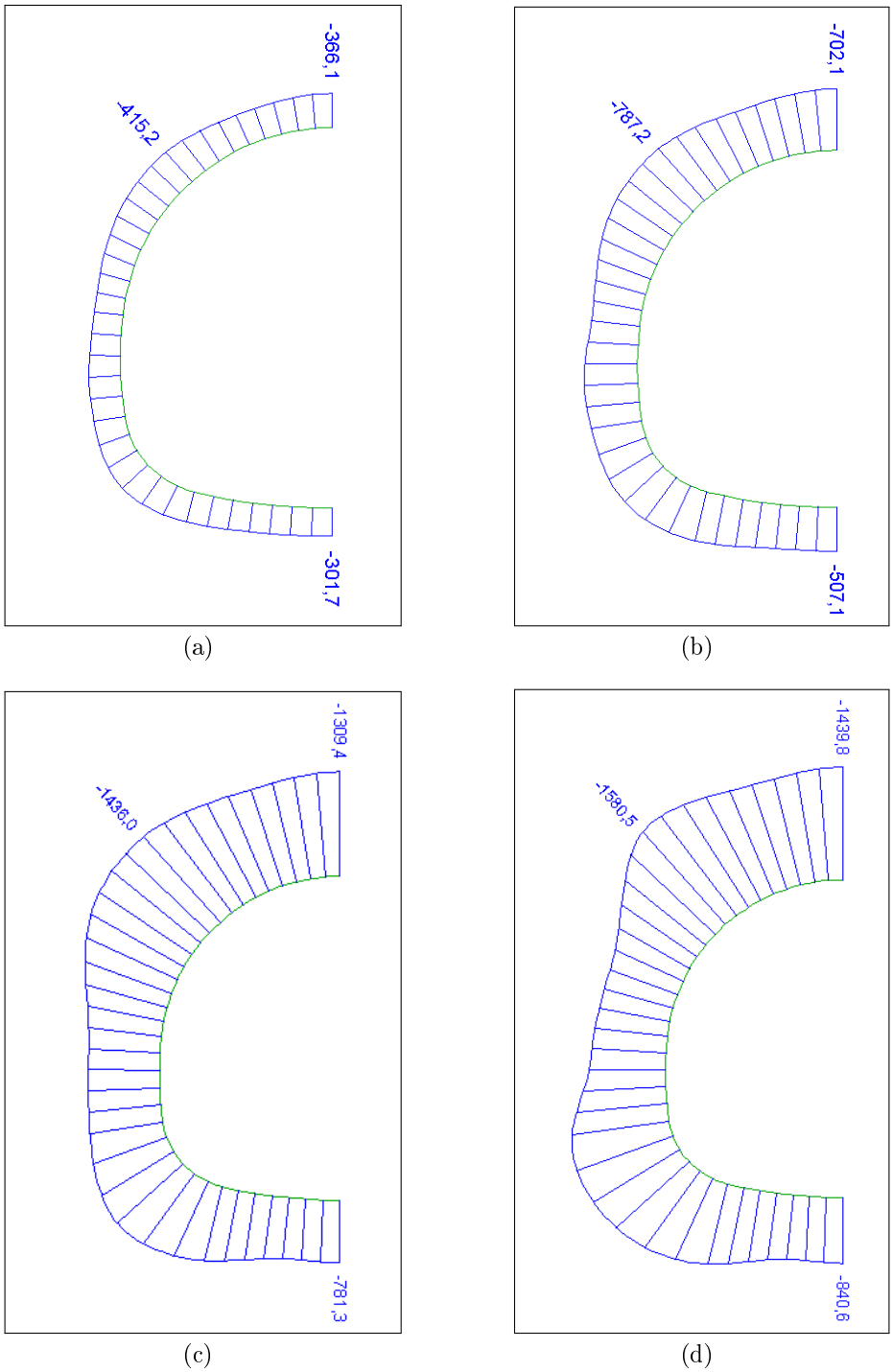

Figure 5.28: The normal forces (kN/m) in the inner lining with degradation of shotcrete Young's modulus, cohesion and friction angle, (a); 30% degradation of shotcrete, (b); 50% degradation of shotcrete, (c); 80% degradation of shotcrete , (d); 90% degradation of shotcrete.

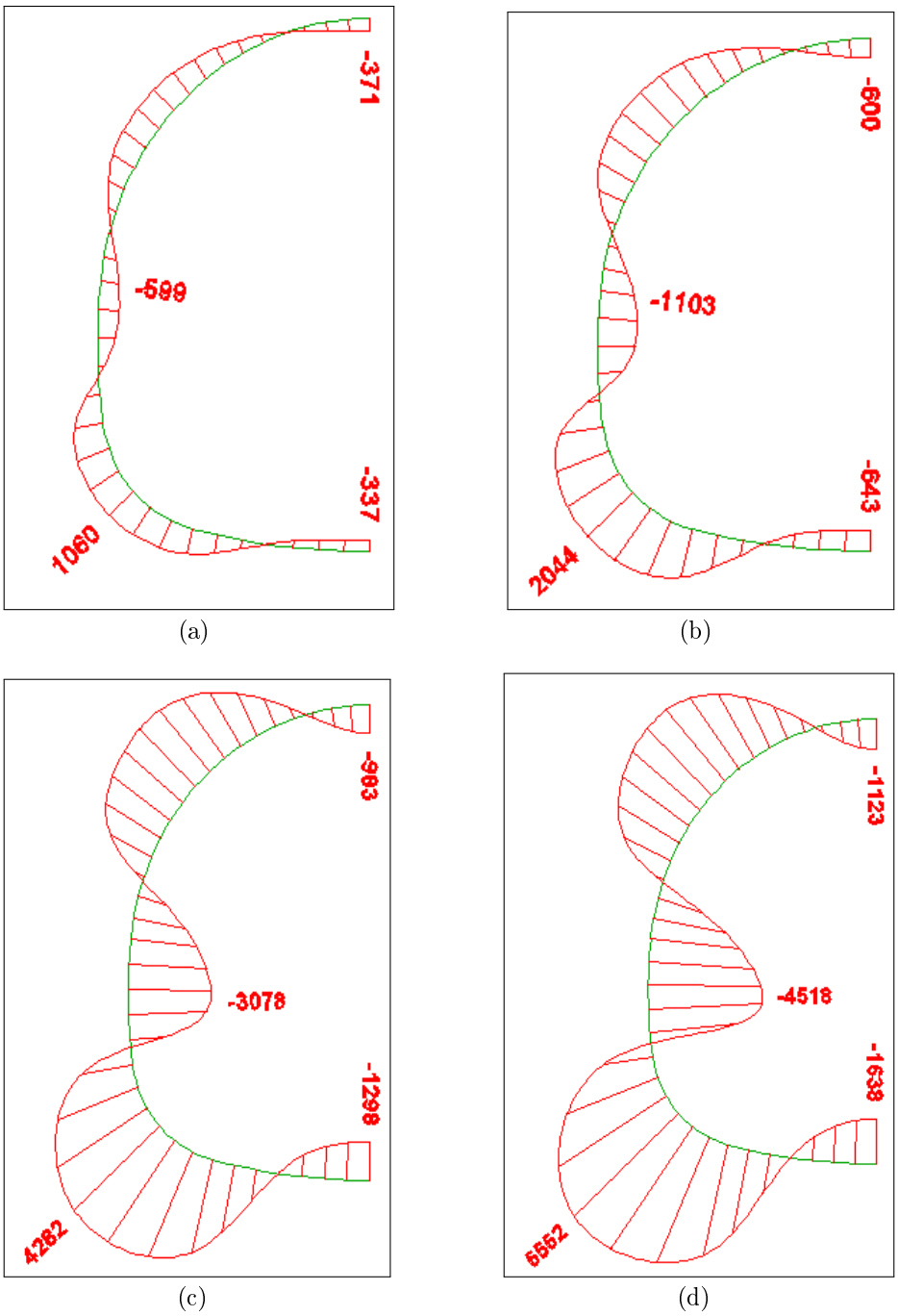

Figure 5.29: The bending moments (Nm/m) in the inner lining with degradation of shotcrete Young's modulus, (a); 30% degradation of shotcrete, (b); 50% degradation of shotcrete, (c); 80% degradation of shotcrete, (d); 90% degradation of shotcrete.

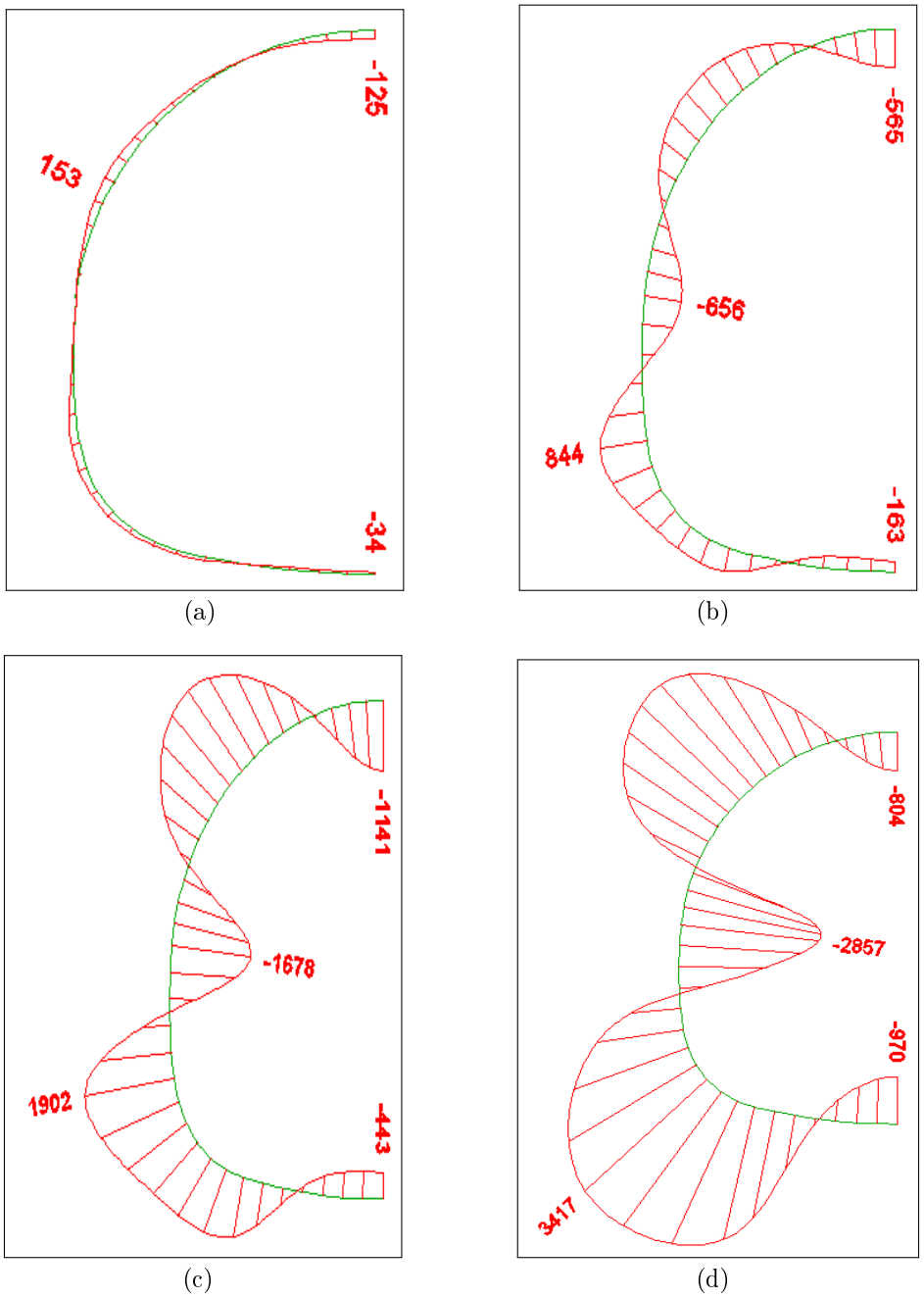

Figure 5.30: The bending moments (Nm/m) in the inner lining with degradation of shotcrete cohesion, (a); 10% degradation of shotcrete, (b); 30% degradation of shotcrete, (c); 50% degradation of shotcrete, (d); 80% degradation of shotcrete.

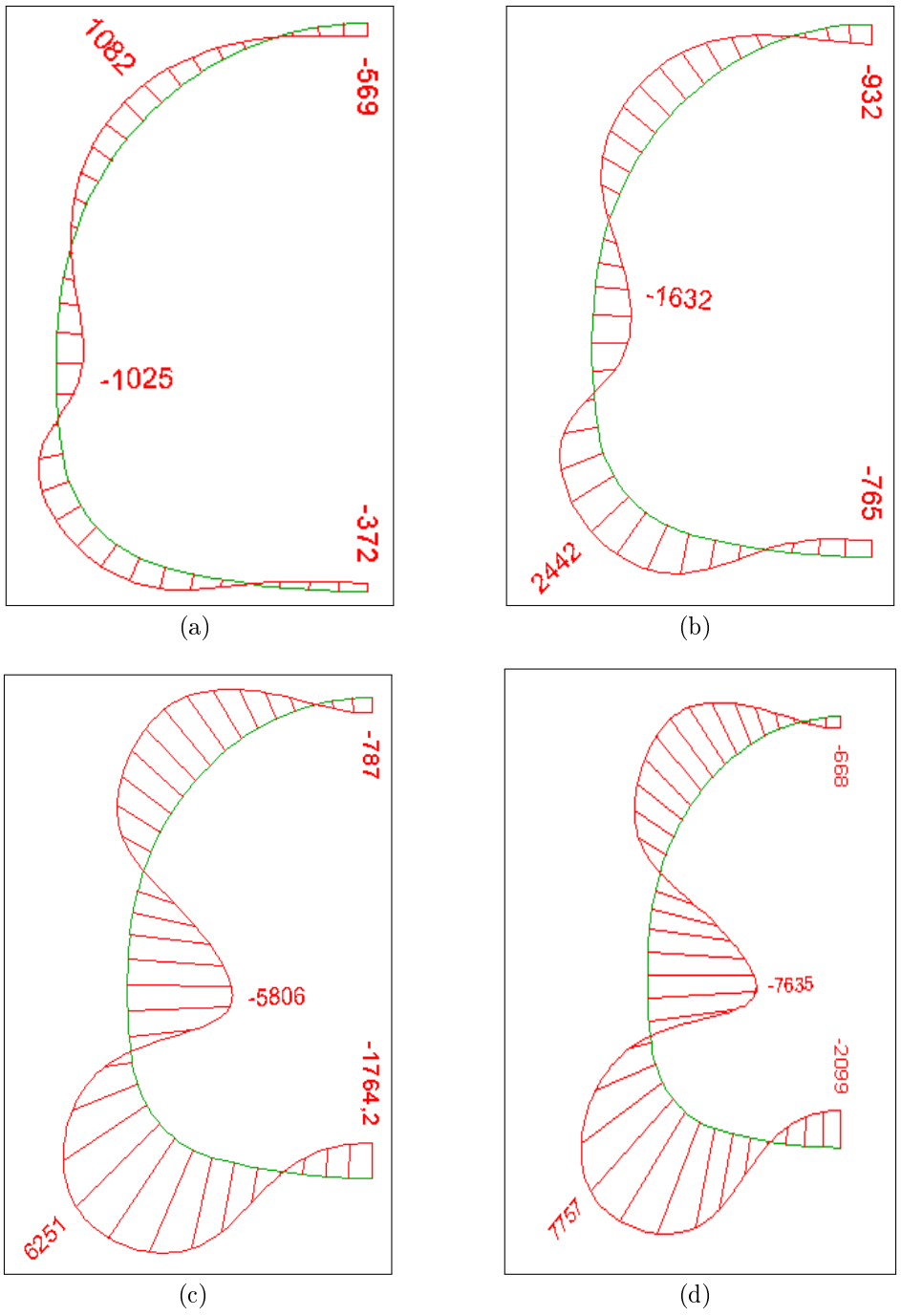

Figure 5.31: The bending moments (Nm/m) acting on the inner lining with degradation of shotcrete Young's modulus, cohesion and friction angle, (a); 30% degradation of shotcrete, (b); 50% degradation of shotcrete, (c); 80% degradation of shotcrete, (d); 90% degradation of shotcrete.

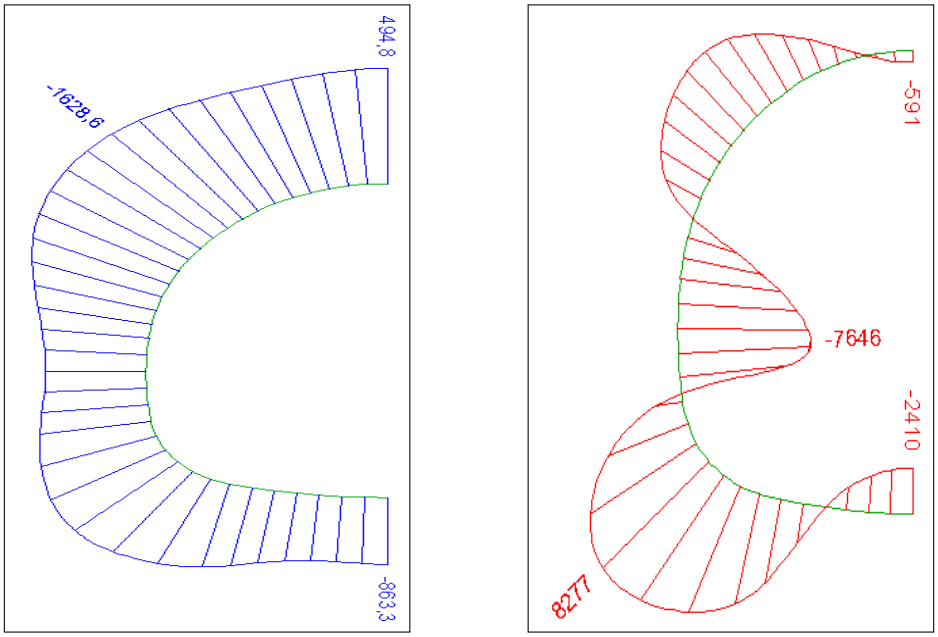

(a) (b)

Figure 5.32: The normal force (N/m) and bending moment (Nm/m) acting on the inner lining with 99% degradation of shotcrete Young's modulus, cohesion and friction angle, (a); normal force in the inner lining, (b); bending moment in the inner lining.

Chapter 6

Conclusions and Future work

6.1 Summary

The main focus of the research was to study the long-time behaviour of support elements in tunnels. The study consisted of the analysis of old samples of support elements in tunnels. The obtained results were included in the numerical analysis of a three-dimensional model of tunnel excavation and support installation. The shotcrete shell deterioration was then simulated to observe how it affects the inner lining. A brief summary of the experimental work conducted and the model capabilities that have been developed are given below:

- Almost thirty years old samples of shotcrete (primary lining), concrete (secondary lining), steel rock bolts and geomembranes were obtained from different cross-cuts of five highways tunnel sites in Austria, named Tanzenberg, Ganzstein, Katschberg, Roppener, and Bosruck.

- Shotcrete samples were tested in the material testing laboratory of the Subsurface and Geotechnical Institute of Montan University Leoben, Austria. After preparation these samples were subjected to different tests such as uniaxial compression and tri-axial compression tests to determine uniaxial compressive strength UCS, Poisson's ratio ν, Young's modulus E, deformation modulus V and shear strength parameters like cohesion c, and angle of friction ϕ using multiple failure tests. The tests were conducted to investigate material degradation and strength reduction with the passage of time.

- The samples of concrete (secondary lining) were tested at the Institute for Rock Mechanics and Tunnelling Technical University Graz, Austria. The tests were conducted to investigate the durability and behavior of inner lining in a dual-lining system after many years of service.

- Steel rock bolts/dowels from all five tunnel sites were tested in the ÖGI (Österreichisches Giesßereiinstitut), which is under the umbrella of Montan University. The purpose of testing was to clarify whether the external influences over 30 years of time

had affected the strength properties, composition and working performance of steel.

- The samples of geomembranes were tested in the Polymer Competence Center Montan University Leoben. Chemical, mechanical and thermomechanical material properties and any physical damage of the old geomembranes were evaluated.

- The evaluated results were included in developing a three-dimensional tunnel model using the finite element code ABAQUS.

- Simulation of shotcrete shell deterioration in stages to see the effect of this degradation on the combined support system comprising of inner lining, shotcrete shell and the surrounding ground.

6.2 Conclusions

As explained in the summary section, the study involved distinct elements of the tunnel support system including shotcrete and concrete, steel bolts and geomembrane. For the sake of clarity and cosistency the conclusions of the long-term degradation analysis of the mentioned elements were given after results and discussion in their respective chapters. The key findings that emerged from the three-dimensional numerical analysis are presented as follows:

- The numerical procedure developed in this study can be used to investigate the effects of stresses on the shotcrete support during step by step excavation of NATM tunneling taking into consideration the interaction between shotcrete shell and rock mass on the one side and shotcrete shell and inner lining on the other side.

- A realistic behaviour of tangential stresses was obtained by a three-dimensional model that provided the possibility for closely observing changes in the stresses, stress free activation of primary support and loading in the following excavation step.

- The stresses in the shotcrete shell substantially increased with the excavation of top heading, bench and invert. The resulting stress values could be used to calculate the required thickness or reinforcement of the shotcrete lining.

- There was no significant difference in the amount of stresses during excavation of top heading, bench and invert using C3D8 and C3D8R type of elements.

- The results illustrated that most of the displacement took place during excavation of the top heading. The visualization of stresses and displacements adjudicate the

salient feature of NATM subdivision of the tunnel cross section into multiple drifts or headings (top heading, bench, invert) to give the initial support sufficient time to stabilize, and limit displacements and stresses during bench and invert excavation.

- Simulating shotcrete shell deterioration by reducing E, c, ϕ or different combination thereof will result in load transfer from the shotcrete shell to the inner liner. Obviously with the reduction of c and ϕ values the compressive strength of the shotcrete was lost and so the shotcrete shell readily relieved of the stresses.

- The results also predicted that using Young's modulus as a deterioration factor of the shotcrete, the load transfer from shotcrete shell to inner lining started earlier but at a slow rate as compared to that of cohesion, in which case the load transfer started later but at a comparatively faster rate.

- The stress dissipation as a consequence of shotcrete shell degradation did not necessarily transfer exclusively into the inner lining, some of the stresses are also transmitted to the surrounding ground.

- At 99% deterioration level, shotcrete shell still supported the load, perhaps due to the fact that the reduced values of parameters were still high enough to sustain considerable share of load.

- Higher bending moments on the side walls with increased level of deterioration will have the tendency to cause tensile forces particularly on the inside of the inner lining.

6.3 Recommendations for Future Work

In the course of this research several important areas were identified where research is needed to probe further into the deterioration of support elements presented in this thesis:

- Further investigations and testing of the shotcrete, concrete, rock bolts and geomembranes samples collected from tunnels with a well known history of the presence of ground water during construction and operation is required to observe the rate of degradation under aggressive environmental conditions. Better evaluation of the level of degradation and service life of the support elements could be done by having knowledge of their composition and properties at the time of installation.

- More complex numerical model should be developed to include the effects of pore water-pressure drained and not drained conditions. The properties of the surrounding ground may change with time. The rock bolts should also be included in the simulation.

- Study of different contact formulations between shotcrete shell and ground and the shotcrete shell and inner liner to characterize the properties of contact as they are also affected with the deterioration of shotcrete.
- The study could be further elaborated by considering different values of shotcrete or ground parameters, overburden and thickness of the shotcrete shell and the inner liner.
- The material properties and load-bearing capacity of the inner liner might be reduced by the phenomenon such as de-icing and salt corrosion. All such factors may change the tunnel equilibrium with time and should be considered in the main degradation processes, and their impacts on the long-term stability of tunnels.

Appendix A

Fortran User Subroutine: USDFLD

```
SUBROUTINE USDFLD(FIELD,STATEV,PNEWDT,DIRECT,T,CELENT, &
TIME,DTIME,CMNAME,ORNAME,NFIELD,NSTATV,NOEL,NPT,LAYER, &
KSPT,KSTEP,KINC,NDI,NSHR,COORD,JMAC,JMATYP,MATLAYO,LACCFLA)

INCLUDE 'ABA_PARAM.INC'
! The following line must be included in the material description
*USER DEFINED FIELD
! Do not forget to make your material property dependent
! on Field Variable(S), e.g.
*ELASTIC, DEPENDENCIES=1
  210000., 0.31, , 0.
  130000., 0.28, , 1.

CHARACTER*80 CMNAME,ORNAME
CHARACTER*3  FLGRAY(15)
DIMENSION FIELD(NFIELD),STATEV(NSTATV),DIRECT(3,3),T(3,3),TIME(2)
DIMENSION ARRAY(15),JARRAY(15),JMAC(*),JMATYP(*),COORD(*)

! Set Field Variable equal to total time at the beginning of
! current the increment
FIELD(1)=TIME(2)
! Store the total time as a solution dependent state variable
STATEV(1)=FIELD(1)

RETURN
END
```

A.1 Input files attached in electronic version

List of Figures

List of Tables

Bibliography

[1] AASHTO, *Technical Manual for Design and Construction of Road Tunnels–Civil Elements. American Association of State Highway and Transportation Officials, Washington D.C.* (2010).

[2] R. Stadelmann, A. Pfeffer, Z. Q. Wei, *Design in tunneling, structural design methods for the inner lining, Geomechanics and Tunnelling.* **2**, 359 (2009).

[3] *Federal highway administration and Federal transit administration U.S. Department of Transportation , Highway and Rail Transit Tunnel Maintenance and Rehabilitation Manual 2004 .*

[4] RVS, 09.01.42. tunnel - geschlossene bauweise im lockergestein unter bebauung. wien: österreichische forschungsgemeinschaft straße und verkehr., *Tech. rep.* (2004).

[5] T. Wang, *Characterizing crack patterns on tunnel linings associated with shear deformation induced by instability of neighboring slopes. Engineering Geology* **115**, 80 (2010).

[6] F. Pacher, *Deformationsmessungen in Versuchstollen als Mittel zur Erforschung des Gebirgsverhalten und zur Bemessung des Ausbaues. Felsmech Ingenieursgeol Suppl* **4**, 149 (1964).

[7] T. Marcher, M. John, M. Ristic, *Determination of Load-Sharing Effects in Sprayed Concrete Tunnel Linings. Underground Construction Conference and Ehhibition Earls Court London, UK* (2011).

[8] H. Moedelhammer, Numerical methods for tunneling using abaqus and investigation of long-time effect of the shotcrete shell and its impact on the combined support system, Master's thesis, University of Leoben (2011).

[9] ÖVBB, Richtlinie innenschalenbeton, wien., *Tech. rep.*, Oesterreichische Vereinigung für Beton-und Bautechnik (2003).

[10] RVS, Tunnel-kontinuierlicher vortrieb von strassentunnel, wien., *Tech. rep.*, Österreichische Forschungsgemeinschaft Straße und Verkehr (2003).

[11] DS, Richtlinie 853„ *Tech. rep.*, Eisenbahntunnel planen, bauen und instand halten. Frankfurt am Main: Deutche Bahn AG (2007).

[12] ÖVBB, Richtlinie spritzbeton, wien., *Tech. rep.*, Oesterreichische Vereinigung für Beton-und Bautechnik (2009).

[13] J. Idris, M. Alheib, T. Verdel, *Numerical modelling of masonry joints degradation in built tunnels. Tunnelling and Underground Space Technology* **24**, 617 (2009).

[14] H. Einstein, *Rock Mechanics and Rock Engineering* **29**, 113 (1996).

[15] J. Idris, M. Alheib, T. Verdel, *Numerical modelling and mechanical behavior analysis of ancient tunnel masonary structures. Tunnelling and Underground Space Technology* **23**, 251 (2008).

[16] S.-W. Nam, A. Bobet, *Liner stresses in deep tunnels below the water table. Tunnelling and Underground Space Technology* **21**, 626 (2006).

[17] I. Akira, I. Shigero, *Road tunnel in japan: Deterioartion and countermeasures, Tunnelling and Underground Space Technology* **11**, 305 (1996).

[18] F. Sandrone, V. Labiouse, *Analysis of the evolution of road tunnels equilibrium conditions with a convergence-confinement approach, Rock Mechanics and Rock Engineering* **43**, 201 (2010).

[19] R. Zachow, Dimensionierung zweischaliger tunnel im fels auf der grundlage von in-situ-messungen., *Tech. rep.*, Dimensionierung zweischaliger Tunnel im Fels auf der Grundlage von in-situ-Messungen. Forschungsergebnisse aus dem Tunnel- und Kavernenbau der Universität Hannover. Hannover: Rokahr R. B. (1995).

[20] T. Marcher, F. Jiricny, *Interaction of primary lining and final lining of a NATM tunnel with respect to relevant long-term effects. Winter Workshop of Rock Mass Mechanics, Zakopane, Poland.* (2004).

[21] J. Marchand, E. Samson, *Predicting the service-life of concrete structures-limitations of simplified models. Cement & Concrete Composites* **31**, 515 (2009).

[22] M. Romer, M. Holzer, L. Pfiffner, *Swiss tunnel structures: concrete damage by formation of thaumasite. Cement & Concrete Composites.* **25**, 1111 (2003).

[23] B. Ladanyi, *Use of the long-term strength concept in the determination of ground pressure on tunnel linings. 3rd International Congress on Rock Mechanics, Denver, (pp. 1150-1156).* (1974).

[24] Y. Yuan, Y. Bai, J. Liu, *Assessment service state of tunnel structure Tunnelling and Underground Space Technology* **xx**, xxxx (2011).

[25] E. Bastidas-Arteaga, M. Sanchez-Silva, A. Chateauneuf, M. Ribas Silva, *coupled reliability model of biodeterioration, chlorides ingress and cracking for reinforced concrete structures. Structure Safety* **30**, 110 (2008).

[26] H. Paul, *Durability of shotcrete strength in case of the Bosruck tunnel, Bachelor thesis Montan university Austria.* (2012).

[27] A. William, L. Richard, eds., *Underground mining methods, Engineering Fundamentals and International Case Studies, SME, Colorado, USA* (2001).

[28] Z. Huan, E. Broch, M. Lu, *Cavern roof stability–mechanism of arching and stabilization by rockbolting. Tunnelling and Underground Space Technology.* **17**, 249 (2002).

[29] C. Charlie, *A new energy-absorbing bolt for rock support in high stress rock masses. International Journal of Rock Mechanics and Mining Sciences.* **47**, 396 (2010).

[30] K. Clapp, M. Maclaughlin, *Preliminary development of a fully grouted rock bolts element for discontinuous deformation analysis. Development and application of discontinuous modeling for rock engineering. Proceedings of the 6th international conference on analysis of discontinuous deformation.* (Swets and Zeitlinger B.V., Lisse. The Netherlands, 2003).

[31] M. Moosav, S. Karimi, *Corrosion Protection of Rock Bolts by Epoxy coating and its Effect on Reducing Bond Capacity. Coal Operators Conference. Wollongong, Australia* (2008).

[32] M. Rahman, S. Divi, D. Chandra, J. Daemen, *Effect of different salts on the corrosion properties of friction type A607 steel rock bolt in simulated concentrated water. Tunneling and Underground Space Technology* **23**, 665 (2008).

[33] E. Gamboa, A. Atrens, *stress corrosion cracking fracture mechanisms in rock bolts. Journal of materials science* **38**, 3813 (2003).

[34] E. Gamboa, A. Atrens, *Material influence on the stress corrosion cracking of rock bolts, Engineering Failure Analysis.* **12**, 201 (2005).

[35] L. Hobst, J. Zajic, *Anchoring in Rock and Soil,* (Elsevier, Amstardam, Oxford, New York, 1983).

[36] S. Divi, D. Chandra, J. Daemen, *Corrosion susceptibility of potential rock bolts in aerated multi-ionic simulated concentrated water. Tunnelling and Underground Space Technology.* **26**, 124 (2011).

[37] A. Burkert, J. Lehmann, J. Mietz, *Damage of stainless steel bars due to atmospheric corrosion. Materials and Corrosion.* **63, No. 3** (2012).

[38] ÖGI, Untersuchungen an alten ankern aus tunnelbau, *Tech. rep.*, Österreichisches Giesßerei-Institut A-8700 Leoben (2011).

[39] ÖGI, Beurteilung von betonankern vergleich alt - neu, *Tech. rep.*, Österreichisches Giesßerei-Institut A-8700 Leoben (2010).

[40] H. Chandler, ed., *Hardness testing.* (ASM International, 1999).

[41] A. Rollen, J. Rigo, *Geomembranes identification and performance testing* (Champan and Hall Australia, Japan, UK, USA., 1991).

[42] R. Rowe, H. Sangam, *Durability of HDPE geomembranes. Geotextile and Geomembranes* **20**, 77 (2002).

[43] R. Erickson, R. Thiel, J. Peters, *The ongoing quality issues regarding polyethylene geomembrane material manufacturing and installation. The First Pan American Geosynthetics Conference and Exhibition Cancun, Mexico* (2008).

[44] J. Scheirs, *A guide to polymeric geomembranes. A practical approach* (John Willey and sons, UK, 2009).

[45] P. Gerard, V. Santvoort, *Geotextiles and Geomembranes in civil engineering.* (A. A. Balkema, Rotterdam, Netherland., 1994).

[46] D. Krevelen, *Properties of Polymers; their correlation with chemical structure, their numerical estimation and prediction from additive group contributions* (Elsevier scientific publishing company, Amsterdam-Oxford- New York- Tokyo, 1991).

[47] J. Scheirs, *A Guide to Polymeric Geomembranes: A Practical Approach* (John Wiley & Sons Ltd, 2009).

[48] R. Koerner, Y. Halse, A. Lord Jr., *Long-term durability and aging of geomembrane. In: Bonaparte, R. (Ed.), Waste Containment Systems: Construction, Regulation, and Performance. ASCE Geotechnical Special Publication No. 26, New York, pp. 106–134* (1990).

[49] P. Lodi, B. Bueno, O. Vilar, *UV Exposure of Polymeric Geomembranes. Proceedings of the 4th Asian Regional Conference on Geosynthetics, Shangai, China* (2008).

[50] K. Brady, W. McMahon, G. Lamming, Thirty-year ageing of plastics. project report 11, *Tech. rep.*, Transport Research Laboratory, E472A/BG, ISSN 0968-4083 (1994).

[51] R. Schmidt, C. Young, J. Helwitt, *Long term field performance of geomembranes—15 years experience. Proceedings of the International Conference on Geomembranes, Vol.II, Denver, Co,* (1984).

[52] H. Fikentscher, *Cellulose-Chemie,* **13**, 58 (1932).

[53] H. Domininghaus, P. Elsner, P. Eyerer, T. Hirth, *Kunststoffe Eigenschaften und Anwendungen. Springer-Verlag, Berlin, Heidelberg, Germany.* (2004).

[54] W. Titov, *PVC Technology* (Elsevier Science Publishing Co., Inc., New York, USA., 1984).

[55] G. Ehrenstein, G. Riedel, P. Trawiel, *Praxis der Thermischen Analyse von Kunststoffen.* (Hanser, MÃijnchen, Germany., 1995).

[56] J. Wylamrzy, Untersuchungen zur auswirkung von anorganischen zusätzen auf die sekundären reaktionen der thermischen dehydrochlorierung von polyvinylchlorid, Ph.D. thesis, Universiy of Duisburg-Essen, Germany. (2004).

[57] B. Benzler, Thermische analyse von polyvinylchlorid (pvc), *Tech. rep.*, USER COM 1/99, Mettler Toledo GmbH, Giessen, Germany. (1999).

[58] PCCL, Characterization of pvc-geomembranes, *Tech. rep.*, Polymer Competence Center Leoben A-8700 (2011).

[59] PCCL, Charakterisierung von pvc-tunnelbahnen, *Tech. rep.*, Polymer Competence Center Leoben A-8700 (2011).

[60] A. Guenaelle, P. Noel, O. Marc, *Easy Identification of Plastics and Rubbers. Rapra Technology, Shrewsbury, UK.* (2001).

[61] L. Rabcewicz, *Die neue österreichische Tunnelbauweise I. Entstehung, Ausführungen und Erfahrungen. Der Bauingenieur* **40**, 289 (1965).

[62] L. Rabcewicz, *The New Austrian Tunneling Method, Part1 and 2, Water Power* (1964).

[63] G. Swoboda, A. Moussa, *Numerical modeling of shotcrete and concrete tunnel linings. Proc. of the Int. congress on Tunneling and Ground Conditions., held in Cairo, Egypt,* (1994).

[64] G. Galli, A. Grimdali, A. Leonardi, *Three-dimensional modeling of tunnel excavation and lining. Computers and Geotechnics* **31**, 171 (2004).

[65] H. Y. Liu, J. C. Small, J. P. Carter, *Full 3D modelling for effects of tunnelling on existing support system in the Sydney region. Tunnelling and Underground Space Technology* **23**, 399 (2008).

[66] ITA, *Tech. rep.*, Austrian Art of Tunnelling in Construction, Cosulting and Research, Ernst&Sohn (2008).

[67] ÖGG, *Tech. rep.*, NATM, The Austrian Practice of Conventional Tunneling, Austrian Society for Geomechanics (2001).

[68] M. Usman, G. G. Gschwandtner, R. Galler, *Three-dimensional Load Analysis of Tunnel Linings using NATM. International Conference on Advances in Geotechnical Engineering, Perth, Australia.* (2011).

[69] H. Meißner, *Tech. rep.*, Empfehlungen des Arbeitskreises " Numerik in der Geotechnik" der Deutschen Gesellschaft für Erd- und Grundbau e.V. (1991).

[70] Hibbitt, Karlsson, Sorensen, *ABAQUS Versions 6.10.1, Rhode Island, USA.* (2010).

[71] W.-F. Chen, *Constitutive Equations for Engineering Materials. Vol. 2. Plasticity and Modeling* (Elsevier Science B.V. Amsterdam-London-New York, 1994).

[72] M. Bolton, *The strength and dilatancy of sands. Geotechnique* **36**, 65 (1986).

[73] J. C. Jaeger, N. G. W. Cook, R. W. Zimmerman, *Fundamentals of Rock Mechanics, Fourth edition* (Blackwell publishing USA-UK-Australia, 2007).

[74] Y. Gueguen, M. Bouteca, eds., *Mechanics of Fluid Saturated Rocks* (Elsevier Inc. UK, USA., 2004).

[75] P. P. Oreste, *Analysis of structural interaction in tunnels using the convergence-confinement approach. Tunnelling and underground space technology* **18**, 347 (2003).

[76] S. Kainrath-Reumayer, E. Neugebauer, F. Charette, R. Galler, M. Plouffe, *Ankerung im untertagebau–Entwicklungen in Theorie und Praxis. Geomechanik und Tunnelbau.* **1**, 345 (2008).

[77] M. Panet, A. Guenot, *Panet, M. and Guenot, A. Analysis of convergence behind the face of a tunnel. Proceedings of the International Symposium. Tunneling, pp. 187-204* (1982).